The Wannier-Functions Software Ecosystem for Materials Simulations

Antimo Marrazzo,¹ Sophie Beck,² Elena R. Margine,³ Nicola Marzari,⁴,⁵ Arash A. Mostofi,⁶ Junfeng Qiao,⁴ Ivo Souza,⁻,¹ Stepan S. Tsirkin,⁻,² Jonathan R. Yates,⁶ and Giovanni Pizzi⁵

¹Dipartimento di Fisica, Università di Trieste, I-34151 Trieste, Italy*

Over the last two decades, following the early developments on maximally-localized Wannier functions, an ecosystem of electronic-structure simulation techniques and software leveraging the Wannier representation has flourished. This environment includes codes to obtain Wannier functions and interfaces with first-principles simulation software, as well as an increasing number of related post-processing packages. Wannier functions can be obtained for isolated or extended systems (both crystalline and disordered), and can be used to understand chemical bonding, to characterize polarization, magnetization, and topology, or as an optimal basis set, providing very accurate interpolations in reciprocal space or large-scale Hamiltonians in real space. In this review, we summarize the current landscape of techniques, materials properties and simulation codes based on Wannier functions that have been made accessible to the research community, and that are now well integrated into what we term a Wannier-functions software ecosystem. First we introduce the theory and practicalities of Wannier functions, starting from their broad domains of applicability to advanced minimization methods using alternative approaches beyond maximal localization. Then we define the concept of a Wannier ecosystem and its interactions and interoperability with many quantum engines and post-processing packages. We focus on some of the key properties that are empowered by such ecosystem—from band interpolations and large-scale simulations to electronic transport, Berryology, topology, electron-phonon couplings, dynamical meanfield theory, embedding, and Koopmans functionals—concluding with the current status of interoperability and automation. The review aims at highlighting basic theory and concepts behind codes, providing relevant pointers to more in-depth references. It also elucidates the relationships and connections between codes and, where relevant, the different motivations and objectives behind their development strategies. Finally, we provide an outlook on future developments, and comment on the goals of biodiversity and sustainability for the whole software ecosystem.

Contents

I.	Introduction			
	A.	$Ab\ initio$ electronic structure and Wannier functions	3	
II.	Wannier functions fundamentals			
	A.	Maximally-localized Wannier functions	4	
		1. Isolated composite groups of bands	4	
		2. Entangled bands	5	
	В.	Major applications of Wannier functions	6	
	C.	Wannier functions for the practitioner	7	
		1. The spread functional in reciprocal space	7	
		2. Accuracy and convergence	9	
	D.	Advanced minimization methods, and beyond		
		maximally-localized Wannier functions	9	

II.	The Wannier ecosystem: theory and software packages				
	A.	Development of widely-available Wannier engines	12		
	В.	The concept of a Wannier-functions software			
		ecosystem	13		
	$\mathbf{C}.$	C. Wannier interpolation and tight-binding models			
		1. Band interpolation	15		
		2. Band derivatives and Boltzmann transport	17		
		3. Interpolation of a generic k-local operator	18		
		4. Wannier function perturbation theory	18		
		5. Porting Wannier Hamiltonians to TB codes	19		
		6. Wannier interpolation beyond density-functional			
		theory	19		
	D.	Ballistic transport and nanostructures	21		
	\mathbf{E} .	Berryology	23		
		1. Motivation	23		
		2. Wannier interpolation of the interband Berry			
		connection	23		
		3. Other Berry-type quantities	24		
	F.	Topological invariants and related properties	25		
	G.		28		
		1. Methodology	28		

² Center for Computational Quantum Physics, Flatiron Institute, 162 5th Avenue, New York, New York 10010, USA

³Department of Physics, Applied Physics, and Astronomy, Binghamton University-SUNY, Binghamton, New York 13902, USA

⁴ Theory and Simulation of Materials (THEOS), and National Centre for Computational Design and Discovery of Novel Materials (MARVEL), École Polytechnique Fédérale de Lausanne, CH-1015 Lausanne, Switzerland

⁵Laboratory for Materials Simulations (LMS), and National Centre for Computational Design and Discovery of Novel Materials (MARVEL), Paul Scherrer Institut (PSI), CH-5232 Villigen PSI, Switzerland

⁶ Departments of Materials and Physics, and the Thomas Young Centre for Theory and Simulation of Materials, Imperial College London, London SW7 2AZ, UK

⁷Centro de Física de Materiales, Universidad del País Vasco, 20018 San Sebastián, Spain

⁸ Ikerbasque Foundation, 48013 Bilbao, Spain

⁹ Department of Materials, University of Oxford, Parks Road, Oxford OX1 3PH, UK

^{*} antimo.marrazzo@units.it

	2. Codes	29		
	H. Beyond DFT with localized orbitals	30		
	1. Dynamical mean-field theory and embedding	31		
	2. Koopmans functionals	33		
	I. Interoperability between codes in the ecosystem	34		
	1. Library mode for the Wannier engines	34		
	2. File I/O generation and parsing	34		
	J. Automation, workflows and high-throughput	35		
IV.	Conclusions and perspectives			
V.	. Acknowledgements			

I. Introduction

Wannier functions (WFs) (Wannier, 1937), and in particular maximally-localized Wannier functions (MLWFs) (Marzari and Vanderbilt, 1997), provide an accurate, compact, and localized representation of the electronic-structure problem, and have become widely used in computational condensed-matter physics and materials science (Marzari et al., 2012).

Thanks to developments in theory, algorithms and implementations over the past few decades, summarized in Sec. II, it has now become possible to apply widely the concept of MLWFs to single-particle theories and in particular to Kohn-Sham (KS) density-functional theory (DFT) simulations, to obtain localized orbitals from Bloch states; the latter can be themselves represented with localized or extended basis sets, such as plane waves. On one hand, these developments have benefited from profound connections between WFs and physical quantities such as electric polarization, orbital magnetization and topological invariants (Soluyanov and Vanderbilt, 2011b; Thonhauser et al., 2005; Vanderbilt, 2018; Vanderbilt and King-Smith, 1993; Xiao et al., 2005). On the other hand, the ability to obtain MLWFs from DFT simulations often allows to calculate physical quantities with high accuracy, but at a fraction of the computational cost, thanks to their role as very accurate interpolators (Lee et al., 2005; Souza et al., 2001; Yates et al., 2007). Finally, although not discussed here, localized representations have long been pioneered by the quantum chemistry community to interpret coordination and bonding (Edmiston and Ruedenberg, 1963), and ML-WFs extend to periodic systems the concept of Foster-Boys localized orbitals (Boys, 1966), thanks to algorithmic breakthroughs in calculating the position operator in solids (Blount, 1962; King-Smith and Vanderbilt, 1993; Nenciu, 1991; Resta, 1992; Zak, 1989).

Wannier functions are typically localized or even exponentially localized (Brouder et al., 2007; Panati, 2007; Panati and Pisante, 2013), and due to the nearsightedness of interacting electrons (Des Cloizeaux, 1964a,b; Kohn, 1996), local electronic properties only depend on the nearby environment (Bianco and Resta, 2011, 2013; Marrazzo and Resta, 2016, 2019). As a consequence,

the resulting Hamiltonian matrix expressed in a localized basis set (such as MLWFs (Calzolari et al., 2004; Lee et al., 2005)) becomes sparse, i.e., it displays negligible matrix elements—or hoppings, in the language of a tight-binding (TB) formalism—if the distance between the corresponding localized basis functions exceeds a given threshold. In this sense, MLWFs are optimal choices as they decay exponentially in real space (Panati and Pisante, 2013) and they minimize a localization functional by design (Marzari et al., 2012; Marzari and Vanderbilt, 1997). The resulting MLWFs can be used as a basis set to build, LEGO[™]-like, the electronic structure of large-scale nanostructures (Lee et al., 2005) that in turn could be solved with linear-scaling methods (Mauri et al., 1993; Nunes and Vanderbilt, 1994; Ordejón et al., 1993), or as a remarkably accurate interpolators of electronic properties, operators and quantities defined as integrals over the Brillouin zone (BZ) of periodic systems (Souza et al., 2001; Yates et al., 2007). Interpolation on dense grids becomes essential when very fine features need to be resolved, as happens when integrals are restricted to lower-dimensional manifolds (such as the Fermi surface, in the case of transport properties of metals).

Nowadays, MLWFs are routinely used in many research areas of condensed-matter physics and materials science. In Sec. II we summarize the past and current challenges, discussing how we reached the current state. Such a flourishment is not only due to theoretical advances, but also strongly driven by the concerted development of accessible and efficient software. Indeed, thanks to the availability of robust software packages (often open-source, encouraging further contributions), and to the user support provided by developers, researchers can now not only easily compute MLWFs, but also use them as core ingredients for advanced simulations. As more codes appear, they adopt the de facto standardization of input and output formats, resulting in a set of interacting and interoperating codes that we will call here the "Wannier-functions software ecosystem."

This review does not aim to provide an extensive discussion of the theory of MLWFs, for which we refer to Marzari et al. (2012), although we do provide a general introduction to the field in Sec. I.A. Instead, the goal is to discuss the nature of the ecosystem and the capabilities of existing codes, focusing in Sec. III on a selection of physical phenomena or quantities that can be efficiently predicted thanks to WFs, and on how WFs are used as an ingredient to extend the accuracy of beyond-DFT simulations. Nevertheless, we will still mention a few notable developments of the past decade, whenever useful to contextualize the theoretical and software developments. Our aim is to provide a reference that can help newcomers and existing practitioners alike navigate the ecosystem: which properties can be computed by which codes, why the use of WFs is beneficial, which quantities are exchanged between codes, and how interoperability

is being addressed.

To discuss the codes, we group them into three major categories: Wannier engines, i.e., codes to obtain WFs; interface codes between the first-principles engines (e.g., DFT or GW codes) and the Wannier engines; and Wannier-enabled codes, which range from relatively simple post-processing tools to more advanced codes that use WFs as one of the ingredients to accelerate accurate simulations. A fourth category of codes that we discuss in Sec. III.J are automation workflows. Indeed, until very recently the generation of WFs typically required human intuition by experienced researchers to provide initial trial orbitals. This barrier has been largely removed by recent algorithmic and automation efforts (see Sec. II.D), enabling the use of WFs both by new users and for high-throughput materials discovery and characterization. In the latter case, managing thousands (or more) simulations poses new challenges, which require not only the use of robust workflow engines, but also the implementation of WF-specific workflows to effectively interconnect multiple codes within the ecosystem.

We will finally conclude in Sec. IV with some perspectives on the field related to the sustainability of the whole effort, current challenges that still need to be addressed, and possible future developments.

A. Ab initio electronic structure and Wannier functions

Electronic-structure simulations aim to determine the behavior of electrons in materials and molecules, as governed by the Schrödinger or Dirac equations. Electrons feel Coulomb interactions among themselves and with the nuclei, in addition to couplings with external fields (e.g., electrical, magnetic, or electromagnetic/photons) or perturbations (e.g., strain, phonons). The core electrons of heavy chemical elements can reach relativistic speeds, requiring to correct the Schrödinger equation with terms obtained from an expansion of the Dirac equation in powers of $1/c^2$, where c is the speed of light. The most relevant relativistic correction is spin-orbit coupling, which is responsible for several important phenomena related to magnetism and to geometrical and topological properties of the electronic manifold (see Sec. III.E and Sec. III.F).

An exact solution of the Schrödinger equation (either the bare one, or with relativistic corrections) would give access to essentially all property of materials. This problem was already clear in 1929, when Paul Dirac declared: "The underlying physical laws necessary for the mathematical theory of a large part of physics and the whole of chemistry are thus completely known, and the difficulty is only that the exact application of these laws leads to equations much too complicated to be soluble" (Dirac, 1929).

For more than fifty years, *ab initio* or first-principles methods have been developed to approximately solve the

Schrödinger equation in realistic settings (Giustino, 2014; Martin, 2020), with more accurate strategies and theories being developed. In parallel, the exponential growth of computational power (Moore's law) has allowed to deploy these new theoretical instruments through numerical simulations, constantly seeking not only to improve accuracy but also targeting more complex and realistic systems. Quickly, numerical solutions became sufficiently accurate to be predictive for a number of properties in relevant systems: the era of first-principles materials modeling had begun (Marzari et al., 2021; Yin and Cohen, 1980).

An iconic example is given by DFT, which made it possible to determine the electronic structure of complex materials with reasonable accuracy at low cost. In DFT, the total energy of the electrons is expressed as a functional of the electronic charge density (Giustino, 2014; Martin, 2020). The theory is supported by two pillars, the Hohenberg-Kohn theorems, which state not only a oneto-one correspondence between the ground-state manybody wavefunction and the ground-state charge density. but also formulate a variational total-energy functional: the solution of the Schrödinger equation can be recast as a minimization problem for the charge density, a remarkably simpler object (a real function of \mathbf{r}) than the manybody wavefunction we started from (a complex function of $3N_e$ variables, where N_e is the number of electrons in the system).

In KS DFT, the interacting many-body problem is mapped onto a non-interacting problem sharing the same ground-state charge density but in presence of a suitable local external potential; the latter is in general unknown. This ansatz allows to capture with accuracy the kinetic energy contribution through the second derivatives of the KS orbitals, otherwise invisible in practice in their square moduli (the density). The success of DFT has been possible also thanks to the discovery and development of simple functionals that approximate the exact, but unknown, total-energy functional. Hence, the KS-DFT approach to solving the many-body Schrödinger equation translates into solving a set of non-interacting one-particle Schrödinger equations in presence of an external potential that depends, self-consistently, upon the charge density only. Although the outstanding importance of DFT has been recognized by the 1998 Nobel Prize in chemistry awarded to Walter Kohn (for DFT) and John Pople (for computational methods in quantum chemistry), its impact on the physics community has been, if possible, even greater: the top ten most highly cited articles published by the American Physical Society deal with DFT and related applications (Talirz et al., 2021).

The electronic structure of materials and molecular systems is, at the same time, very similar and yet very different. To some extent, extended materials can be seen as very large molecules and one could focus on the local electronic structure in real space, which is periodi-

cally repeated in the case of a crystalline materials (e.g., metals, semiconductors, oxides). This viewpoint is supported by the mathematical structure of the Schrödinger equation and its solutions, as observed by Kohn (Kohn, 1996): the electronic structure is fundamentally a local property, "near sighted" to what happens at further distance in real space. The effect of chemical bonding and the presence of the lattice can be seen as perturbations to the case of isolated atoms, with their well-defined s, p, dand f orbitals. This perspective is powerful and foundational for linear-scaling methods, which target the simulation of large systems and leverage a description based on localized orbitals. Yet materials are not just very large molecules, and "more is different" (Anderson, 1972). Extended systems are practically infinite and can thus be described using periodic boundary conditions (PBCs). As will be discussed in more formal terms in Sec. II, the electronic structure of a material in PBC is more naturally described in terms of Bloch orbitals, which are not localized in real space. Indeed, a different perspective often drives the discussion of the electronic structure of periodic crystals: the behavior in reciprocal (i.e., Fouriertransformed) space. A textbook example is semiconductor physics, that is in general much better understood (and taught) by studying solutions of the Schrödinger equation in such reciprocal space. This approach, somewhat orthogonal to the large-molecule perspective, is indeed also very powerful both at a conceptual and practical level. As a side note, many electronic-structure codes for materials actually adopt a completely delocalized basis (e.g., plane waves) to describe the periodic part of the Bloch orbitals (Martin, 2004, 2020; Pickett, 1989).

How can we reconcile these two, almost opposite, perspectives? Remarkably, one can use the fundamental "gauge freedom" of quantum mechanics: First, any quantum state is defined modulo a phase factor. Second, if one considers a set of single-particle states separated in energy from other states, then any trace operation on this manifold is invariant with respect to any unitary transformation among the orbitals; we call this a "generalized" gauge freedom. However, and this is the crucial aspect, the localization properties of that set of states strongly depend on their gauge.

WFs provide a rigorous and insightful way to reconcile the real-space and localized perspective with the reciprocal-space (Fourier) and delocalized one. As it will be clear in the next section, MLWFs in particular exploit the generalized gauge freedom to transform delocalized orbitals into localized ones (and vice versa), by constructing the proper unitary matrices.

II. Wannier functions fundamentals

The electronic structure of periodic crystals is most commonly described in terms of Bloch waves $\psi_{n\mathbf{k}}(\mathbf{r}) = u_{n\mathbf{k}}(\mathbf{r})\,e^{i\mathbf{k}\cdot\mathbf{r}}$, where \mathbf{k} is the crystal momentum, and n is the band index. This is the case in textbooks on solid-state theory, but also for the many software packages that solve the KS equations for crystalline solids. A few years after Felix Bloch developed the theory of electron waves in periodic crystals (Bloch, 1929), Gregory Wannier introduced an alternative representation in terms of an orthonormal set of localized functions (Wannier, 1937), the Wannier functions. Given an isolated Bloch band n, the WF $w_{n\mathbf{R}}(\mathbf{r}) = \langle \mathbf{r} | \mathbf{R} n \rangle = w_{n\mathbf{0}}(\mathbf{r} - \mathbf{R})$ associated with the unit cell labelled by lattice vector \mathbf{R} is defined as (Wannier, 1937)

$$|\mathbf{R}n\rangle = \frac{V_{\text{cell}}}{(2\pi)^3} \int_{\mathbf{RZ}} d\mathbf{k} \, e^{-i\mathbf{k}\cdot\mathbf{R}} |\psi_{n\mathbf{k}}\rangle,$$
 (1)

where V_{cell} is the unit-cell volume.

Since their inception, WFs have been employed as a conceptual tool to tackle problems in solid-state physics (see, e.g., Kivelson (1982)). However, in the first sixty years following Wannier's paper, there were few actual calculations of WFs for real materials (see, e.g., Callaway and Hughes (1967); Satpathy and Pawlowska (1988); and Sporkmann and Bross (1994)). The main obstacle was the fact that WFs are strongly non-unique, being sensitive to the generalized gauge freedom discussed earlier, e.g., to k-dependent phase changes $|\psi_{n\mathbf{k}}\rangle \to e^{-i\beta_{n\mathbf{k}}} |\psi_{n\mathbf{k}}\rangle$ with $\beta_{n\mathbf{k}} \in \mathbb{R}$ (gauge transformations) of the Bloch eigenstates. Moreover, the energy bands of real materials typically become degenerate at points, lines, or even entire planes in the BZ. The presence of degeneracies leads to poor localization properties of the WFs obtained from Eq. (1), because no matter how the phase factors $e^{-i\beta_{n\mathbf{k}}}$ are chosen, the Bloch eigenfunctions are non-differentiable functions of \mathbf{k} at the degeneracy points.

A. Maximally-localized Wannier functions

In the following, we discuss the original Wannierization methods introduced in Marzari and Vanderbilt (1997) and Souza *et al.* (2001), while we refer the reader to Sec. II.D for an overview of more recent and advanced minimization methods.

1. Isolated composite groups of bands

Consider a group of J Bloch bands of orthonormal $|\psi_{n\mathbf{k}}\rangle$ Bloch states that may be connected among themselves by degeneracies, but are isolated from all lower or higher bands, e.g., the six valence bands in Fig. 1. Given such a composite group, the most general expression for

the associated WFs is (Marzari and Vanderbilt, 1997)

$$|\mathbf{R}j\rangle = \frac{V_{\text{cell}}}{(2\pi)^3} \int_{\mathbf{RZ}} d\mathbf{k} \, e^{-i\mathbf{k}\cdot\mathbf{R}} |\psi_{j\mathbf{k}}^{\mathbf{W}}\rangle ,$$
 (2a)

$$|\psi_{j\mathbf{k}}^{\mathbf{W}}\rangle = \sum_{n=1}^{J} |\psi_{n\mathbf{k}}\rangle U_{\mathbf{k},nj},$$
 (2b)

where the $U_{\mathbf{k}}$ are $J \times J$ unitary matrices that describe the generalized (multiband) gauge freedom within the Bloch manifold at each \mathbf{k} . The superscript W denotes a Wannier gauge, as opposed to a Hamiltonian gauge (later denoted by H) where the Hamiltonian matrix is diagonal. Note that at variance with Eq. (1), in Eq. (2) there is not a one-to-one correspondence between the band index nand the intra-cell Wannier index j.

Marzari and Vanderbilt (MV) introduced the concept of MLWFs, in which the $U_{\mathbf{k}}$ matrices are chosen so as to minimize the total quadratic spread of the WFs (Marzari and Vanderbilt, 1997):

$$\Omega = \sum_{j=1}^{J} \left[\langle \mathbf{0}j | r^2 | \mathbf{0}j \rangle - |\langle \mathbf{0}j | \mathbf{r} | \mathbf{0}j \rangle|^2 \right]. \quad (3)$$

As discussed later (see Sec. II.C.1) the spread (a.k.a. localization) functional Ω and its gradient with respect to an infinitesimal gauge transformation can be expressed in reciprocal space; furthermore, the BZ integration in Eq. (2a) is replaced by a discrete sum $(1/N)\sum_{\mathbf{k}}$ where N is the number of k-points in the finite grid used in the numerical simulations, and the optimal $U_{\mathbf{k}}$ matrices are found by iteratively minimizing the functional Ω (see also Marzari and Vanderbilt (1997) for the mathematical details).

From general Fourier-transform considerations (Duffin, 1953), the good real-space localization properties of the MLWFs on the left-hand side of Eq. (2a) mean that the Bloch-like states $|\psi_{j\mathbf{k}}^{W}\rangle$ appearing on the right-hand side are smooth functions of \mathbf{k} for the optimal choice of $U_{\mathbf{k}}$ matrices in Eq. (2b) (or for any other choice leading to well-localized WFs).

The details of the MV methodology can be found in Marzari et al. (2012) and Marzari and Vanderbilt (1997); in the case of single k-point sampling (large unit cells), it is equivalent to the Foster-Boys scheme used in quantum chemistry to construct localized molecular orbitals (Boys, 1966). It should be noted that other localization criteria can be used for the purpose of obtaining localized orbitals, e.g., the Edmiston–Ruedenberg (Edmiston and Ruedenberg, 1963) and Pipek–Mizey (Pipek and Mezey, 1989) approaches, based on maximizing the Coulomb self-repulsion of the orbitals and the sum of the squares of the Mulliken charges (Mulliken, 2004) associated with the orbitals, respectively. Whilst these are more challenging to adapt to a periodic, multi-k-point formulation, there has been recent work to obtain

WFs for periodic systems using the Pipek–Mezey localization criterion (Clement *et al.*, 2021; Jónsson *et al.*, 2017). Nevertheless, the MV approach of minimizing the quadratic spread is still the most widely used approach for periodic systems.

2. Entangled bands

The MV approach described above provides a means to construct well-localized WFs from isolated groups of bands, such as the valence bands of insulators. However, it is often useful to obtain WFs from non-isolated (or "entangled") groups of bands. Typical examples include the low-lying conduction bands or the valence plus conduction bands of insulators (see Fig. 1), and the bands crossing the Fermi level in metals.

A possible strategy to deal with such cases is to first identify an appropriate J-dimensional Bloch manifold at each k-point from a larger set of $\mathcal{J}_{\mathbf{k}}$ Bloch eigenstates $|\psi_{m\mathbf{k}}\rangle$, e.g., the ones within some energy window. Formally, this band-disentanglement step can be expressed as

$$|\tilde{\psi}_{n\mathbf{k}}\rangle = \sum_{m=1}^{\mathcal{J}_{\mathbf{k}}} |\psi_{m\mathbf{k}}\rangle \,\tilde{V}_{\mathbf{k},mn} \,,$$
 (4)

where the $\tilde{V}_{\mathbf{k}}$ are $\mathcal{J}_{\mathbf{k}} \times J$ matrices satisfying $\tilde{V}_{\mathbf{k}}^{\dagger} \tilde{V}_{\mathbf{k}} = \mathbbm{1}_{J \times J}$. In 2001, Souza, Marzari and Vanderbilt (Souza et al., 2001) (SMV) introduced a practical scheme to extract an optimally-smooth Bloch-like subspace $\hat{P} = \sum_{n=1}^{J} |\tilde{u}_{n\mathbf{k}}\rangle \langle \tilde{u}_{n\mathbf{k}}|$ across the BZ, from which a set of MLWFs could then be obtained using the MV prescription. The resulting "disentangled WFs" are given by Eq. (2) with the ab initio Bloch eigenstates $|\psi_{n\mathbf{k}}\rangle$ therein replaced by $|\tilde{\psi}_{n\mathbf{k}}\rangle$, that is,

$$|\mathbf{R}j\rangle = \frac{1}{N} \sum_{\mathbf{k}} e^{-i\mathbf{k}\cdot\mathbf{R}} |\psi_{j\mathbf{k}}^{\mathbf{W}}\rangle ,$$
 (5a)

$$|\psi_{j\mathbf{k}}^{\mathbf{W}}\rangle = \sum_{n=1}^{\mathcal{J}_{\mathbf{k}}} |\psi_{n\mathbf{k}}\rangle V_{\mathbf{k},nj},$$
 (5b)

where the $\mathcal{J}_{\mathbf{k}} \times J$ matrices $V_{\mathbf{k}} = \tilde{V}_{\mathbf{k}} U_{\mathbf{k}}$ encode the net result of the disentanglement (subspace-selection) and maximal localization (gauge-selection) steps. As in the case of Eq. (2), the states $|\psi_{j\mathbf{k}}^{W}\rangle$ in Eq. (5) are smooth functions of \mathbf{k} whenever the associated WFs are well localized.

The disentanglement step can be carried out in such a way that the *ab initio* eigenstates are described exactly within a "frozen" or "inner" energy window that is contained by the "outer" energy window mentioned earlier (Souza *et al.*, 2001). This is useful, for example, when studying transport properties, for which one would like to obtain a faithful description of the states within some

small energy range around the Fermi level. Note that because of these energy windows, the needed input from the first-principles calculation includes the energy eigenvalues $\varepsilon_{n\mathbf{k}}$ in addition to the overlap matrices Eq. (8).

Over the years, many alternative approaches and algorithms have been developed—from partially-occupied Wannier functions (Fontana et al., 2021; Thygesen et al., 2005) to quasiatomic orbitals (Qian et al., 2008), to the selected columns of the density matrix (SCDM) (Damle et al., 2015, 2017), and to projectability disentanglement and manifold remixing (Qiao et al., 2023a,b); these and others will be discussed in Sec. II.D.

B. Major applications of Wannier functions

a. Interpolation The efficient interpolation in reciprocal space of k-dependent quantities is arguably the most common application of WFs, enabling the calculation of simple (e.g., the band structure) or complex (e.g., electron-phonon coupling) electronic structure properties. A large part of this review is devoted to the fundamentals of WF interpolation (Sec. III.C) and their applications, including ballistic transport (Sec. III.D), Berry-phase related properties (Sec. III.E) and electronphonon interactions (Sec. III.G). As discussed in more detail in Sec. III.C, the reason for such widespread set of applications (not all of them covered in this review) is that WFs can be applied to any generic operator that is local in reciprocal space. Equally important is that WFs allow to reproduce the correct band connectivity: in particular, avoided crossings are not mistaken for actual crossings. This distinguishes Wannier interpolation from other methods based on direct Fourier interpolation of the energy eigenvalues. In other words, WFs allow to exploit the fundamental locality ("nearsightedness" according to Kohn (Des Cloizeaux, 1964a,b; Kohn, 1996)) of the electronic structure and the related exponential localization of WFs to construct a potentially exact representation of an operator in real space, such that any interpolation back to reciprocal space is exact as well. The procedure is also systematic as WFs are guaranteed to exist and the convergence is exponential with the linear sampling density (Brouder et al., 2007; Panati, 2007; Panati and Pisante, 2013); prefactors and coefficients might depend on electronic structure properties such as the band gap, and on the specific operator under consideration.

b. Geometry and Topology WFs have several profound connections with quantum-geometrical and topological aspects of the electronic structure (Vanderbilt, 2018); some of them are discussed in Sec. III.E and III.F. In the following, we refer to topological properties as a subset of geometrical properties that are quantized and

hence represented by integer topological invariants robust to certain classes of perturbations. A prime example of geometrical—and in some circumstances also topological—quantity is the electric polarization of periodic solids, which can be calculated in reciprocal space as a Berry phase (Vanderbilt, 2018) (see Sec. III.E). Electric polarization can also be equivalently computed by summing over WFs centers in real space (Marzari et al., 2012; Marzari and Vanderbilt, 1997; Vanderbilt, 2018), which provides a more intuitive formulation of the modern theory of polarization (King-Smith and Vanderbilt, 1993; Resta, 1992, 1994; Vanderbilt, 2018) and restores some justification to the classical Clausius-Mossotti (Clausius, 1879; Mossotti, 1850) viewpoint. While electronicstructure geometry in reciprocal space speaks the language of differential geometry (e.g., curvatures, parallel transport, smoothness of manifolds), WFs allow to express the same quantities in terms of matrix elements of the Hamiltonian and position operator $\hat{\mathbf{r}}$. The reciprocalspace smoothness, which is measured by the quantum geometric tensor (Provost and Vallee, 1980), can be equivalently analyzed in real space by measuring the degree of WFs localization.

To some extent, the connection between WFs and topological invariants is even stronger, where the former provide not only powerful approaches to calculate invariants for real materials (see Sec. III.F for a discussion) but also fundamental understanding of topological phases. In fact, topological insulators are essentially systems that cannot be connected adiabatically to atomic insulators, hence it is impossible to truly represent their ground state with WFs (Thonhauser and Vanderbilt, 2006; Vanderbilt, 2018). In reciprocal space, non-trivial topological invariants translate into unavoidable obstructions to choosing a smooth gauge over the BZ (Bernevig and Hughes, 2013; Vanderbilt, 2018). The fundamental connection between non-trivial topology of electronic bands and the corresponding absence of a Wannier representation has been recently generalized and made systematic in the context of elementary band representation (Michel and Zak, 1999; Zak, 1982), leading to the so-called topological quantum chemistry (Bradlyn et al., 2017; Cano et al., 2018; Vergniory et al., 2017) (see also related efforts on symmetry-based indicators by Khalaf et al. (2018); Kruthoff et al. (2017); Po et al. (2017); and Song et al. (2018)), allowing to screen materials databases and identify non-trivial materials of various classes (Tang et al., 2019; Vergniory et al., 2019; Wieder et al., 2022; Zhang et al., 2019).

c. Advanced electronic-structure methods DFT simulations of periodic solids can be conveniently (but definitely not necessarily) performed by adopting a plane-wave basis set, in conjunction with smooth pseudopotentials that reproduce the interaction between valence electrons and

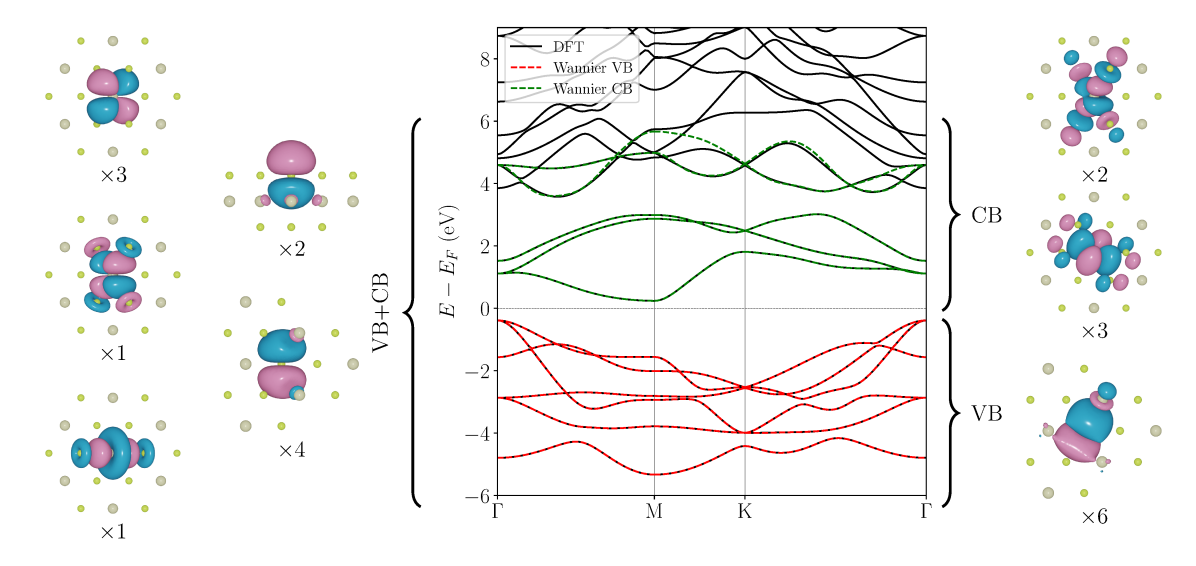


FIG. 1 MLWFs and band structure of the 2D material HfSe₂. In the center, the comparison between the DFT band structure (black lines) and the Wannier-interpolated band structure from valence MLWFs only (VB, red dashed lines) and from low-lying conduction MLWFs only (CB, green dashed lines) are shown. Note that the Wannier-interpolated bands from both valence + conduction MLWFs together (VB+CB) are not shown since they are visually indistinguishable from the combination of the VB and CB MLWFs. On the left, we show the real-space shapes of (in total 11) valence + conduction MLWFs, obtained starting from Hf d and Se p initial guess orbitals, followed by disentanglement (see Sec. II.A.2) from high-energy conduction states: specifically, three of them resemble $d_{xy,xz,yz}$ orbitals, one resembles a d_{z^2} orbital, one resembles a $d_{x^2-y^2}$ orbital, and the remaining six resemble p orbitals. Some small hybridization with orbitals from nearby atoms is visible. On the right, we show the real-space shapes of (in total 6) valence MLWFs (lower panel) and (in total 5) conduction MLWFs (upper panel). The valence MLWFs span an isolated group of bands (see Sec. II.A.1) and are composed by six hybridized bonding orbitals, where the Hf d and Se p orbitals overlap constructively. The conduction MLWFs are instead five hybridized anti-bonding orbitals, where Hf d and Se p orbitals overlap destructively, forming nodal planes close to bond centers. (The notation ×n below each shape denotes the multiplicity of the corresponding MLWF, i.e., n MLWFs having similar shapes but different spatial orientation.)

nuclei plus core electrons (Martin, 2020). The resulting KS eigenstates are also not particularly localized functions, and DFT is invariant under unitary rotations of the occupied electronic states. However several electronicstructure methods, aiming at improving or complementing the capabilities of DFT, fundamentally require to be formulated in terms of localized orbitals (see Sec. III.H). In addition, several of these beyond-DFT methods are not deployed directly on the crystal structure, but operate more as corrections to starting DFT calculations. Also, beyond-DFT methods can be computational rather intensive, and it is common practice to apply them only on a subset of bands extracted from the entire manifold. In this context, WFs provide a robust way to bridge DFT with advanced electronic-structure methods by allowing to systematically construct orthogonal localized states that represent the manifold of interest: WFs are first constructed on the KS DFT solution and then fed into beyond-DFT methods; a technical overview of how this is carried out in practice is the subject of Sec. III.H.

C. Wannier functions for the practitioner

1. The spread functional in reciprocal space

The Blount identities (Blount, 1962) provide the matrix elements of the position operator between WFs, and, remarkably, prefigure the link between macroscopic properties and integrals (Berry phases) of Berry connections (King-Smith and Vanderbilt, 1993):

$$\langle \mathbf{R}i | \mathbf{r} | \mathbf{0}j \rangle = i \frac{V_{cell}}{(2\pi)^3} \int d\mathbf{k} \, e^{i\mathbf{k}\cdot\mathbf{R}} \langle u_{i\mathbf{k}} | \nabla_{\mathbf{k}} | u_{j\mathbf{k}} \rangle$$
 (6)

and

$$\langle \mathbf{R}i|r^2|\mathbf{0}j\rangle = -\frac{V_{cell}}{(2\pi)^3} \int d\mathbf{k} \, e^{i\mathbf{k}\cdot\mathbf{R}} \langle u_{i\mathbf{k}}|\nabla_{\mathbf{k}}^2|u_{j\mathbf{k}}\rangle \quad . \tag{7}$$

It is through these identities that one can recast the spread functional Ω using reciprocal-space expressions, where the gradients and higher derivatives are obtained from finite differences. The building blocks for these finite-difference expressions are the overlap matrices

$$M_{ij}^{(\mathbf{k},\mathbf{b})} = \langle u_{i\mathbf{k}} | u_{j\mathbf{k}+\mathbf{b}} \rangle \tag{8}$$

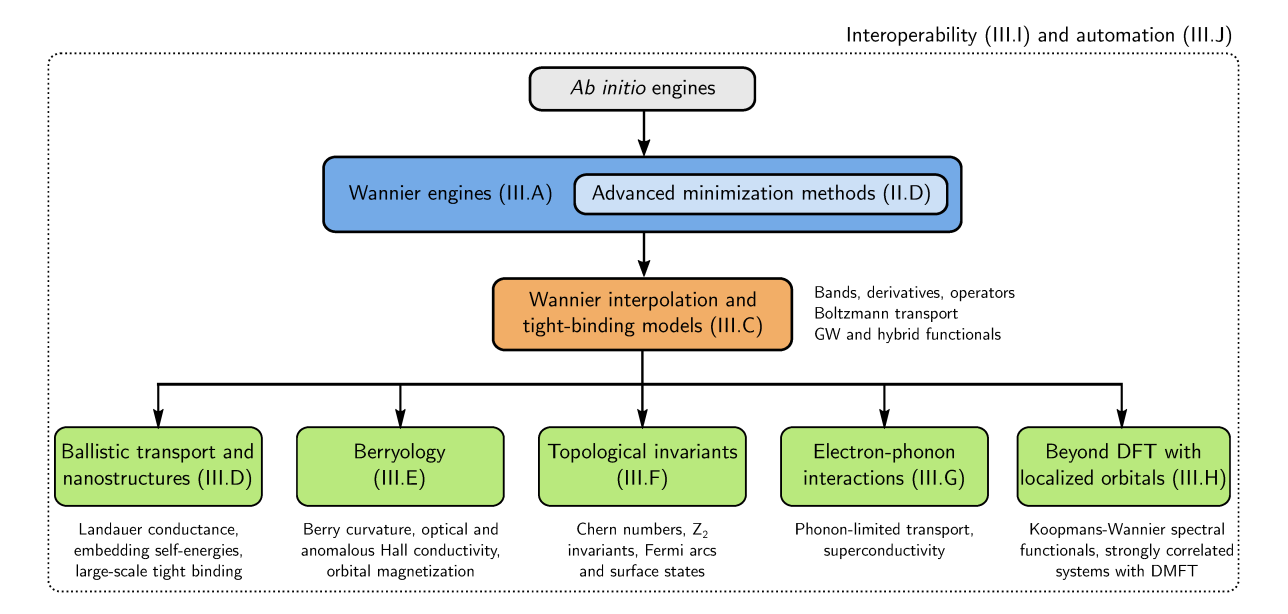


FIG. 2 Overall schematics of how different codes in the ecosystem interact. This figure serves also as a "table of contents" to this review, where sections describing the relevant blocks are indicated in the figure. At the top, the *ab initio* engines (grey block) generate the data that is transferred to a Wannier engine (blue block), that might implement also advanced methods discussed in Sec. II.D. Once WFs are obtained, they are typically used to generate a TB model and perform interpolation of the Hamiltonian and other operators (orange block). Such interpolated quantities are used for a number of different applications; the ones that are discussed in more detail in this review are indicated in the green blocks. As schematically indicated by the outer dotted rectangle, all these codes forming the Wannier ecosystem may be automated with workflow tools, which also coordinate data transfer between them.

between cell-periodic Bloch eigenstates $|u_{n\mathbf{k}}\rangle$ at neighboring points on a regular grid in the BZ (the **b** vectors connect one k-point to its neighbors on a regular discrete grid); in the limit of very dense meshes the **b** vectors tend to zero and the gradient in **k** is recovered. This finite-difference construction remains valid even in the case of Γ -sampling, where the neighboring **k**-points are given by the primitive reciprocal lattice vectors **G**, with the Bloch orbitals differing just by phase factors $\exp(i\mathbf{G} \cdot \mathbf{r})$. Now, we note that the gradient in **k** of a function $f(\mathbf{k})$ can be written as

$$\nabla f(\mathbf{k}) = \sum_{\mathbf{b}} w_b \, \mathbf{b} \left[f(\mathbf{k} + \mathbf{b}) - f(\mathbf{k}) \right] + \mathcal{O}(b^2)$$
 (9)

using stars ("shells") of neighboring **k**-points, where each shell has a weight w_b (see Appendix B in Marzari and Vanderbilt, 1997 and Mostofi et al., 2008 for a detailed description); this is easily proven taking a linear function $f(\mathbf{k}) = f_0 + \mathbf{g} \cdot \mathbf{k}$, where the exact result $\nabla_{\alpha} f(\mathbf{k}) = g_{\alpha}$ is recovered. In the simple case of cubic Bravais lattices, the first shell of reciprocal-space nearest neighbors (6, 8 or 12 for Bravais lattices in direct space that are simple cubic, FCC, or BCC) is sufficient; the general case where several shells need to be chosen automatically is detailed in Mostofi et al. (2008). While the procedure is automated, for unusual cases (e.g., very elongated cells) it might be convenient to find manually the most symmetric choice of shells (Posternak et al., 2002). With these

definitions, the diagonal matrix elements of the position operator can be evaluated by finite differences as

$$\langle \mathbf{0}i|\mathbf{r}|\mathbf{0}i\rangle = -\frac{1}{N}\sum_{\mathbf{k},\mathbf{b}} w_b \,\mathbf{b} \,\mathrm{Im} \,\ln M_{ii}^{(\mathbf{k},\mathbf{b})},$$
 (10)

where N is the number of k-points of the reciprocal-space grid. More complex expressions for the second derivatives and for the entire spread functional can then be obtained; among many alternatives (all correct to leading order in b), the choices made in Marzari and Vanderbilt (1997) transform correctly under a transformation that shifts $|\mathbf{R}i\rangle$ by a lattice vector. We also note that when using such finite-difference formalism, the spread functional converges slowly (polynomially) with reciprocal-space sampling, and hence some care must be paid in comparing its actual values in case of calculations performed with different discrete samplings.

Importantly, the finite-differences construction is particularly convenient for constructing MLWFs in a code-agnostic form, as the only input needed from the original first-principles calculation is encoded in the overlap matrices $M_{ij}^{(\mathbf{k},\mathbf{b})}$. Thus, once the $M_{ij}^{(\mathbf{k},\mathbf{b})}$ have been calculated, no further interaction is necessary with the electronic-structure code that calculated the ground state wavefunctions, making the entire Wannierization procedure a code-independent post-processing step (see, e.g., Ferretti et al., 2007 for the extension to ultrasoft pseudopotentials and the projector-augmented wave method,

and Freimuth et al., 2008; Kune et al., 2010; and Posternak et al., 2002 for the full-potential linearized augmented planewave method). As regards the disentanglement procedure, note that because of energy windows the needed input from the first-principles calculation includes the energy eigenvalues $\varepsilon_{n\mathbf{k}}$ in addition to the overlap matrices Eq. (8).

2. Accuracy and convergence

While the main focus of this review is on the powerful applications of WFs, their successful use relies on the Wannierization process being done correctly: in the following, we briefly comment on fundamental tests and established procedures to assess and improve the quality of WFs.

Two major convergence parameters control the quality (and the cost) of the Wannierization procedure: the spread minimization and the k-point grid used to obtain the initial Hamiltonian eigenstates (e.g., the cell-periodic part of Bloch states, if working with PBCs).

The spread minimization is generally performed with a steepest-descent algorithm until results do not change within a certain tolerance. While the iterative algorithm is in general robust, the minimization can become trapped in local minima. The strategy to avoid that is to select a very good starting point: if the initial spread is sufficiently close to the absolute minimum, it is more likely to reach it by following the local gradient. Hence, particular care needs to be paid to select good projection functions to obtain the initial unitary matrix of Eq. (5b), to be then iteratively optimized. In absence of chemical intuition, a common strategy is to calculate a projected density of states on the pseudoatomic orbitals and identify the orbital character in the energy region of interest: the atomic orbitals which project more on the relevant bands can be used as initial projection. Note that ML-WFs are often not atom-centered, and atomic orbitals are not always good starting projections, as it the case of the valence bands of monolayer MoS₂ (Gibertini et al., 2014). In Sections II.D and III.J we cover advanced methods to automate the selection of the starting point for the minimization procedure.

The spread functional measures the degree of localization in real space and, to some extent, the efficiency of the interpolation: more localized WFs decay faster in real space, hence they require a smaller Born–von Kármán (BvK) supercell to include all non-vanishing matrix elements of the Hamiltonian and the other operators, which in turn allows adopting coarser k-point grids in the starting electronic-structure simulation that is performed in reciprocal space. Indeed, the accuracy of band interpolation can be considered a proxy for the quality of the underlying WFs not only as regards k-point convergence: especially in the case of entangled bands (see Sec. II.A.2),

poor interpolation might signal problems in the disentanglement procedure. In addition, it is worth to emphasize that in general the Wannierization procedure is not forced to preserve symmetries (unless dedicated methods designed to do so are employed, see Sec. II.D). Hence, the spurious splitting of symmetry-protected degeneracies in the interpolated band structure might signal convergence problems related to the minimization, to the k-point convergence or to the choice of projection functions. This holds true not only for crystalline symmetries, but also for time-reversal symmetry, which is particularly relevant in non-collinear simulations of non-magnetic materials in presence of spin-orbit coupling (e.g., topological insulators).

Among other indicators of the quality of WFs we mention the ratio between their imaginary (Im) and real (Re) part: for isolated bands (and not considering spin-orbit coupling), MLWFs at the global minimum should be real functions (Marzari and Vanderbilt, 1997). Note that the calculation of the Im/Re part, and anything related to WFs themselves and their visualization, requires to have access to the full Bloch orbitals, not just the overlap matrices. It is also important to emphasize that different quantities derived from WFs—such as the WF spread and centers, as well as unitary matrices $\tilde{V}_{\mathbf{k}}$, $U_{\mathbf{k}}$ —converge in general with different speeds, also depending on the specific formulation adopted (Stengel and Spaldin, 2006).

Finally, we remark that many of the complications related to producing WFs for periodic solids are related to construction of a smooth gauge across the BZ. Hence, supercell Wannierizations with Γ -only sampling are typically more straightforward and less prone to be trapped in local minima. The challenge there is more on algorithmic efficiency due the large size of the systems involved; a number of Γ -only dedicated methods have been developed (Gygi et al., 2003; Silvestrelli, 1999).

D. Advanced minimization methods, and beyond maximally-localized Wannier functions

As discussed in section II, there is in principle large freedom in choosing the recipe to obtain well-localized WFs. Not only one can replace the MV spread functional with other cost functions, but also different minimization procedures and their starting points can be chosen, hence affecting the resulting WFs and their localization properties. Over the years, a number of methods have been developed to address all these different aspects of the Wannierization procedure. It is worth emphasizing that for many of these methods, the initial guess already provides well-localized WFs, so that an iterative minimization can in principle be avoided. The unitary matrices $U_{\mathbf{k}}$ of these "projection-only" WFs are set directly by the initial projection functions. While this choice cannot guarantee optimal localization properties, it has the ad-

vantage of enforcing some degree of symmetry induced by the choice of atomic orbitals used as projection functions. However, in all these cases it is possible—and in some cases even recommended—to minimize the MV spread or some other functional as a final step.

The prime decision deals with the functional that is to be minimized in order to determine the unitary matrices of Eq. (5). The most popular choice is the MV MLWF procedure (Marzari and Vanderbilt, 1997) for composite bands (see Sec. II.A.1) and the SMV disentanglement scheme for entangled bands (Souza et al., 2001) (see Sec. II.A.2). The minimization of the spread functional leads to very well localized WFs, hence reducing the size of the BvK supercell needed to represent operators (e.g., the Hamiltonian) in a WF basis. While MLWFs and disentanglement represent the most convenient choice in the vast majority of applications, substantial work has been done to augment the MLWF scheme or develop alternatives which satisfy the needs of specific applications.

The MLWF procedure leads to optimal real-space localization, but is not guaranteed to yield orbitals that preserve desirable crystal symmetries. This is only partially relieved using symmetric initial projections, as typically obtained by a proper selection of atomic-like orbitals (we further discuss initial projections later on in this section). Symmetry-preserving WFs are appealing in providing the correct orbital or site symmetries for many-body approaches like dynamical meanfield theory (DMFT). Hence, it is not surprising that several non-MLWF procedures directly or indirectly include crystal symmetries in the functional to minimize. In the symmetry-adapted Wannier function (SAWF) method (Sakuma, 2013), symmetric WFs are obtained through additional constraints on the unitary matrices $U_{\mathbf{k}}$ which are based on symmetry operations of the sitesymmetry group. The SAWF method is fully compatible with the maximal-localization procedure and the SMV disentanglement (and has also been recently extended to the case where a frozen window is used (Koretsune, 2023)), although the additional constraints imply a possibly larger total spread, even if some individual WFs can actually be more localized than in the MLWF procedure. Currently, the implementation of the SAWF method in the code Wannier90 (more about software in Sec. III.A) is interfaced with the Quantum ESPRESSO distribution and. if the site-symmetry group is equivalent to the full space group of the crystal, then symmetry operations can be calculated directly by the interface code. Otherwise, if the site-symmetry group contains fewer operations than the full space group, then symmetry operations can be provided by an external file. We note that it is also necessary to specify the site location and orbital symmetry of the SAWFs through the projection functions.

While the SAWF method provides a rigorous way to include symmetries in the maximal-localization procedure, it requires quite some prior knowledge of the electronic

structure of the material under study. An alternative and simpler approach is to construct selectively-localized Wannier functions (SLWFs), where the MLWF procedure is applied only to a subset of the entire WFs considered (Wang et al., 2014). In addition, some WF centers can be constrained (SLWF+C) to specific positions by adding a quadratic penalty term to the spread functional. While the SLWF+C approach does not enforce symmetries, it has been observed that the resulting WFs typically exhibit the site symmetries corresponding to the constrained centers (Wang et al., 2014). The SLWF+C can be used in the case of entangled bands, where the SMV disentanglement step is performed as usual, while the selective localization and constrained centers are applied only to the final Wannierization step. A more indepth review of the SAWF and SLWF+C methods, including their implementation and usage in Wannier90, can be found in Pizzi et al. (2020).

The localization and possibly the symmetry can crucially depend on the number of WFs considered in a given energy range. The so-called partly occupied Wannier functions (POWFs) (Thygesen et al., 2005) formalize this observation by including the relevant unoccupied states which lead to the minimal spread functional, essentially implementing a bonding-antibonding closing procedure. POWFs can have a high degree of symmetry, while the bonding-antibonding criterion has been shown to correspond to the condition of maximal average localization (Thygesen et al., 2005). Notably, in the POWF scheme the total spread functional $\Omega = \Omega_I + \tilde{\Omega}$ is minimized at once, at variance with the SMV scheme where first the gauge-invariant part Ω_I is minimized through the disentanglement step, and only after the gaugedependent part Ω is minimized through the usual MV scheme. The iterative minimization of the total spread Ω has been further developed by Damle, Levitt and Lin in Damle et al. (2019). They reformulated the Wannierization, which is a constrained non-linear optimization problem, as unconstrained optimization on matrix manifolds, where the SMV disentanglement procedure can be interpreted as a splitting method which represents an approximate solution.

We stress that even if minimization of the full the spread functional Ω guarantees the highest degree of overall localization, several of the methods discussed here can actually produce WFs such that a subset of them might individually be more localized than their maximally-localized counterparts. Along those lines, Fontana et al. developed the spread-balanced WFs (Fontana et al., 2021), where they added a penalty term to the spread functional, proportional to the variance of the spread distribution among all WFs of the system. This scheme could be less prone to produce solutions with one or several poorly localized WFs, at the price of an increased total spread for the whole set. The addition of terms to the spread functional can also be used to pre-

serve some degree of locality in energy, such as in the case of mixed Wannier-Bloch functions (Giustino and Pasquarello, 2006) and dually localized Wannier functions (Mahler et al., 2022). These approaches are based on a generalized spread functional (Gygi et al., 2003) designed to carry both spatial localization (Wannier character) and limited spectral broadening (Bloch character), by minimizing a functional that contains not only a spatial variance (as for MLWF) but also an energy variance.

Once a choice for the functional to be minimized is made (the total spread as in the MLWF scheme, or any other choice), there is still a lot of flexibility on the choice of algorithm to perform the minimization. First, one needs to define a starting guess for the unitary matrices $U_{\mathbf{k}}$, which is customarily obtained by specifying a set of localized projection functions. While for composite bands a set of randomly centered spherically-symmetric Gaussian orbitals might work, in general more sophisticated choices are required. Typically, atomic orbitals are used as projection functions, such as s, p, d-orbitals as well as hybrid orbitals (e.g., sp^3), which are often centered either on atoms or along bond directions. As discussed in Sec. II.C.2, the choice of the right atomic orbitals is typically based on chemical intuition and can be partly informed by inspecting the projected density of states in the energy region of interest. Still, the choice of the right projection orbitals—i.e., those providing a good starting point for a successful minimization of the target functional—can often be a non-trivial task, especially in the context of automated high-throughput materials screening and, more generally, when one wants to study a novel material never investigated before (especially in case of unfamiliar orbital composition). Hence, in the last decade substantial efforts have been targeted at developing automated algorithms removing the need for users to define appropriate initial projections. A first approach in this direction is the optimized projection functions (OPFs) method (Mustafa et al., 2015) for composite bands. In OPF, a larger set of functions that overspan the space of MLWFs is built and used as a starting point. While in plane-wave codes the OPF approach (Mustafa et al., 2015) still needs the user to provide a list of initial projections, for instance atomic-like local orbitals (LOs). ab initio codes operating with localized (or mixed planewave/localized) basis sets can leverage the built-in localized orbitals. For instance, the full-potential linearized augmented-plane wave (LAPW) method can be extended by adding the so-called LOs, which are atomic-like, very localized, and can be employed in the construction of WFs. Tillack et al. (2020) combined the SMV disentanglement with the OPF method (Mustafa et al., 2015) to construct initial guesses for MLWFs from a set of LOs in an automated way. Finally, another set of parameters that require tuning in the standard SMV disentanglement scheme are the inner and outer energy windows. Gresch et al. (2018) targeted the removal of the need for

manual input by focusing on the automated optimization of both windows.

On the algorithmic side, in the quest for fully automating the generation of localized WFs, various general and practical approaches have been recently proposed, targeting the construction of well-localized WFs using algorithms that are often non-iterative; this not only makes them more automatable, but also provides an excellent starting point for a final Wannierization, if required: the SCDM approach (Damle and Lin, 2018; Damle et al., 2015, 2017), the continuous Bloch gauges (Cancès et al., 2017; Gontier et al., 2019), and the projectability disentanglement and manifold remixing approaches (Qiao et al., 2023a,b).

SCDM is based on QR factorization with column pivoting (QRCP) of the reduced single-particle density matrix. The approach can be used either to produce well-localized WFs without performing an iterative minimization, or it can be considered a linear-algebra method to identify a good starting point for a MLWF procedure. The SCDM method is implemented (Vitale et al., 2020) in the interface code to Quantum ESPRESSO, with an algorithm for the QRCP factorization that works on a smaller matrix instead of the full density matrix (Damle and Lin, 2018; Damle et al., 2015, 2017). For a set of composite bands, SCDM is parameter-free. A comprehensive study on 81 insulators (Vitale et al., 2020) has shown how the MLWF procedure applied to SCDM initial projections (SCDM+MLWF) improves the interpolation accuracy and localization of the resulting WFs, although SCDM-only WFs perform already remarkably well, both in terms of accuracy of band structure interpolation and in terms of localization. In the case of entangled bands, SCDM requires to specify an energy-window function, its center and width, as well as the number of WFs to consider. Vitale et al. (2020) introduced a recipe to automatically select those parameters (more details in Sec. III.J), which was tested on 200 bulk materials. Unlike in the case of isolated groups of bands, for entangled bands the SCDM+MLWF method greatly improved the localization of the WFs with respect to SCDM-only. Notably, however, the reduced spread induced by the MV procedure might result in lower band-interpolation accuracy. Although the SCDM projections could be used together with the SMV disentanglement scheme, this more complex procedure does not provide systematic gain in accuracy, such that a SCDM-only or SCDM+MLWF (with MV minimization for $\tilde{\Omega}$) is recommended (Vitale *et al.*, 2020). In addition, we note that SCDM requires realspace wavefunctions as input, and therefore has a higher computational and memory cost with respect to other methods discussed later in this section, which are implemented in reciprocal space.

Another non-iterative approach for composite bands is based on ensuring a continuous Bloch gauge over the entire BZ (Cancès *et al.*, 2017; Gontier *et al.*, 2019), re-

sulting in good localization properties of the WFs and not requiring any chemical intuition for their construction. The main idea is that one can construct a sequence of gauge matrices that are not only continuous across the BZ but also satisfy its periodicity at the BZ edges. This is achieved by first adopting parallel transport for the gauge matrix, starting from a chosen k-point (usually the Γ point) and propagating along a line (e.g. the k_x line). This allows to fix the periodicity at the two end points of the line, while preserving the continuity. Then, for each k-point on the line, parallel transport is applied to each of the gauge matrices along an orthogonal direction (e.g. in the k_y direction), and all gauge matrices are fixed again at the endpoints, to ensure periodicity of the 2D plane. Finally, for each k-point on the 2D plane, one can apply a similar procedure to construct gauge matrices along the third direction, therefore obtaining a global continuous gauge across the full BZ. Often, the resulting gauge is continuous but not smooth enough: a subsequent conventional MV iterative minimization can improve the localization and reach the MLWF gauge. Such algorithm is able to construct MLWFs for difficult cases such as \mathbb{Z}_2 topological insulators (Gontier *et al.*, 2019).

Lastly, a very robust approach has emerged in the form of projectability disentanglement (Qiao et al., 2023b), where the inner and outer energy windows are replaced by projectability thresholds. For each state $|u_{n\mathbf{k}}\rangle$, a projectability (Agapito et al., 2013; Vitale et al., 2020) onto localized atomic orbitals (typically, those coming from the pseudopotentials) is calculated. states that have very high projectability are retained identically (exactly as done for states inside the inner frozen window in the SMV method); states that have low projectability are discarded altogether (since they do not provide useful contributions to MLWFs); and states that span the intermediate projectability values are treated with the standard SMV disentanglement. This approach leads naturally and robustly to atomic-like projectability-disentangled Wannier functions (PDWFs), spanning both occupied and unoccupied states corresponding to Bloch sums of bonding/anti-bonding combinations of atomic orbitals.

These PDWFs can in turn be remixed into linear combinations that aim to describe target submanifolds; e.g., the valence states only, the conduction states only, or certain groups of bands that are separated in energy from the rest. This may be beneficial for finding optimal target states for beyond-DFT methods (see Sec. III.H).

This remixing is particularly valuable for Koopmans functionals (see Sec. III.H.2), which require separate sets of MLWFs for the valence and conduction manifolds, or for transport calculations. For this purpose, the manifold-remixed Wannier functions (MRWFs) (Qiao et al., 2023a) are obtained by starting from the PDWFs spanning the whole manifold (valence plus conduction), which is then split by rotating the gauge matrices into

a block-diagonal structure across all the k-points, while simultaneously maintaining the gauge smoothness for each block. This is achieved by a combination of automated Wannierization of the whole manifold, diagonalization of the Wannier Hamiltonian, parallel transport, and maximal localization. The automated Wannierization of the whole manifold can be obtained using the PDWF method; the Hamiltonian diagonalization splits the manifold into desired submanifolds (e.g., two for valence and conduction, respectively); the parallel transport fixes the gauge randomness to construct two sets of localized WFs; the final maximal localization smoothens the gauge, leading to subsets of MLWFs for the respective submanifolds. Qiao et al. (2023a) demonstrates that, when combined with PDWFs, the MRWF method can be fully automated, and can also be extended to other types of band manifolds gapped in energy, such as the single top valence band of MoS₂, or the 3d and t_{2q}/e_q submanifolds of SrVO₃. For high-throughput results of PDWF and MRWF, see Sec. III.J.

III. The Wannier ecosystem: theory and software packages

A. Development of widely-available Wannier engines

The MV and SMV methods described in Marzari and Vanderbilt (1997) and Souza et al. (2001) were originally implemented in Fortran 77. The code would compute the overlaps in Eq. (8) and the projection of the periodic part of the Bloch orbitals onto trial localized states, by reading the former evaluated on a regular k-point grid by a DFT code—originally by an early version of CASTEP (Clark et al., 2005; Marzari et al., 1997). To provide a more general model, driven by the need to interface with a DFT code based on the LAPW method (Posternak et al., 2002), the choice was made to keep the calculation of all the scalar products involving Bloch orbitals needed by the Wannier code within the electronic-structure code of choice, typically as a postprocessing step, and to establish well-defined protocols to exchange this information writing/reading files to/from disk; the format of those files was defined in the accompanying documentation, and the Wannier77 code was released under a GPL v2 license in March 2004.

In 2005, two of the current authors (AAM and JRY), then working in the groups of NM and IS respectively, rewrote the routines using modern modular Fortran, relying on their experience of software development gained from working on the ONETEP (Prentice et al., 2020) and CASTEP (Clark et al., 2005) DFT programs. The resulting program, Wannier90 (Mostofi et al., 2008), was released under a GPL license in April 2006. Following the early layout in the Wannier77 code, Wannier90 was designed to be easily interfaced to any electronic structure code, irrespective of its underlying basis set. The first release

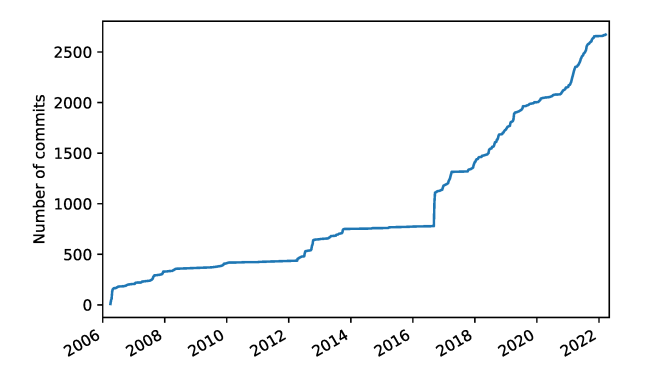


FIG. 3 Total number of commits over time for the Wannier90 repository (CVS until August 2016, then transferred to Git and hosted on GitHub). Note the significant increase during and right after the community developer workshop in September 2016.

of Wannier90 came with extensive documentation, tutorials, and two validation tests. Development used CVS as a version control system. GP joined the development effort in 2012, and a new parallel post-processing code (postw90) was developed and released in Wannier90 version 2 (Mostofi et al., 2014) in October 2013.

While the development of Wannier90 as an opensource interoperable code was innovative in 2006, by 2016 it was clear that the development tools being used did not make use of what was then considered best practice. For example, having only a few developers with access to the main repository presented a barrier to adding new functionality to the program. A decision was made to move to a community development model, and the Wannier90 repository was migrated to GitHub with the adoption of a "fork and pull request" approach. This new model was launched with a community developer workshop held in San Sebastián in September of 2016. This event is clearly recognizable in Fig. 3, which shows the number of commits to the code repository over time, with a large number of commits contributed during (or right after) the 2016 event. Moreover, once the code made its transition to a community development model, the rate of commits significantly increased, as well as the number of individual contributors (over 35 different people contributed code, tests or documentation via commits by the end of 2022). Essential to this change was the development of an extensive suite of tests, which runs automatically to validate every pull request. In 2019, Wannier90 version 3 was released, including all community contributions to the code (Pizzi et al., 2020).

In addition to Wannier90, there are a few electronic structure software packages that nowadays implement internal functionality for computing WFs in periodic systems. These include GPAW (Enkovaara

et al., 2010), QBOX (Gygi, 2008), CP2K (Kühne et al., 2020), exciting (Tillack et al., 2020), OpenMX (Weng et al., 2009), RESPACK (Nakamura et al., 2021) and CRYSTAL (Zicovich-Wilson et al., 2001). However, in this review we want to use the term "Wannier engines" to describe software packages that generate WFs and are designed to be used interoperably with other software packages: e.g., with the electronic structure codes for solving the electronic ground state, used as input to a Wannier engine, and with post-processing codes that use the WFs from a Wannier engine to calculate advanced electronic properties. Wannier90 is clearly an example of a Wannier engine, but it is not the only readilyavailable one—another notable example is the Atomic Simulation Environment (ASE) (Larsen et al., 2017), which also implements routines based on the minimization of the quadratic spread of the WFs, but uses a different approach (Fontana et al., 2021; Thygesen et al., 2005) to that described above (see also Sec. II.D). In addition, the recent Wannier.jl package (Qiao et al., 2023d) implements several Wannierization algorithms using manifold optimization techniques, and brings the methodology of WFs to the Julia (Bezanson et al., 2017) community. In this review, we focus on those codes that interface to the Wannier90 code; nevertheless, we note that often the other Wannier engines have adopted the same file formats first defined by Wannier77/Wannier90 (see discussion in Sec. III.B), thus being fully compatible with the ecosystem.

B. The concept of a Wannier-functions software ecosystem

Complex software can adopt a variety of architecture design approaches, often differing substantially in the level of modularity (or lack thereof) of their components. Historically, most computer programs started as monolithic applications: self-contained and independent codes made of tightly coupled functions. This is a natural choice when writing new software from scratch, and it reduces the installation burden for users, who do not need to deal with the management of many dependencies. Over time, however, features and postprocessing tools tend to get added, making the codebase very large and complex. This results in serious challenges for development and maintenance, which become critical when the code needs to be adapted and optimized for newer hardware architectures. Furthermore, this leads to reimplementation of common routines in each code, which could instead be written and optimized only once, and then used as a library. The library approach is already common in the electronicstructure community for linear-algebra and diagonalization routines, where the code calls functions via standard interfaces defined by the BLAS (Blackford et al., 2002) and LAPACK (Anderson et al., 1999) libraries,

and the executables are linked to performance-optimized versions on high-performance computing (HPC) clusters. While a similar approach is often used for other low-level routines, such as fast-Fourier-transform (FFT) computation (Frigo and Johnson, 2005) or to support file formats such as netCDF (Rew and Davis, 1990) or HDF5 (The HDF Group, 2023), it was until recently far less common for higher-level materials-science-oriented routines.

To address the challenges of monolithic codes, many electronic structure codes are being redesigned or rewritten using a more modular approach, where core modules are—when possible—generalized and separated into a library of reusable routines, then called by higher-level functions to execute complex tasks. Some of these codes have evolved into distributions, i.e., a set of relatively independent but interoperable executables reusing common core routines. However, even with this approach, the different modules can often operate only within the distribution, and the development of all modules needs to be constantly in sync.

Ultimate interoperability is obtained when code (such as core routines or full functionality) is reused by different independent software distributions, maintained by non-overlapping developer groups. A crucial challenge to enable such a level of interoperability is to design a clear application programming interface (API) defining which data needs to be transferred between codes, and in which format. This requires discussions and coordination, which can be catalyzed via targeted coordination efforts; an example worth mentioning is the CECAM Electronic Structure Library project (CECAM-ESL, 2023). At an even higher level, one can address code interoperability by defining common interfaces (e.g., input/output schemes) for workflows computing a quantity of interest, independent of the underlying simulation code, such as the common workflow interface of Huber et al. (2021) to perform crystal-structure relaxation and to compute equations of state. The workflow only requires as input, in a common format, the crystal structure and a few basic input parameters, and is then interfaced with 11 different DFT codes to run the actual simulations. Such universal interfaces make workflows accessible to a broader audience and codes fully interoperable, allowing researchers to switch between them without the need to learn from scratch the details of each one. In addition, they can be seamlessly applied to perform cross-code verification studies (Bosoni et al., 2023).

When codes have to exchange data, the interfaces between them can be actual code APIs (e.g., in C or Fortran), where the library is directly compiled and linked with the main code, but also simply files in a well-documented format, written by the first application and read by the second one (see also later discussion of this approach in Sec. III.I). The actual choice depends on the interdependency between the algorithmic steps and on performance considerations. The use of files is typically

favored when the corresponding simulation workflows imply a sequential execution of codes rather than interconnected loops between them, when the exchanged data is small (up to few GB), and when the individual steps are computationally demanding, so that I/O overhead is only a small fraction of the total execution time. (In a few advanced cases, other interfaces such as network sockets have been used to keep the applications decoupled while still reducing the I/O overhead for simulations that are not very computationally demanding (Kapil et al., 2019).) In addition, by writing intermediate results to files, the steps do not need to be combined in the same run, but can be executed at differed points in time (e.g., days later) or by different researchers.

In this context, WFs represent a remarkable and elegant method to decouple the ab initio simulation of the electronic structure from the calculation of the physical properties. This is possible thanks to two core aspects of WFs. First, WFs are independent of the basis set used in the first-principles electronic structure code: the MLWF algorithm requires the sole knowledge of a handful of vectors and matrices, such as the overlap matrices on a coarse grid of k points. Wavefunctions, typically stored in very large files, are not required during Wannierization, but only used optionally in few post-processing steps, e.g., when representing the WFs on a real-space grid. Second, many physical quantities can be obtained efficiently once a WF basis is constructed, only with the knowledge of relevant operators represented as small matrices directly in the Wannier basis, such as the Hamiltonian or the position operator. Indeed, while extended basis sets such as plane waves are particularly convenient to obtain charge densities and wavefunctions of periodic systems, reciprocal space integrals can be more efficiently calculated using a Fourier-interpolated basis set, originating from a compact maximally-localized representation in real space. From a computer-science perspective, we can say that these two aspects of the Wannierization process make it an effective data-compression encoding, avoiding the need to transfer large wavefunctions between the ab initio codes and the property calculators, while retaining an equivalent level of accuracy.

Thanks to the first aspect, i.e., basis-set independence, the Wannier code (Marzari and Vanderbilt, 1997) evolved from being a standalone code focused on the minimization procedure to one with a well-defined format for the input data (overlap and projection matrices), which also defined and documented the corresponding files (e.g., for the overlap matrices in .mmn format and the projection matrices in .amn format). The calculation of the latter was delegated to specific interfaces implemented within the corresponding first-principles packages (Posternak et al., 2002). This design persisted in the Wannier90 code (Mostofi et al., 2008; Pizzi et al., 2020) and as a result the Wannier90 engine can now be interfaced with virtually any electronic-structure code as already dis-

cussed in Sec. III.A, with interfaces currently available for many widespread codes, including ABINIT (Gonze et al., 2020), BigDFT (Ratcliff et al., 2020), Elk (Elk, 2023), FLEUR (Wortmann et al., 2023), GPAW (Enkovaara et al., 2010), Octopus (Tancogne-Dejean et al., 2020), OpenMX (Ozaki and Kino, 2005), pySCF (Sun et al., 2018, 2020), Quantum ESPRESSO (Giannozzi et al., 2017, 2009), SIESTA (Soler et al., 2002), VASP (Kresse and Joubert, 1999) and WIEN2k (Blaha et al., 2020).

Because of the second aspect, i.e., the possibility of efficiently obtaining many physical quantities in the Wannier basis, Wannier90 started to include a large number of efficient post-processing utilities for materials properties, ranging from simple band-structure interpolation to more complex properties such as the ordinary and anomalous Hall conductivities, Seebeck coefficients, orbital magnetization, and many more (Pizzi et al., 2020). However, in the last decade the community has spontaneously moved towards a decentralized software ecosystem (as opposed to a centralized, albeit modular, Wannier distribution), where different packages interact through APIs and a common data format. The decentralized model was again facilitated by a clear and documented interface to generate data as input to the next steps (e.g., the _tb.dat file containing the full TB model: WF centers, on-site energies, and hopping energies). The community has been rapidly growing, and several independent packages exploiting MLWFs exist nowadays, targeting diverse properties such as TB models (Sec. III.C), ballistic transport (Sec. III.D), Berryphase related properties (Sec. III.E), topological invariants (Sec. III.F), electron-phonon coupling (Sec. III.G), beyond-DFT methods (Sec. III.H), high-throughput calculations (Sec. III.J), and more.

This review article formalizes the existence of such a community of symbiotic packages, forming a research and software ecosystem built upon the concept of MLWFs. We illustrate this schematically in Fig. 2.

C. Wannier interpolation and tight-binding models

A very common application of WFs is to evaluate various k-space quantities and BZ integrals by "Wannier interpolation". This name has come to refer to a type of Slater–Koster interpolation where the needed on-site and hopping integrals are calculated explicitly in the WF basis (Calzolari et al., 2004; Lee et al., 2005; Souza et al., 2001; Yates et al., 2007), as opposed to being treated as fitting parameters as done in empirical TB theory. Here we review the basic procedure as it applies to energy bands and other simple quantities, leaving more sophisticated applications to later sections. Before proceeding, let us mention that the Wannier interpolation scheme has been adapted to work with non-orthogonal localized orbitals instead of (orthogonal) WFs (Buongiorno Nardelli

et al., 2018; Jin et al., 2021; Lee et al., 2018; Wang et al., 2019a).

1. Band interpolation

To interpolate the band structure, one needs the matrix elements of the KS Hamiltonian in the WF basis,

$$H_{ij}^{W}(\mathbf{R}) = \langle \mathbf{0}i|\hat{H}|\mathbf{R}j\rangle;$$
 (11)

here $H_{ii}(\mathbf{0})$ are on-site energies, and the remaining matrix elements are hoppings. One way to evaluate these matrix elements is to start from Eq. (5a) for the WFs in terms of the KS Bloch eigenstates on the *ab initio* k-grid. Inserting that expression in Eq. (11) gives

$$H_{ij}^{W}(\mathbf{R}) = \frac{1}{N} \sum_{\mathbf{k}} e^{-i\mathbf{k} \cdot \mathbf{R}} \sum_{n=1}^{\mathcal{J}_{\mathbf{k}}} V_{\mathbf{k},ni}^* \varepsilon_{n\mathbf{k}} V_{\mathbf{k},nj}.$$
 (12)

This procedure is particularly convenient in the framework of the MV and SMV Wannierization schemes, which are formulated as post-processing steps after a conventional *ab initio* calculation is carried out on a uniform $\{\mathbf{k}\}$ grid; Eq. (12) only involves the $V_{\mathbf{k}}$ matrices generated by the Wannier engine starting from the *ab initio* overlap matrices and energy eigenvalues (see Sec. II.A), and the energy eigenvalues themselves. An alternative to Eq. (12) would be to express the WFs in a real-space basis, e.g., localized orbitals or a grid, and then evaluate Eq. (11) directly on that basis.

In view of the localized character of the WFs, $|H_{ij}^{W}(\mathbf{R})|$ is expected to become negligibly small when the distance $|\mathbf{R} + \boldsymbol{\tau}_i - \boldsymbol{\tau}_i|$ between the centers of the two WFs becomes sufficiently large (here, $\tau_i = \langle \mathbf{0}j | \hat{\mathbf{r}} | \mathbf{0}j \rangle$). However, due to the finite size N of the ab initio grid, the WFs obtained from Eq. (5a) are actually periodic over a realspace supercell of volume NV_{cell} ; accordingly, the matrix elements given by Eq. (12) are also supercell-periodic: $H^{\mathrm{W}}_{ij}(\mathbf{R}+\mathbf{T})=H^{\mathrm{W}}_{ij}(\mathbf{R})$, for any supercell lattice vector \mathbf{T} . To minimize spurious effects associated with this artificial periodicity, the hopping matrix should be truncated by setting $H_{ij}^{W}(\mathbf{R}) = 0$ whenever the vector $\mathbf{R} + \mathbf{T} + \boldsymbol{\tau}_{j}$ lies outside the Wigner-Seitz (WS) supercell centered at the origin. Provided that this supercell is sufficiently large to ensure negligible overlap between a WF and its periodic images, the truncation error will be insignificant. This means that in practice one can achieve well-converged numerical results with a relatively coarse ab initio grid. Note, however, that the matrix elements do not decay exactly to zero for finite-size WS supercells. Therefore, when multiple R vectors lie on the boundary of the WS supercell and are connected by a supercell vector T, it is better to consider all these equivalent vectors with appropriate weights, rather than picking only one of them, which would introduce spurious symmetry breaking in the Hamiltonian. The details of this approach and its

implementation in Wannier90 are discussed in Sec. 4.2 of Pizzi *et al.* (2020).

Once the on-site energies and hoppings have been tabulated, the Hamiltonian matrix is interpolated onto an arbitrary BZ point \mathbf{k}' by performing an inverse Fourier transform,

$$H_{\mathbf{k'},ij}^{\mathbf{W}} = \sum_{\mathbf{R}}^{\mathbf{WS}} \frac{1}{\mathcal{N}_{\mathbf{R},ij}} \sum_{l=1}^{\mathcal{N}_{\mathbf{R},ij}} e^{i\mathbf{k'}\cdot(\mathbf{R} + \mathbf{T}_{\mathbf{R},ij}^l)} H_{ij}^{\mathbf{W}}(\mathbf{R}). \quad (13)$$

The summation runs over the lattice vectors \mathbf{R} (which lie in the WS supercell centered at the origin. as discussed above) with $\mathcal{N}_{\mathbf{R}} > 1$ whenever $\mathbf{R} + \mathbf{T}_{\mathbf{R},ij}^l + \boldsymbol{\tau}_j$ falls on the boundary of the WS supercell centered at $\boldsymbol{\tau}_i$. To optimize the quality of the interpolation, for each combination of i, j, and \mathbf{R} the supercell lattice vector \mathbf{T} appearing in Eq. (13) is chosen as the one that minimizes $|\mathbf{R} + \mathbf{T} + \boldsymbol{\tau}_j - \boldsymbol{\tau}_i|$ (Pizzi *et al.*, 2020). Finally, the interpolated energy eigenvalues are obtained by diagonalizing the above matrix,

$$\left[\mathcal{U}_{\mathbf{k}'}^{\dagger} H_{\mathbf{k}'}^{W} \mathcal{U}_{\mathbf{k}'}\right]_{mn} = \delta_{mn} \varepsilon_{n\mathbf{k}'}^{H}, \qquad (14)$$

so that the column vectors of the unitary matrix $\mathcal{U}_{\mathbf{k}'}$ are eigenvectors of $H^{\mathrm{W}}_{\mathbf{k}'}$.

Since the interpolation steps (13) and (14) only involve Fourier transforming and diagonalizing $J \times J$ matrices that are typically small, the overall procedure tends to be much less expensive than a direct DFT calculation at every interpolation point, especially when a dense interpolation grid $\{\mathbf{k}'\}$ is needed. The efficient evaluation of the Hamiltonian matrix and band derivatives (see below) allows to explore BZ integration beyond the standard equispaced scheme when fine features in k-space need to be resolved using adaptive integration methods (Assmann et al., 2016; Kaye et al., 2023).

The above interpolation scheme has been shown to accurately reproduce—within the frozen energy window—the energy eigenvalues obtained by a direct DFT calculation. As an example, we show in Fig. 4 a detail of the interpolated band structure of ferromagnetic bodycentred cubic (BCC) Fe along the H- Γ line (Yates et al... 2007). The vertical gray lines indicate points on the $\{k\}$ mesh used for constructing the WFs. For comparison, we plot as plus symbols the ab initio dispersion around a weak spin-orbit-induced avoided crossing between two bands of opposite spin. It is apparent that the Wannier interpolation procedure succeeds in resolving details on a scale much smaller than the spacing between those points. In particular, the correct band connectivity is obtained, so that avoided crossings, no matter how weak, are not mistaken for actual crossings. This characteristic, which distinguishes Wannier interpolation from methods based on direct Fourier interpolation of the energy eigenvalues (Madsen et al., 2018; Madsen and Singh, 2006),

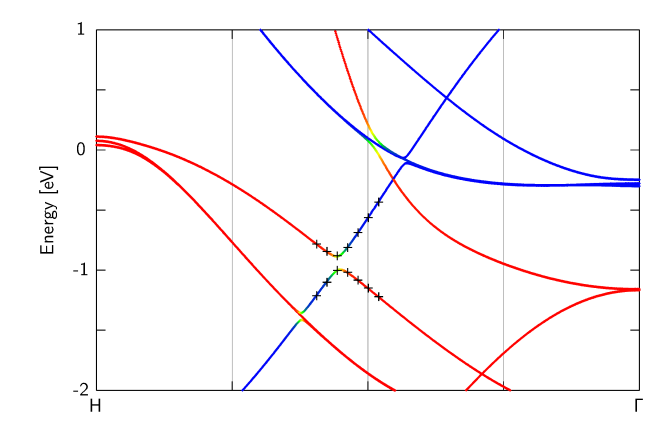


FIG. 4 Wannier-interpolated bands of BCC Fe along the H- Γ line. The bands are color-coded according to the value of the spin expectation value $\langle \psi_{nk} | \hat{S}_z | \psi_{nk} \rangle$: red for spin up, and blue for spin down. The energies are given in eV, and the Fermi level is at 0 eV. The vertical gray lines indicate k-points on the ab initio mesh used for constructing the WFs.

makes it a powerful tool for studying topological properties (Sec. III.F), and for evaluating BZ integrals involving quantities that change rapidly over small regions of k-space, such as the Berry curvature (Sec. III.E) and electron-phonon matrix elements (Sec. III.G).

Wannier interpolation works for the same reason that empirical TB does: the short range of the real-space Hamiltonian matrix (12) ensures that its Fourier transform (13) is a smooth function in reciprocal space. This can also be seen by writing the left-hand side of Eq. (13) as

$$H_{\mathbf{k}',ij}^{\mathbf{W}} = \langle \psi_{i\mathbf{k}'}^{\mathbf{W}} | \hat{H} | \psi_{j\mathbf{k}'}^{\mathbf{W}} \rangle, \qquad (15)$$

where

$$|\psi_{j\mathbf{k}'}^{\mathbf{W}}\rangle = \sum_{\mathbf{R}} e^{i\mathbf{k}'\cdot\mathbf{R}} |\mathbf{R}j\rangle$$
 (16)

interpolates the smooth Bloch functions defined on the ab initio grid by Eq. (5b). We may also write the left-hand side of Eq. (14) as

$$H_{\mathbf{k}',mn}^{\mathrm{H}} = \langle \psi_{m\mathbf{k}'}^{\mathrm{H}} | \hat{H} | \psi_{n\mathbf{k}'}^{\mathrm{H}} \rangle, \qquad (17)$$

where

$$|\psi_{n\mathbf{k'}}^{\mathrm{H}}\rangle = \sum_{j=1}^{J} |\psi_{j\mathbf{k'}}^{\mathrm{W}}\rangle \mathcal{U}_{\mathbf{k'},jn}$$
 (18)

describes a unitary transformation from the Wannier gauge W to the Hamiltonian gauge H. Inside the frozen energy window, the states $|\psi_{n\mathbf{k}'}^{\mathrm{H}}\rangle$ interpolate—up to arbitrary phase factors—the *ab initio* eigenstates $|\psi_{n\mathbf{k}}\rangle$.

In summary, performing Fourier interpolation in the W gauge followed by a unitary transformation to the H gauge allows interpolating quantities—band energies,

Bloch eigenstates, and matrix elements thereof (see below)—that can vary rapidly in k-space, and even become non-analytic at degeneracies. This strategy retains the accuracy of a full-blown ab initio calculation, while benefiting from the efficiency of Slater–Koster interpolation.

2. Band derivatives and Boltzmann transport

The interpolation procedure outlined above can be adapted to evaluate band velocities, inverse effectivemass tensors, and higher k-derivatives of the energy eigenvalues (Yates *et al.*, 2007); as in the empirical TB method (Graf and Vogl, 1995), this is achieved without relying on finite-difference methods, which become problematic in the vicinity of band crossings and weak avoided crossings, where the band ordering can change from one grid point to the next.

Band derivatives are needed, for instance, to evaluate transport coefficients such as the electrical conductivity σ , the Seebeck coefficient S, or the electronic contribution to the thermal conductivity K. Within the semiclassical Boltzmann transport equation (BTE) framework, one defines a scattering time $\tau_{n\mathbf{k}}$ for an electron on band n at wavevector \mathbf{k} (incidentally, the contributions from electron—phonon scattering to $\tau_{n\mathbf{k}}$ can be efficiently computed exploiting Wannier functions, see Sec. III.G). Then, the expressions for the transport tensors are given by (Ziman, 1972):

$$\sigma_{ab}(\mu, T) = e^2 \int_{-\infty}^{+\infty} dE \left(-\frac{\partial f(E, \mu, T)}{\partial E} \right) \Sigma_{ab}(E), \tag{19}$$

$$[\sigma S]_{ab}(\mu, T) = \frac{e}{T} \int_{-\infty}^{+\infty} dE \left(-\frac{\partial f(E, \mu, T)}{\partial E} \right) (E - \mu) \Sigma_{ab}(E), \tag{20}$$

$$K_{ab}(\mu, T) = \frac{1}{T} \int_{-\infty}^{+\infty} dE \left(-\frac{\partial f(E, \mu, T)}{\partial E} \right) (E - \mu)^2 \Sigma_{ab}(E), \tag{21}$$

where μ is the chemical potential, T is the temperature, a and b are Cartesian indices, σS denotes the matrix product of the two tensors, $\partial f/\partial E$ is the derivative of the Fermi–Dirac distribution function with respect to the energy, and $\Sigma_{ab}(E)$ is the transport distribution function. The latter is defined by

$$\Sigma_{ab}(E) = \frac{1}{V_{cell}} \sum_{n\mathbf{k}} v_{n\mathbf{k}}^a v_{n\mathbf{k}}^b \tau_{n\mathbf{k}} \delta(E - E_{n\mathbf{k}}), \qquad (22)$$

where the summation is over all bands n and over all the BZ, $\varepsilon_{n\mathbf{k}}$ is the energy for band n at \mathbf{k} and $v_{n\mathbf{k}}^a$ is the a component of the band velocity at (n, \mathbf{k}) .

Obtaining converged quantities for Eqs.(19)–(21), therefore, requires to compute the band derivatives $\mathbf{v}_{n\mathbf{k}}$ while sampling the BZ over dense k-point grids (Madsen and Singh, 2006; Schulz et al., 1992; Uehara and Tse, 2000), since the term $\partial f/\partial E$ is non-zero only in a narrow energy region (of typical size k_BT , where k_B is the Boltzmann constant) around the chemical potential μ . Wannier interpolation allows carrying out this task efficiently and accurately even when (avoided) crossings occur close to the Fermi level: band derivatives at a given k-point are obtained with an analytical expression, without resorting to finite-difference methods (Yates et al., 2007). Moreover, computation on dense k-point grids is very efficient, as already discussed earlier for band interpolation. This WF-based Boltzmann-transport methodology

is implemented in Wannier90 and used to compute transport tensors in its BoltzWann module (Pizzi et al., 2014), as well as in other codes (see, e.g., the electron-phonon section, Sec. III.G), and is also used for post-processing calculations in many-body theory (see Sec. III.H.1).

Furthermore, many transport coefficients (e.g., linear and non-linear (AHCs) (Sodemann and Fu, 2015; Yao et al., 2004), anomalous Nernst thermoelectric conductivity (Xiao et al., 2006), magnetoresistance (Gao et al., 2017), and magnetochiral anisotropy (Yokouchi et al., 2023)) depend on the Berry curvature and other quantum-geometric quantities (Gao, 2019; Vanderbilt, 2018; Xiao et al., 2010). As they involve k-derivatives of the Bloch states themselves, such quantities cannot be obtained from the energy dispersions. Moreover, those quantities tend to become strongly enhanced when weak avoided crossings occur near the Fermi level; when that happens, very dense k-point grids must be employed to converge the calculation (Yao et al., 2004). Compared to band interpolation, the interpolation of Berry-type quantities is more involved because it requires setting up matrix elements of the position operator $\hat{\mathbf{r}}$, which is non-local in reciprocal space (Blount, 1962). We defer a discussion of that case to Sec. III.E, and below we describe how to interpolate the matrix elements of a generic k-local operator \hat{X} .

3. Interpolation of a generic k-local operator

Replacing $\hat{H} \to \hat{X}$ in Eq. (11) and using Eq. (5) yields

$$X_{ij}^{W}(\mathbf{R}) = \frac{1}{N} \sum_{\mathbf{k}} e^{-i\mathbf{k} \cdot \mathbf{R}} \sum_{m,n=1}^{\mathcal{J}_{\mathbf{k}}} V_{\mathbf{k},mi}^{*} \langle \psi_{m\mathbf{k}} | \hat{X} | \psi_{n\mathbf{k}} \rangle V_{\mathbf{k},nj} ,$$
(23)

which reduces to Eq. (12) for $\hat{X} = \hat{H}$. The considerations made earlier regarding the spatial decay and truncation of the $H^{W}(\mathbf{R})$ matrix apply equally well to $X^{W}(\mathbf{R})$. The Fourier-transform step is also analogous to Eq. (13),

$$X_{\mathbf{k}',ij}^{W} = \sum_{\mathbf{R}} e^{i\mathbf{k}'\cdot\mathbf{R}} X_{ij}^{W}(\mathbf{R}) = \langle \psi_{i\mathbf{k}'}^{W} | \hat{X} | \psi_{j\mathbf{k}'}^{W} \rangle, \qquad (24)$$

and the final step is to apply to $X_{\mathbf{k}'}^{\mathbf{W}}$ the same unitary transformation that was used in Eq. (14) to diagonalize $H_{\mathbf{k}'}^{\mathbf{W}}$. Using Eq. (18), we find

$$X_{\mathbf{k}',mn}^{\mathrm{H}} = \left(\mathcal{U}_{\mathbf{k}'}^{\dagger} X_{\mathbf{k}'}^{\mathrm{W}} \mathcal{U}_{\mathbf{k}'} \right)_{mn} = \left\langle \psi_{m\mathbf{k}'}^{\mathrm{H}} | \hat{X} | \psi_{n\mathbf{k}'}^{\mathrm{H}} \right\rangle. \tag{25}$$

In particular, diagonal elements of $X_{\mathbf{k'}}^{\mathbf{H}}$ give the expectation values of \hat{X} in the interpolated states. With $\hat{X} = \hat{\mathbf{S}}$, for example, one obtains their spin polarization, which is how the color-coding in Fig. 4 was generated.

Note that in addition to the overlap matrices and energy eigenvalues, interpolating a generic operator $\hat{X} \neq \hat{H}$ requires setting up its matrix elements $\langle \psi_{m\mathbf{k}} | \hat{X} | \psi_{n\mathbf{k}} \rangle$ on the *ab initio* grid; this should be done by the same interface code that computes the overlap matrices.

4. Wannier function perturbation theory

Several important materials properties can be calculated as the linear response of the system to an external perturbation \hat{V} . A common example is the calculation of phonon dispersions and electron-phonon coupling through density-functional perturbation theory (DFPT) (Baroni *et al.*, 2001), the latter case is discussed in Sec. III.G.

We follow Lihm and Park (2021), and write the Hamiltonian eigenstates of the perturbed system in terms of the ones of the unperturbed system plus the wavefunction perturbation,

$$|\psi_{n\mathbf{k}}\rangle = |\psi_{n\mathbf{k}}\rangle^{(0)} + \lambda |\psi_{n\mathbf{k}}\rangle^{(1)} + \mathcal{O}(\lambda^2),$$
 (26)

where the wavefunction perturbation can be calculated with a sum over empty states,

$$|\psi_{n\mathbf{k}}\rangle^{(1)} = \sum_{n'\mathbf{k'}} |\psi_{n\mathbf{k}}\rangle^{(0)} \frac{\langle \psi_{n'\mathbf{k'}} | \hat{V} | \psi_{n\mathbf{k}}\rangle^{(0)}}{\epsilon_{n\mathbf{k}} - \epsilon_{n'\mathbf{k'}}}.$$
 (27)

The primed sum means that terms for which the denominator vanishes are excluded.

Alternatively, the wavefunction perturbation can be calculated without summing over high-energy states by solving the Sternheimer equation (Baroni *et al.*, 2001). Lihm and Park (Lihm and Park, 2021) have shown that such perturbation theory can be formulated in the Wannier representation, where the WFs of the perturbed system can be written as

$$|\mathbf{R}j\rangle = |\mathbf{R}j\rangle^{(0)} + \lambda |\mathbf{R}j\rangle^{(1)} + \mathcal{O}(\lambda^2).$$
 (28)

The expression for $|\mathbf{R}j\rangle^{(1)}$, reported in Eqs. (8) and (9) of Lihm and Park (2021), consists of two terms: the first can be calculated with the Sternheimer equation to obtain the states $|\psi_{n\mathbf{k}}\rangle^{(1)}$, while the second contains matrix elements of \hat{V} and the projector over the WFs of the unperturbed system. Crucially, both terms only require energies and matrix elements within the Wannier outer window introduced in Sec. II.A.2. Thus, the Wannier function perturbation can be calculated without making explicit use of the states outside that energy window.

For a monochromatic static perturbation with wavevector **q**, the first-order wavefunction perturbation can be interpolated as (Lihm and Park, 2021)

$$|\psi_{n\mathbf{k}',\mathbf{q}}^{\mathrm{H}}\rangle^{(1)} = \frac{1}{\sqrt{N}} \sum_{j,\mathbf{R}} e^{i\mathbf{k}'\cdot\mathbf{R}} |\mathbf{R}_{\mathbf{q}}j\rangle^{(1)} \mathcal{U}_{\mathbf{k}',jn}$$
$$+ \sum_{m=1}^{N_W} |\psi_{m\mathbf{k}'+\mathbf{q}}^{\mathrm{H}}\rangle^{(0)} \frac{\tilde{g}_{mn\mathbf{k}',\mathbf{q}}^{\mathrm{H}}}{\epsilon_{n\mathbf{k}'}^{(0)} - \epsilon_{m\mathbf{k}'+\mathbf{q}}^{(0)}}, (29)$$

where the WF perturbations are expanded as a sum of monochromatic perturbations

$$|\mathbf{R}j\rangle^{(1)} = \sum_{\mathbf{q}} |\mathbf{R}_{\mathbf{q}}j\rangle^{(1)} \tag{30}$$

while the superscript H marks the Hamiltonian gauge of the unperturbed (0) and perturbed (1) system, $\mathcal{U}_{\mathbf{k}'}$ is the unitary matrix that diagonalizes the unperturbed Hamiltonian according to Eq. (14), and $\tilde{g}_{mn\mathbf{k},\mathbf{q}}^{H}$ is obtained by performing the Fourier transform of the matrix elements of \hat{V} between WFs of the unperturbed states, and then rotating to the Hamiltonian gauge using $\mathcal{U}_{\mathbf{k}'}$.

A key aspect is that Wannier function perturbations are localized in real space, so the perturbed Hamiltonian and its eigenstates can be efficiently interpolated by considering coarse k-point grids. This allows to efficiently interpolate various matrix elements involving the wavefunction perturbation, such as in the case of electron-phonon self-energies and Kubo formulas. Wannier function perturbation theory (WFPT) has been applied to describe temperature-dependent electronic band structures and indirect optical absorption, shift spin currents and spin Hall conductivities (Lihm and Park, 2021). WFPT will be made available in a future release of the EPW code (Lee et al., 2023).

5. Porting Wannier Hamiltonians to TB codes

In TB theory, two phase conventions are commonly used to perform the Fourier transforms from real to reciprocal space (Vanderbilt, 2018): the one adopted in Eqs. (13), (16) and (24) ("original convention"), and the alternative one ("modified convention") where the phase factors in those equations are modified as

$$e^{i\mathbf{k}'\cdot\mathbf{R}} \to e^{i\mathbf{k}'\cdot(\mathbf{R}+\boldsymbol{\tau}_j-\boldsymbol{\tau}_i)}$$
. (31)

Although the interpolated eigenvalues $\varepsilon_{n\mathbf{k}'}^{\mathrm{H}}$ and matrix elements $X_{\mathbf{k}',mn}^{\mathrm{H}}$ come out the same with both conventions (as they should), the modified convention is more natural for the purpose of evaluating quantities, such as Berry connections and curvatures, that are sensitive to the real-space embedding of the TB model via the position matrix elements $\langle 0i|\hat{\mathbf{r}}|\mathbf{R}j\rangle$ (see Sec. III.E). This has to do with the fact that with the original convention, TB eigenvectors (the column vectors of $\mathcal{U}_{\mathbf{k}'}$) behave like full Bloch eigenstates $|\psi_{n\mathbf{k}'}\rangle$, whereas with the modified convention they behave like their cell-periodic parts $|u_{n\mathbf{k}'}\rangle$ (Vanderbilt, 2018); and it is in terms of the latter that Berry-type quantities are most naturally expressed.

The modified phase convention is the one adopted in the TB codes PythTB (PythTB, 2023a) and TBmodels (TBmodels, 2023); both are able to import the Wannier Hamiltonian $H_{ij}^{W}(\mathbf{R})$, along with the Wannier centers $\{\boldsymbol{\tau}_i\}$, from the seedname_tb.dat file written by Wannier90. PythTB was originally written for pedagogical purposes, as part of a course on Berry phases in electronic structure theory that was later turned into a textbook (Vanderbilt, 2018). It is feature-rich but is not optimized for speed, as it was designed with TB toy models in mind (however, a high-performance implementation is available (Numba-PythTB, 2023)). Instead, TBmodels has fewer post-processing functionalities, but it delivers critical speed-up and improved scaling. Among other Wannier-TB codes, it is worth mentioning Wannier Tools (Wu et al., 2018), which implements sparse Hamiltonians for large systems, band unfolding, and several other features related to Berry-type quantities (see Sec. III.E).

6. Wannier interpolation beyond density-functional theory

As discussed above, one of the most powerful and effective applications of WFs is the interpolation of band structures and other electronic-structure properties. While this is already very useful in the context of DFT calculations, it becomes even more compelling for beyond-DFT methods, such as hybrid functionals (Becke, 1988, 2014; Heyd et al., 2003; Kümmel and Kronik, 2008; Lee et al., 1988; Martin, 2020; Perdew et al., 1996), manybody perturbation theory (MBPT) such as G_0W_0 (Golze et al., 2019), and non-diagrammatic approaches such

as the Koopmans-compliant functionals (Borghi et al., 2014; Colonna et al., 2022, 2018, 2019; Dabo et al., 2010; De Gennaro et al., 2022; Elliott et al., 2019; Nguyen et al., 2018). In fact, in DFT the potential can always be recalculated from the sole knowledge of the ground-state electronic charge density; therefore, the corresponding KS Hamiltonian can be directly calculated at any arbitrary k-point. Instead, for most beyond-DFT methods this is no longer the case, and band structure calculations on a high-symmetry path cannot be performed as a series of independent diagonalizations. For hybrid functionals and GW, the eigenvalues at a given k-point requires the knowledge of the wavefunctions and eigenenergies on all $(\mathbf{k} + \mathbf{q})$ -points, where the \mathbf{q} -points are defined on a uniform grid which has to be converged. In other words, reasonably dense sampling on high-symmetry paths can only be obtained with some form of interpolation.

While electronic structure codes typically offer generalpurpose interpolation methods, often based on Fourier series (Koelling and Wood, 1986; Pickett et al., 1988), WFs provide two concrete advantages. First, they are a physically motived and optimal basis set, which exhibits exponential convergence and is guaranteed to deliver the exact result for a sufficiently dense k-point grid, so the accuracy can be systematically increased simply by considering denser grids. If MLWFs are chosen, the efficiency is maximal and rather coarse grids are often sufficient to faithfully reproduce the entire band structure. Second, once a WF basis is constructed, not only it yields interpolated eigenvalues (e.g., the band structure) but it also allows to represent the Hamiltonian and many other operators in a compact real space representation. Once the relevant operators in a WF basis are available, one gets access to the full spectrum of theories and software packages that are part of the Wannier ecosystem, capable of much more complex tasks than just band interpolation. Notably, once a Wannierization is performed with hybrid functionals or at the G_0W_0 level, all other Wannier-interpolated quantities can be obtained at the same level of theory with no extra effort or cost. Finally, thanks to all the recent work in advanced minimization techniques (Sec. II.D) and automation (Sec. III.J), the Wannier interpolation does not require much more human intervention than other standard methods such as smooth Fourier interpolation. In the following, we briefly outline the motivation and the corresponding procedure to deploy Wannier interpolation for two of the most popular excited-state approaches: hybrid functionals, and many-body perturbation theory at the G_0W_0 level.

a. Hybrid functionals. A very popular approach to improve the accuracy of *ab initio* band structures is to combine explicit density-dependent functionals with Hartree–Fock terms, which leads to orbital-dependent functionals called "hybrids" (Becke, 1988, 2014; Heyd

et al., 2003; Kümmel and Kronik, 2008; Lee et al., 1988; Martin, 2020; Perdew et al., 1996). The procedure to obtain WFs is similar to that in vanilla DFT, except that non-self-consistent field calculations cannot be performed. Hence, the self-consistent field calculation must already include all the empty states (if any) to be included in the Wannierization. In addition, ground-state calculations are typically performed on the irreducible Brillouin zone (IBZ) by exploiting crystalline symmetries, while Wannier90 requires a uniform grid on the full Brillouin zone (FBZ). As performing the self-consistent calculation on the FBZ is certainly possible but rather inefficient, the typical procedure involves unfolding the ground-state orbitals and band structure from the IBZ to the FBZ as a post-processing step to be performed after the self-consistent calculation and before producing the overlap matrices and the other input required to obtain WFs. For example, in the Quantum ESPRESSO distribution (Giannozzi et al., 2017, 2009) this is done through the open_grid.x code. Notably, WFs can be used to speed up the core hybrid-functionals calculations, as they allow reducing the number of exchange integrals to be computed (Carnimeo et al., 2019; DiStasio et al., 2014; E et al., 2007; García-Cervera et al., 2009; Mountjoy et al., 2017; Wu et al., 2009).

b. G_0W_0 . Most of what has been discussed for hybrid functionals also holds for MBPT calculations in the G_0W_0 approximation, with two important remarks. First, G_0W_0 is a one-shot approach in the quasiparticle (QP) approximation which is typically performed on top of a DFT calculation: so the orbitals remain at the KS level and only the energy eigenvalues are corrected, hence neglecting off-diagonal elements of the self-energy in the KS basis. Second, as only the energies are changed at the G_0W_0 level, the KS states might swap their band indices and not be ordered in energy anymore. A typical case where this might manifest clearly are topological insulator candidates (and systems with band inversions in general) such as monolayer TiNI (Marrazzo et al., 2019), which is topological in DFT and trivial at the G_0W_0 level. The practicalities of obtaining G_0W_0 WFs and related quantities depend on whether the DFT and MBPT calculations are performed with the same distribution (e.g., VASP (Kaltak, 2015)) or with two separate codes (as for example with Quantum ESPRESSO (Giannozzi et al., 2017, 2009) and Yambo (Sangalli et al., 2019)). In general, G_0W_0 QP corrections $\Delta \epsilon_i^{\text{QP}} = \epsilon_i^{G_0W_0} - \epsilon_i^{\text{DFT}}$ need to be computed on a uniform grid in the FBZ, which can be made efficient by unfolding from the IBZ to the FBZ (in Yambo, this operation is carried out by the post-processing utility ypp). While orbitals remain at the DFT-KS level, Wannier90 requires the states to be ordered with ascending energy and, in addition, some input matrices (e.g., the uHu) need to be updated with QP corrections. If this is not performed by the ab initio engine, it can be taken care by the Wannier90 utility gw2wannier90.py if the DFT eigenvalues and QP corrections are provided in the standard format seedname.eig. After this step, the Wannierization can proceed as usual, and it is available in both Wannier90 (Pizzi et al., 2020) and WanT (Ferretti et al., 2012). Note that in G_0W_0 , QP corrections need to be computed on a subset of the k-point grid required to calculate the self-energy: this can be exploited to speedup the calculation, especially for 2D materials as discussed in Sangalli et al. (2019), because Wannierization typically requires relatively coarse k-point grids. Finally, we briefly touch on beyond- G_0W_0 development of interest from a WF perspective. While Aguilera et al. have shown that off-diagonal components of the self-energy—which are not included in standard perturbative approaches—are very relevant in case of band inversions (Aguilera et al., 2013) (such as for topological insulators), Hamann and Vanderbilt have found (Hamann and Vanderbilt, 2009) that, in general, differences between MLWFs obtained with local-density approximation (LDA) and self-consistent GW (QSGW) are minimal.

c. Bethe–Salpeter equation In order to address neutral excitations, as opposed to the charged excitations of GW, one needs to describe the bound state of an excited electron with the hole that has been created. This is accomplished either using time-dependent density-functional theory or Green's function methods (Onida et al., 2002); in the latter case, the Bethe–Salpeter equation (BSE) is solved on top of the GW solutions. Within the Tamm–Dancoff approximation (Dancoff, 1950; Hirata and Head-Gordon, 1999; Onida et al., 2002), the BSE can be recast into an effective two-particle eigenvalue problem (Onida et al., 2002; Rohlfing and Louie, 2000), which in the electron-hole (e-h) basis reads

$$\sum_{v'c'} \left[D_{vc,v'c'} + 2K_{vc,v'c'}^{\mathbf{x}} - K_{vc,v'c'}^{\mathbf{d}} \right] A_{v'c'}^{\lambda} = E_{\lambda} A_{vc}^{\lambda}, \tag{32}$$

where the v,v' and c,c' indices run over valence and conduction states, E_{λ} are the neutral excitation energies (the poles of the density-density response function), and A_{vc}^{λ} are the coefficients of the excitonic wavefunctions (that are related to oscillator strengths) in the e-h basis. The effective 2-particle Hamiltonian is made by i) a diagonal term $D_{vc,v'c'} = (\varepsilon_c^{\rm QP} - \varepsilon_v^{\rm QP})\delta_{vv'}\delta_{cc'}$ representing the "bare" e-h transitions (i.e., without accounting for the electron-hole interaction) from the QP theory, ii) an exchange-like term

$$K_{vc,v'c'}^{\mathbf{x}} = \int d\mathbf{r} d\mathbf{r}' \,\phi_c^*(\mathbf{r}) \phi_v(\mathbf{r}) |\mathbf{r} - \mathbf{r}'|^{-1} \phi_{v'}^*(\mathbf{r}') \phi_{c'}(\mathbf{r}'),$$
(33)

and iii) a direct screened Coulomb term

$$K_{vc,v'c'}^{d} = \int d\mathbf{r} d\mathbf{r}' \,\phi_c^*(\mathbf{r})\phi_{c'}(\mathbf{r})W(\mathbf{r},\mathbf{r}')\phi_{v'}^*(\mathbf{r}')\phi_v(\mathbf{r}')$$
(34)

responsible for an effective attractive interaction between the electron and the hole. Here $\{\phi_i\}$ and $\{\varepsilon_i^{\mathrm{QP}}\}$ are the QP wavefunctions and QP energies, respectively. The solution of Eq. (32) in the e-h basis would require the explicit computation of a significant number of empty states, which becomes in turn a critical convergence parameter. This can be conveniently avoided (Giustino et al., 2010; Marsili et al., 2017; Rocca et al., 2010; Umari et al., 2011) resorting to well established techniques from DFPT (Baroni et al., 2001) by introducing i) the projector over the conduction manifold Q = $\mathbb{1} - \hat{P} = \mathbb{1} - \sum_{v} |\phi_{v}\rangle\langle\phi_{v}|$, and ii) a set of auxiliary functions $\xi_{v}(\mathbf{r}) = \sum_{c} A_{cv}\phi_{c}(\mathbf{r})$, usually called a *batch* representation (Rocca et al., 2008; Walker et al., 2006). These are N_v (where N_v is the number of occupied states) auxiliary functions that live in the unperturbed empty-states manifold and provide an equivalent but more compact representation of the excitonic wavefunction $\Theta(\mathbf{r}, \mathbf{r}') = \sum_{vc} A_{cv} \phi_v^*(\mathbf{r}) \phi_c(\mathbf{r}') = \sum_v \phi_v(\mathbf{r}) \xi_v(\mathbf{r}')$. In this representation, the effective 2-particle Hamiltonian is completely specified by its action on the components of the batch (Rocca et al., 2010):

$$\sum_{v'} D_{vv'} |\xi_{v'}\rangle = \sum_{v'} (\hat{H}^{QP} - \varepsilon_{v'} \mathbb{1}) \delta_{vv'} |\xi_{v'}\rangle$$
 (35)

$$\sum_{v'} K_{vv'}^{\mathbf{x}} |\xi_{v'}\rangle = \sum_{v'} \hat{Q} \left(\int \frac{1}{|\mathbf{r} - \mathbf{r}'|} \phi_{v'}^{*}(\mathbf{r}') \xi_{v'}(\mathbf{r}') d\mathbf{r}' \right) |\phi_{v}\rangle$$
(36)

$$\sum_{v'} K_{vv'}^{\mathbf{d}} |\xi_{v'}\rangle = \sum_{v'} \hat{Q} \left(\int W(\mathbf{r}, \mathbf{r}') \phi_{v'}^{*}(\mathbf{r}') \phi_{v'}(\mathbf{r}') d\mathbf{r}' \right) |\xi_{v'}\rangle.$$
(37)

The advantage of this formulation is that there is no explicit reference to the empty states (hidden inside the projector \hat{Q} and the batch representation), and only the N_v auxiliary functions $\{|\xi_v\rangle\}$ need to be determined solving the BSE in the batch representation.

A further computational speed-up (and an improvement on the overall scaling (Marsili et al., 2017)) can be achieved by moving from the KS orbitals to MLWFs and by exploiting their localization to greatly reduce the number of operations needed to evaluate the action of the BSE Hamiltonian on a trial state $|\xi_v\rangle$. This is particularly relevant for the direct term (Eq. (37)), which represents the real bottleneck of the calculations. In the Wannier representation, this becomes

$$\sum_{v'} K_{vv'}^{\mathrm{d}} |\tilde{\xi}_{v'}\rangle = \hat{Q} \left(\sum_{v'} \int W(\mathbf{r}, \mathbf{r}') \omega_{v'}^*(\mathbf{r}') \omega_{v'}(\mathbf{r}') d\mathbf{r}' \right) |\tilde{\xi}_{v'}\rangle,$$
(38)

where $\{\omega_v(\mathbf{r})\}\$ are the MLWFs and $\tilde{\xi}_v(\mathbf{r})$ is the batch component in the Wannier representation (simply obtained by rotating the original $\xi_v(\mathbf{r})$ with the unitary matrix rotation that transforms the manifold from the canonical to the MLWF representation). Exploiting locality, one can define a threshold for which a given pair of MLWFs overlap. By excluding non-overlapping pairs of MLWFs from the summation in Eq. (38), it becomes possible to lower the scaling of the evaluation of the action of the direct term on trial states from $\mathcal{O}(N^4)$ to $\mathcal{O}(N^3)$ (Marsili et al., 2017), an approach that has been established and applied in the community (Elliott et al., 2019; Marsili et al., 2017; Umari et al., 2011). Tightbinding and phenomenological models based on localized representation have also recently appeared (Dias et al., 2023: Uría-Álvarez *et al.*, 2023).

D. Ballistic transport and nanostructures

MLWFs can be used to build the electronic structure of large nanostructures (Lee et al., 2005; Lihm and Park, 2019) and to determine their ballistic transport when connected to semi-infinite leads (Calzolari et al., 2004; Lee et al., 2005). In this latter case, the formalism of Green's functions is used to embed a conductor into the surrounding environment. In all cases, the building blocks are Hamiltonian matrix elements between the localized MLWFs that are used to construct, LEGO[™]like, either the desired non-self-consistent Hamiltonian of a much larger nanostructure, or the self-energies embedding the conductor of interest into semi-infinite leads. Importantly, any solid (or surface) can be viewed as an infinite (or semi-infinite, in the case of surfaces) stack of "principal layers" interacting only with neighboring layers (Lee and Joannopoulos, 1981a,b). In this way, the infinite-dimensional real-space Hamiltonian can be divided into finite-sized Hamiltonian matrices; for a bulk system (i.e., infinite and periodic) the only independent components are H_{00} and H_{01} , where the former represents the interaction between MLWFs located in the same principal layer, and the latter the interaction between orbitals in one principal layer and the next.

As discussed by Nardelli (Nardelli, 1999), one can consider a system composed of a conductor C connected to two semi-infinite leads, R and L (C, R, and L are in themselves composed by a finite or infinite number of principal layers). The conductance through C is related to the scattering properties of C itself via the Landauer formula (Landauer, 1970):

$$\mathcal{G}(E) = \frac{2e^2}{h}\mathcal{T}(E),\tag{39}$$

where \mathcal{T} is the transmission function, \mathcal{G} is the conductance, and \mathcal{T} is the probability that an electron injected at one end of the conductor will transmit to the other end.

This transmission function can be expressed in terms of the Green's functions of the conductors and of its coupling to the leads (Lee and Joannopoulos, 1981a,b) as

$$\mathcal{T} = \text{Tr}(\Gamma_L G_C^r \Gamma_R G_C^a), \tag{40}$$

where $G_C^{\{r,a\}}$ are the retarded and advanced Green's functions of the conductor, respectively, and $\Gamma_{\{L,R\}}$ are functions that describe the coupling of the conductor to the two leads. To compute the Green's function of the conductor, one starts from the equation for the Green's function of the whole system:

$$(\epsilon - H)G = 1 \tag{41}$$

where $\epsilon = E + i\eta$ with η arbitrarily small, and $\mathbbm{1}$ is the identity matrix. The matrix representation of G in a WFs basis can be partitioned as

$$\begin{pmatrix}
G_L & G_{LC} & G_{LCR} \\
G_{CL} & G_C & G_{CR} \\
G_{LRC} & G_{RC} & G_R
\end{pmatrix} = (42)$$

$$\begin{pmatrix} (\epsilon - H_L) & H_{LC} & 0 \\ H_{LC}^{\dagger} & (\epsilon - H_C) & H_{CR} \\ 0 & H_{CR}^{\dagger} & (\epsilon - H_R) \end{pmatrix}^{-1}.$$

We can then write the conductor Green's function as

$$G_C(E) = (\epsilon - H_C - \Sigma_L - \Sigma_R)^{-1}, \tag{43}$$

where the effect of the semi-infinite leads on the conductor is described by the self-energies $\Sigma_{L,R}$, and the coupling functions $\Gamma_{\{L,R\}}$ are obtained from the self-energies as

$$\Gamma_{\{L,R\}} = i[\Sigma_{\{L,R\}}^r - \Sigma_{\{L,R\}}^a];$$
 (44)

here, the advanced self-energy is the Hermitian conjugate of the retarded one, and we solve for the latter. Given that the semi-infinite leads are also made of principal layers, one can construct the self-energies as (Nardelli, 1999)

$$\Sigma_{L} = H_{LC}^{\dagger} (\epsilon - H_{00}^{L} - (H_{01}^{L})^{\dagger} \overline{T}_{L})^{-1} H_{LC},$$

$$\Sigma_{R} = H_{CR} (\epsilon - H_{00}^{R} - H_{01}^{R} T_{R})^{-1} H_{CR}^{\dagger},$$
(45)

where, e.g., H_{00} describes the intralayer interactions and H_{01} the interlayer couplings. The transfer matrices $\overline{T}_{L,R}$ and $T_{L,R}$, defined such that $G_{10} = TG_{00}$ and $G_{00} = \overline{T}G_{10}$, are calculated following the iterative procedure by Lopez-Sancho et al. (Sancho et al., 1984). The only inputs are the matrix elements of the Hamiltonian H_{mn} in a localized representation; the accuracy of the results depends on having principal layers that do not couple beyond next neighbors, i.e., on having a well-localized basis. The knowledge of the conductor Green's

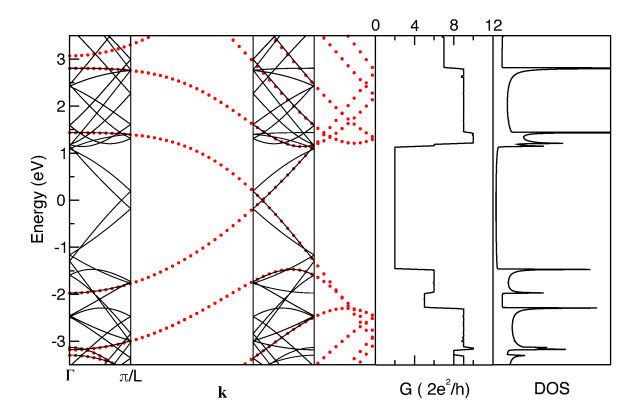


FIG. 5 Comparison of band structures calculated for a (5,5) single-walled carbon nanotube, either from MLWFs obtained from a supercell calculation (100 atoms, Γ sampling), and then Wannier-interpolated (solid thin line) or from a full diagonalization of the Hamiltonian (20-atom primitive cell, sampled with 5 k-points, red dots). The center and right panels show also the ballistic conductance and density of states calculated from the Green's functions (see text). Notably, only states at Γ are used in the disentanglement and Wannierization, where the system exhibits a pseudogap greater than 2 eV; still, this leads to a perfect description of the metallic bands and the van Hove singularities anywhere in the BZ, highlighting the role of MLWFs as excellent interpolators and building blocks for the non-self-consistent electronic structure of large-scale nanostructures (see also Lee et al. (2005)).

function G_C also gives direct information on the electronic spectrum via the spectral density of the electronic states: $N_C(E) = -(1/\pi) \text{Im}(\text{Tr}G_C(E))$.

As an example, we take a (5,5) single-wall carbon nanotube, described with a supercell containing 100 carbon atoms (five times the primitive cell); the disentanglement and Wannierization procedure results in 150 sp^2 orbitals and 100 p_z orbitals. Such supercell size is large enough to allow for Γ -sampling only in the BZ, and to have negligible overlap with the MLWFs belonging to the second next supercell. We show in Fig. 5 the results for the band structure, quantum conductance, and density of states, adapted from Lee et al. (2005). The metallic nanotube, notwithstanding its ~ 2 eV pseudogap at Γ , shows a band structure in perfect agreement with that obtained from a very fine sampling of the BZ, and perfect agreement between the steps in conductance and the peaks in the van Hove singularities, with the maxima and the minima of the band dispersions at arbitrary points in the BZ. While these methodologies based on WFs have been implemented either as an extension of Wannier90 (Shelley et al., 2011) or standalone in the WF-based WanT code (Ferretti et al., 2012), analogous techniques have been developed for other types of localized orbitals and implemented in simulation codes such as TranSiesta/Atomistix Toolkit (Brandbyge et al.,

2002), SMEAGOL (Rocha et al., 2006), OpenMX (Ozaki et al., 2010), NEMO5 (Fonseca et al., 2013), nextnano (Birner et al., 2007), NanoTCAD Vides (Bruzzone et al., 2014; Fiori and Iannaccone, 2007), KWANT (Groth et al., 2014), some of which also provide an interface with the Wannier ecosystem.

E. Berryology

1. Motivation

Berry phases and related quantities are central to the description of the electronic properties of crystals (Vanderbilt, 2018; Xiao et al., 2010). Here are some representative examples.

1. The electronic contribution to the electric polarization of an insulator is given by

$$\mathbf{P}_{\text{el}} = -e \sum_{n}^{\text{occ}} \int_{\text{BZ}} \frac{d^3 k}{(2\pi)^3} \, \mathbf{A}_{\mathbf{k},nn} \,, \tag{46}$$

where -e is the electron charge and $\mathbf{A}_{\mathbf{k},nn}$ are diagonal elements of the Berry connection matrix,

$$\mathbf{A}_{\mathbf{k},mn} = i \langle u_{m\mathbf{k}} | \nabla_{\mathbf{k}} u_{n\mathbf{k}} \rangle. \tag{47}$$

2. Off-diagonal elements of $\mathbf{A_k}$ describe electric-dipole transition moments, allowing the interband optical conductivity to be expressed as

$$\sigma_{ab}(\omega) = \frac{ie^2}{\hbar} \sum_{m,n} \int_{BZ} \frac{d^3k}{(2\pi)^3} \left(f_{m\mathbf{k}} - f_{n\mathbf{k}} \right) \times \frac{\varepsilon_{m\mathbf{k}} - \varepsilon_{n\mathbf{k}}}{\varepsilon_{m\mathbf{k}} - \varepsilon_{n\mathbf{k}} - \hbar(\omega + i0^+)} A^a_{\mathbf{k},nm} A^b_{\mathbf{k},mn} , \quad (48)$$

where $f_{n\mathbf{k}}$ is the Fermi-Dirac occupation factor.

3. The Berry curvature is defined as the curl of the Berry connection,

$$\Omega_{n\mathbf{k}} = \nabla_{\mathbf{k}} \times \mathbf{A}_{\mathbf{k},nn} = -\text{Im} \langle \nabla_{\mathbf{k}} u_{n\mathbf{k}} | \times | \nabla_{\mathbf{k}} u_{n\mathbf{k}} \rangle$$
, (49)

and its integral over the occupied states gives the intrinsic AHC,

$$\sigma_{yx} = \frac{e^2}{\hbar} \int_{BZ} \frac{d^3k}{(2\pi)^3} \sum_{\mathbf{n}} f_{n\mathbf{k}} \Omega_{n\mathbf{k}}^z.$$
 (50)

4. The ground-state orbital magnetization reads

$$\mathbf{M}_{\text{orb}} = \int_{\text{BZ}} \frac{d\mathbf{k}}{(2\pi)^3} \sum_{n} f_{n\mathbf{k}} \left[\mathbf{m}_{n\mathbf{k}}^{\text{orb}} + \frac{e}{\hbar} \left(\varepsilon_{\text{F}} - \varepsilon_{n\mathbf{k}} \right) \mathbf{\Omega}_{n\mathbf{k}} \right],$$
(51)

with $\varepsilon_{\rm F}$ the Fermi energy and

$$\mathbf{m}_{n\mathbf{k}}^{\text{orb}} = \frac{e}{2\hbar} \text{Im} \langle \nabla_{\mathbf{k}} u_{n\mathbf{k}} | \times \left(\hat{H}_{\mathbf{k}} - \varepsilon_{n\mathbf{k}} \right) | \nabla_{\mathbf{k}} u_{n\mathbf{k}} \rangle$$
 (52)

the intrinsic orbital moment of a Bloch state.

5. To first order in applied fields ${\bf E}$ and ${\bf B}$, the semiclassical equations of motion for a wavepacket in a Bloch band read

$$\dot{\mathbf{r}} = \frac{1}{\hbar} \nabla_{\mathbf{k}} \tilde{\varepsilon}_{n\mathbf{k}} - \dot{\mathbf{k}} \times \mathbf{\Omega}_{n\mathbf{k}}, \qquad (53a)$$

$$\dot{\mathbf{k}} = -\frac{e}{\hbar}\mathbf{E} - \frac{e}{\hbar}\dot{\mathbf{r}} \times \mathbf{B}, \qquad (53b)$$

where

$$\tilde{\varepsilon}_{n\mathbf{k}} = \varepsilon_{n\mathbf{k}} - \left(\mathbf{m}_{n\mathbf{k}}^{\text{spin}} + \mathbf{m}_{n\mathbf{k}}^{\text{orb}}\right) \cdot \mathbf{B}$$
 (54)

is the Zeeman-shifted band energy.

The motivation to apply Wannier interpolation to Berry-type quantities came from pioneering ab initio calculations of the AHC in the ferromagnets $SrRuO_3$ (Fang et al., 2003) and BCC Fe (Yao et al., 2004), which revealed the integrand of Eq. (50) to be strongly peaked in the vicinity of avoided crossings between occupied and empty bands; resulting in the need to sample the BZ over millions of k-points to reach convergence. An efficient Wannier-interpolation scheme for evaluating the AHC was developed in Wang et al. (2006), and since then the methodology has been applied to many other properties.

Wannier interpolation of Berry-type quantities was introduced in version 2 of Wannier90 as part of its postprocessing code postw90 (Mostofi et al., 2014), with the ability to compute AHC (Wang et al., 2006), interband optical conductivity (Yates et al., 2007), and orbital magnetization (Lopez et al., 2012). The list of available properties has grown considerably since then, and more recently the WannierBerri code package (Tsirkin, 2021) introduced several methodological improvements including "pruned FFT" (Markel, 1971; Sorensen and Burrus, 1993) (a combination of fast and slow Fourier transforms), and the use of symmetries and of the tetrahedron method for BZ integrals. Other codes, including WannierTools (Wu et al., 2018) and linres (Železný, 2023), implement some functionalities but with additional approximations (see discussion of Eq. (60) below). The reader should consult the documentation of the codes for an up-to-date description of their capabilities.

In the following, we outline the basic interpolation strategy for Berry-type quantities, using the off-diagonal Berry connection as an example (the diagonal Berry connection that enters the Berry phase requires a separate treatment, see Sec. III.F). For discussion purposes, we adopt the modified phase convention for Bloch sums indicated in Eq. (31).

2. Wannier interpolation of the interband Berry connection

We wish to evaluate off-diagonal elements of the Berry connection matrix in the Hamiltonian gauge. Inserting in Eq. (47) the relation (18) between interpolated Bloch states in the Hamiltonian and Wannier gauges, we obtain

$$\mathbf{A}_{\mathbf{k}'}^{\mathrm{H}} = i \mathcal{U}_{\mathbf{k}'}^{\dagger} \mathbf{\nabla}_{\mathbf{k}'} \mathcal{U}_{\mathbf{k}'} + \mathcal{U}_{\mathbf{k}'}^{\dagger} \mathbf{A}_{\mathbf{k}'}^{\mathrm{W}} \mathcal{U}_{\mathbf{k}'}. \tag{55}$$

Note the extra (first) term compared to the gauge-transformation rule (25) for a k-local matrix object. Recalling from Eq. (14) that the columns of $\mathcal{U}_{\mathbf{k}'}$ are eigenvectors of $H^{\mathrm{W}}_{\mathbf{k}'}$, the off-diagonal matrix elements of that term can be evaluated from non-degenerate perturbation theory as

$$\left(\mathcal{U}_{\mathbf{k}'}^{\dagger} \nabla_{\mathbf{k}'} \mathcal{U}_{\mathbf{k}'}\right)_{mn} = \frac{\left[\mathcal{U}_{\mathbf{k}'}^{\dagger} \left(\nabla_{\mathbf{k}'} H_{\mathbf{k}'}^{\mathbf{W}}\right) \mathcal{U}_{\mathbf{k}'}\right]_{mn}}{\varepsilon_{n\mathbf{k}'}^{\mathbf{H}} - \varepsilon_{m\mathbf{k}'}^{\mathbf{H}}}.$$
 (56)

All quantities on the right-hand side can be obtained from Eqs. (13) and (14) starting from $\langle \mathbf{0}i|\hat{H}|\mathbf{R}j\rangle$ and $\boldsymbol{\tau}_j = \langle \mathbf{0}j|\hat{\hat{\mathbf{r}}}|\mathbf{0}j\rangle$ (the latter appears in the modified phase factors in Eq. (31)). For the second term in Eq. (55), we also need

$$\mathbf{A}_{\mathbf{k}',ij}^{\mathrm{W}} = \sum_{\mathbf{R}} e^{i\mathbf{k}' \cdot (\mathbf{R} + \boldsymbol{\tau}_j - \boldsymbol{\tau}_i)} \mathbf{d}_{ij}(\mathbf{R}), \qquad (57)$$

which follows from inserting in Eq. (47) the Bloch sum (16) with the modified phase factors. Here $\mathbf{d}_{ij}(\mathbf{R})$ are the off-diagonal matrix elements of $\hat{\mathbf{r}}$ in the Wannier basis, that is,

$$\langle \mathbf{0}i|\hat{\mathbf{r}}|\mathbf{R}j\rangle = \delta_{\mathbf{R},\mathbf{0}}\delta_{ij}\boldsymbol{\tau}_j + \mathbf{d}_{ij}(\mathbf{R}).$$
 (58)

The matrix elements $\langle \mathbf{0}i|\hat{\mathbf{H}}|\mathbf{R}j\rangle$ are evaluated using Eq. (12), and the corresponding procedure for $\langle \mathbf{0}i|\hat{\mathbf{r}}|\mathbf{R}j\rangle$ is as follows. First, we can use Eq. (5a) to write $\langle \mathbf{0}i|\hat{\mathbf{r}}|\mathbf{R}j\rangle$ as $(1/N)\sum_{\mathbf{k}}e^{-i\mathbf{k}\cdot\mathbf{R}}A_{\mathbf{k},ij}^{\mathrm{W}}$. Since the Bloch functions are smooth in the Wannier gauge, $\mathbf{A}_{\mathbf{k},ij}^{\mathrm{W}}$ can be evaluated on the *ab initio* grid by discretizing the **k** derivative appearing in Eq. (47). Adopting the finite-differences scheme described in Marzari and Vanderbilt (1997) and Mostofi *et al.* (2008) we obtain

$$\langle \mathbf{0}i|\hat{\mathbf{r}}|\mathbf{R}j\rangle = \frac{i}{N} \sum_{\mathbf{k}} e^{-i\mathbf{k}\cdot\mathbf{R}} \sum_{\mathbf{b}} w_b \mathbf{b} \times \sum_{\mathbf{m},n} V_{\mathbf{k},mi}^* M_{mn}^{(\mathbf{k},\mathbf{b})} V_{\mathbf{k}+\mathbf{b},nj}, \qquad (59)$$

where **b** are vectors connecting neighboring grid points, w_b are appropriately chosen weights, $M^{(\mathbf{k},\mathbf{b})}$ are the overlap matrices defined by Eq. (8), and $V_{\mathbf{k}}$ are the Wannierization matrices in Eq. (5b); since the overlap matrices were computed in preparation for the WF construction procedure, and the Wannierization matrices were obtained at the end of that procedure, both are readily available.

Once $\langle 0i|\hat{H}|\mathbf{R}j\rangle$ and $\langle 0i|\hat{\mathbf{r}}|\mathbf{R}j\rangle$ have been tabulated, the interband Berry connection can be evaluated from Eqs. (55)–(57), with the matrices $\mathcal{U}_{\mathbf{k}'}$ therein (along with

the interpolated energy eigenvalues) given by Eq. (14). Finally, the Berry connection and energy eigenvalues are inserted in Eq. (48) to obtain the interband optical conductivity (Yates *et al.*, 2007).

Equation (59) entails a numerical error of order $(\Delta k)^2$, where Δk is the *ab initio* mesh spacing (Marzari and Vanderbilt, 1997; Mostofi *et al.*, 2008). The direct realspace mesh integration method mentioned below Eq. (12) should be free of such errors, but it is not as practical in the context of k-space Wannierization schemes. It is therefore desirable to develop improved discretized k-space formulas for $\langle 0i|\hat{\mathbf{r}}|\mathbf{R}j\rangle$ and related matrix elements. A higher-order generalization of the discretization scheme of Marzari and Vanderbilt (1997) and Mostofi *et al.* (2008) was recently introduced (Cistaro *et al.*, 2023), and further improvements are currently under way (Ghim, 2022; Lihm, 2022).

In empirical tight-binding, it is customary to approximate the position matrix elements by dropping the second term in Eq. (58) (Foreman, 2002; Vanderbilt, 2018),

$$\langle \mathbf{0}i|\hat{\mathbf{r}}|\mathbf{R}j\rangle \approx \delta_{\mathbf{R},\mathbf{0}}\delta_{ij}\boldsymbol{\tau}_{j}$$
 (60)

In this approximation, and when the modified phase convention (31) is used, the matrix $\mathbf{A}_{\mathbf{k}'}^{W}$ in Eq. (57) vanishes; Eq. (55) for $\mathbf{A}_{\mathbf{k}'}^{H}$ then reduces to its first term, which can be interpreted as the "internal" Berry connection of the tight-binding eigenvectors; this is how tight-binding codes such as PythTB evaluate Berry phases and curvatures (PythTB, 2023b), which is quite natural in the context of toy-model calculations.

The above approximation is harder to justify when using ab initio WFs, given that the discarded $\mathbf{d}_{ij}(\mathbf{R})$ matrix elements are readily available, as mentioned above; even so, that approximation is made by some codes, including WannierTools (Wu et al., 2018) and linres (Železný, 2023). The role of intra-atomic $\mathbf{d}_{ij}(\mathbf{R})$ matrix elements in tight-binding calculations of the linear dielectric function was studied in Pedersen et al. (2001); in Ibañez-Azpiroz et al. (2022), that analysis was extended to inter-atomic matrix elements and to non-linear optical responses, using Wannier interpolation.

3. Other Berry-type quantities

The interpolation of the Berry curvature $\Omega_{\bf k}$ proceeds along similar lines, allowing to compute the AHC from Eq. (50) (Wang et al., 2006), and the procedure can be extended to spin Hall conductivity (SHC) (Qiao et al., 2018; Ryoo et al., 2019) or non-linear responses. For example, non-linear optical and AHCs involve k-derivatives of ${\bf A_k}$ and ${\bf \Omega_k}$, respectively (Aversa and Sipe, 1995; Sodemann and Fu, 2015); in the same way as band derivatives (see Sec. III.C.2), both are conveniently evaluated by Wannier interpolation (Ibañez Azpiroz et al., 2018; Liu et al., 2023; Wang et al., 2017). To interpolate ${\bf A_k}$, ${\bf \Omega_k}$,

and their k-derivatives, only $\langle \mathbf{0}i|\hat{H}|\mathbf{R}j\rangle$ and $\langle \mathbf{0}i|\hat{\mathbf{r}}|\mathbf{R}j\rangle$ are needed, but other quantities require additional matrix elements. For example, the orbital moment in Eq. (52) requires $\langle \mathbf{0}i|\hat{H}(\hat{\mathbf{r}}-\mathbf{R})|\mathbf{R}j\rangle$ and $\langle \mathbf{0}i|\hat{r}_a\hat{H}(\hat{r}-R)_b|\mathbf{R}j\rangle$ (Lopez et al., 2012); and while the former can be evaluated on the ab initio grid using the same ingredients entering Eqs. (12) and (59) for $\langle \mathbf{0}i|\hat{H}|\mathbf{R}j\rangle$ and $\langle \mathbf{0}i|\hat{\mathbf{r}}|\mathbf{R}j\rangle$, the latter also requires $\langle u_{m\mathbf{k}+\mathbf{b_1}}|\hat{H}_{\mathbf{k}}|u_{n\mathbf{k}+\mathbf{b_2}}\rangle$, which must be calculated separately (Lopez et al., 2012). As in the case of Eq. (55) for $A_{k'}$, the resulting interpolation formula contains an "internal" term analogous to Eq. (52) itself, but expressed in terms of the TB eigenvectors and Hamiltonian. That term can be evaluated from $\langle \mathbf{0}i|\hat{H}|\mathbf{R}j\rangle$ and $\boldsymbol{\tau}_{j}$ alone, but it leaves out important atomic-like contributions that are encoded in the other matrix elements needed for a full calculation (Lopez et al., 2012; Nikolaev and Solovyev, 2014).

The *ab initio* matrix elements needed for various interpolation tasks are listed in Table I. The files *.eig and *.mmn are required already for constructing the WFs, and therefore they are provided by the interface code of every *ab initio* code that is compatible with Wannier90. The file *.spn is provided by the interface of both Quantum ESPRESSO and VASP. As for the other matrix elements listed in Table I, at present they are only implemented in pw2wannier90.x, the interface of Quantum ESPRESSO.

As a workaround for obtaining these quantities from the output of other *ab initio* engines, one can resort to a sum-over-states procedure. For example, the uHu matrix elements may be expressed as

$$\langle u_{m\mathbf{k}+\mathbf{b_1}}|\hat{H}_{\mathbf{k}}|u_{n\mathbf{k}+\mathbf{b_2}}\rangle \approx \sum_{l}^{l_{\text{max}}} \langle u_{m\mathbf{k}+\mathbf{b_1}}|u_{l\mathbf{k}}\rangle \varepsilon_{l\mathbf{k}}\langle u_{l\mathbf{k}}|u_{n\mathbf{k}+\mathbf{b_2}}\rangle$$
(61)

in terms of the energy eigenvalues and overlap matrices, and the relevant matrices for spin Hall conductivity can be obtained similarly (Qiao et al., 2018). Since the summation is done before Wannierization, the number $l_{\rm max}$ of states included in the non-selfconsistent ab initio calculation can be systematically increased until the desired level of convergence is reached.

The above procedure is implemented for uHu, uIu, sHu and sIu in the utility mmn2uHu (WannierBerri, 2023) provided with the WannierBerri code package (Tsirkin, 2021). Besides its use as a workaround, it can serve as a benchmark for testing future implementations of those matrix elements in various interface codes between ab initio and Wannier engines.

F. Topological invariants and related properties

The topological aspects of band theory have been studied intensively over the past two decades (Hasan and Kane, 2010; Vanderbilt, 2018), and *ab initio* calculations have been central to that effort (Wang and Zhang, 2017):

they are used for identifying candidate topological materials, to determine topological invariants, and to calculate surface bands that can be compared with angle-resolved photoemission measurements.

WFs feature prominently in topological band theory. For example, quantum anomalous Hall insulators (Haldane, 1988) (a.k.a. Chern insulators) can be defined as 2D systems where it is not possible ¹ to construct a set of exponentially-localized WFs (Brouder et al., 2007; Thonhauser and Vanderbilt, 2006; Vanderbilt, 2018): this is known as a "topological obstruction". More generally, symmetry-protected topological insulators can typically be defined as insulators for which it is not possible to construct a set of WFs spanning the valence bands without breaking the protecting symmetry in the choice of gauge (Bradlyn et al., 2017; Soluyanov and Vanderbilt, 2011a). Prominent examples include 2D quantum spin Hall insulators (Bernevig and Zhang, 2006; Kane and Mele, 2005a,b) and 3D \mathbb{Z}_2 topological insulators (Fu et al., 2007), where the protecting symmetry is time reversal, and topological crystalline insulators, which are instead protected by crystalline symmetries (Fu, 2011).

A second example is the "Wannier spectrum" defined by the centers of hybrid (a.k.a. hermaphrodite) orbitals (Sgiarovello et al., 2001) that are Wannier-like along $\hat{\mathbf{z}}$ and Bloch-like along $\hat{\mathbf{x}}$ and $\hat{\mathbf{y}}$. The surface energy spectrum $\varepsilon_n(k_x,k_y)$ can be continuously deformed into the bulk Wannier spectrum $z_n(k_x,k_y)$ obtained by Wannierizing along the surface normal (Fidkowski et al., 2011; Neupert and Schindler, 2018), allowing to infer the topological flow of the surface energy bands from that of the bulk Wannier bands (Taherinejad et al., 2014). In some cases, the topological indices can be deduced from the Wannier band structure (Gresch et al., 2017; Varnava et al., 2020).

WFs also play a more practical role in the study of topological materials, as several of the electronic-structure packages that are commonly used to characterize them rely on a Wannier/TB representation (despite the obstruction mentioned above (Bradlyn et al., 2017; Soluyanov and Vanderbilt, 2011a), topological insulators still afford a Wannier representation, provided that the WFs span a few low-lying conduction states along with the valence bands).

In particular, both PythTB (PythTB, 2023a) and WannierTools (Wu et al., 2018) work with orthogonal TB models, and have the option to import TB Hamiltonians generated by a Wannier engine using either the *_hr.dat or the *_tb.dat file format (as mentioned above, the latter also includes the matrix elements of

Very recent work (Gunawardana et al., 2023) suggests that it might be possible to construct optimally localized WFs even in presence of non-vanishing Chern numbers, at least for the simple case of one isolated band.

Matrix element	Wannier90 file	Needed for	Implemented in	Computed by mmn2uHu from
$\langle u_{m\mathbf{k}} \hat{H}_{\mathbf{k}} u_{n\mathbf{k}}\rangle = \varepsilon_{n\mathbf{k}}\delta_{mn}$	*.eig	Transport, optics, $\mathbf{m}_{\mathbf{k}}^{\mathrm{orb}}$	All	
$\langle u_{m\mathbf{k}} \hat{\boldsymbol{\sigma}} u_{n\mathbf{k}}\rangle$	*.spn	$\mathbf{m}_{\mathbf{k}}^{ ext{spin}}$	QE,VASP	
$\langle u_{m\mathbf{k}} u_{n\mathbf{k}+\mathbf{b}}\rangle$	*.mmn	$\mathbf{A_k},\mathbf{\Omega_k},\mathbf{m_k^{\mathrm{orb}}},\mathrm{all}\mathrm{below}$	All	
$\langle u_{m\mathbf{k}+\mathbf{b}_1} \hat{H}_{\mathbf{k}} u_{n\mathbf{k}+\mathbf{b}_2}\rangle$	*.uHu	$\mathbf{m}^{\mathrm{orb}}_{\mathbf{k}}$	QE	*.eig, *.mmn
$\langle u_{m\mathbf{k}+\mathbf{b}_1} u_{n\mathbf{k}+\mathbf{b}_2}\rangle$	*.uIu	$q_{f k}^{ab}$	QE	*.mmn
$\langle u_{m\mathbf{k}} \hat{\boldsymbol{\sigma}}\hat{H}_{\mathbf{k}} u_{n\mathbf{k}+\mathbf{b}}\rangle$	$ \hat{\sigma}\hat{H}_{\mathbf{k}} u_{n\mathbf{k}+\mathbf{b}}\rangle$ *.sHu SHC in Ryoo et al. (2019)		QE	*.eig, *.mmn, *.spn
$\langle u_{m\mathbf{k}} \boldsymbol{\sigma} u_{n\mathbf{k}+\mathbf{b}}\rangle$	*.sIu	\ \ \ \ \ \ \ \ \ \ \ \ \ \ \ \ \ \ \	QE	*.mmn, *.spn

TABLE I Ab initio matrix elements that are used explicitly in setting up the WF matrix elements needed to perform common interpolation tasks, SHC stands for spin Hall conductivity. * denotes the seedname specified in the input file of Wannier90. QE = Quantum ESPRESSO, A_k is the Berry connection or electric dipole matrix (47), Ω_k is the Berry curvature (49), $\mathbf{m}_k^{\text{orb}}$ is the intrinsic orbital magnetic dipole (52), and q_k^{ab} is the intrinsic electric quadrupole (for the matrix definitions of $\mathbf{m}_k^{\text{orb}}$ and q_k^{ab} , see Óscar Pozo Ocaña and Souza (2023)). The optical conductivity (48) in the electric-dipole approximation involves $\varepsilon_{n\mathbf{k}}$ and A_k , the AHC (50) involves $\varepsilon_{n\mathbf{k}}$ and Ω_k , and the orbital magnetization (51) involves $\varepsilon_{n\mathbf{k}}$, Ω_k and $\mathbf{m}_k^{\text{orb}}$. Spatially-dispersive responses such as natural optical activity depend on $\varepsilon_{n\mathbf{k}}$, \mathbf{A}_k , $\mathbf{m}_k^{\text{orb}}$, $\mathbf{m}_k^{\text{spin}}$, and q_k^{ab} (Óscar Pozo Ocaña and Souza, 2023). The mmn (and eig) matrix elements are needed for constructing the (disentangled) WFs, and hence they are used implicitly when interpolating any physical quantity.

the position operator in the Wannier basis, and the coordinates of the lattice vectors). The key point is that the Wannierized Hamiltonian preserves the topological features of the original first-principles electronic structure; the identification and characterization of those features can therefore be carried out entirely in the Wannier representation, which is often more convenient and/or efficient than proceeding directly from the *ab initio* Bloch states.

The simplest example of a topological band-structure feature is an isolated touching between a pair of bands, known as a "Weyl point" (Armitage et al., 2018; Vanderbilt, 2018). Weyl points are fundamentally different from weak avoided crossings, but most band interpolation schemes are unable to tell them apart; instead, Wannier interpolation correctly distinguishes between the two. The distinction is rooted in the fact that a Weyl node acts as a monopole source or sink of Berry curvature in **k** space, allowing to associate with it a topological invariant known as the "chiral charge."

The chiral charge χ (typically ± 1 , but sometimes ± 2 or ± 3 (Fang *et al.*, 2012; Tsirkin *et al.*, 2017)) can be determined in two different ways: (i) from the quantized Berry-curvature flux through a small surface $\mathcal S$ enclosing the Weyl point (Gosálbez-Martínez *et al.*, 2015; Vanderbilt, 2018),

$$\int_{\mathcal{S}} \mathbf{\Omega}_{n\mathbf{k}} \cdot \hat{\mathbf{n}} = -2\pi\chi \,, \tag{62}$$

where $\hat{\mathbf{n}}$ is a unit vector in the direction of $\nabla_{\mathbf{k}} \varepsilon_{n\mathbf{k}}$; (ii) by evaluating the Berry phase

$$\phi_n(\mathcal{C}) = \oint_{\mathcal{C}} \mathbf{A}_{nn\mathbf{k}} \cdot d\mathbf{k} \tag{63}$$

around contours C at fixed latitude on an enclosing spherical surface, and then tracking its evolution from zero at the south pole to $2\pi\chi$ at the north pole (Gresch *et al.*, 2017).

The latter procedure is implemented in both Z2Pack (Z2pack, 2023) and WannierTools. All that is required is the TB Hamiltonian $\langle 0i|\hat{H}|\mathbf{R}j\rangle$, from which one obtains the eigenvectors on a discrete mesh $\{\mathbf{k}_j\}$ of points along each contour; the Berry phase is then evaluated by finite differences from the overlaps between TB eigenvectors on consecutive points along $\mathcal C$ as follows (Vanderbilt, 2018),

$$\phi_n^{(\text{int})}(\mathcal{C}) = -\text{Im } \ln \Pi_j \langle\!\langle \phi_{n\mathbf{k}_j} |\!| \phi_{n\mathbf{k}_{j+1}} \rangle\!\rangle, \qquad (64)$$

where $||u_{n\mathbf{k}_j}||$ denotes a column vector of the matrix $\mathcal{U}_{\mathbf{k}_j}$ defined by Eq. (14). The above expression corresponds, in the language of Sec. III.E, to the internal part of the Berry phase (63), which also contains an external part

$$\phi_n^{(\text{ext})}(\mathcal{C}) = \sum_{i} \langle \langle u_{n\mathbf{k}_j} | | \mathbf{A}_{\mathbf{k}}^{W} | | u_{n\mathbf{k}_j} \rangle \cdot \Delta \mathbf{k}, \qquad (65)$$

where $\Delta \mathbf{k} = (\mathbf{k}_{j+1} - \mathbf{k}_{j-1})/2$ (Wang et al., 2007). The two parts arise from discretizing the integral along \mathcal{C} of the two terms in Eq. (55) for the interpolated Berry connection; the internal term only depends on $\langle \mathbf{0}i|\hat{H}|\mathbf{R}j\rangle$, while the external one also requires $\langle \mathbf{0}i|\hat{\mathbf{r}}|\mathbf{R}j\rangle$. The 2π indeterminacy in the Berry phase comes from the former, while the latter is single-valued and hence it does not contribute to the quantized change in Berry phase from the south to the north pole of a spherical surface; this is why χ can be determined from the TB Hamiltonian alone.

Weyl crossings can occur at arbitrary points in the BZ, which makes it difficult to spot them in the band structure. By allowing to quickly evaluate energy eigenvalues and band velocities at arbitrary k-points, Wannier interpolation provides a practical solution to this problem (Gosálbez-Martínez et al., 2015): to locate the degeneracies between bands n and n+1, define a gap function $\varepsilon_{n+1\mathbf{k}} - \varepsilon_{n\mathbf{k}}$, and search for its minima using a

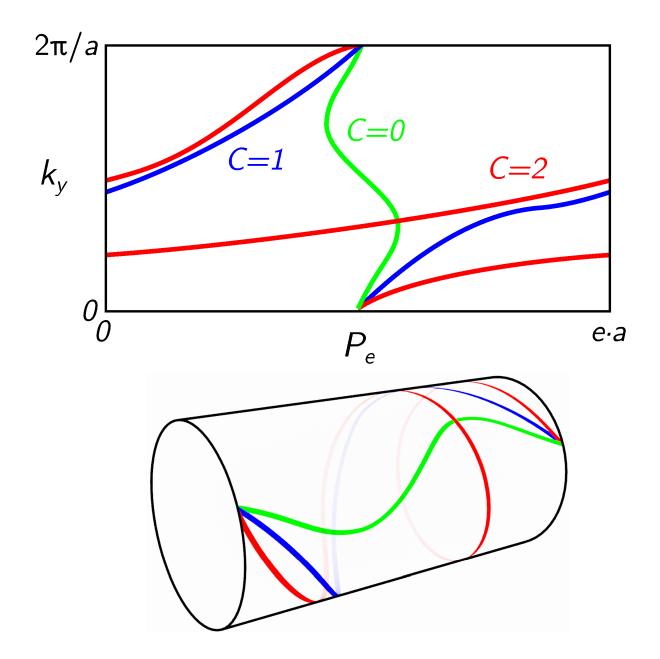


FIG. 6 Sketch of some possible evolutions of hybrid polarization $P_e(k_y)$, i.e. the sum of hybrid Wannier charge centers, across the BZ. Chern numbers C correspond to different winding numbers. See Gresch *et al.* (2017) for an in-depth discussion.

minimization method such as conjugate-gradient, starting from a sufficiently dense grid of k-points. After discarding local minima where the gap function is above some numerical threshold, one is left with candidate degeneracies that can be further characterized; they include not only point nodes such as Weyl and Dirac nodes (Armitage $et\ al.,\ 2018$), but also nodal lines (Fang $et\ al.,\ 2018$). This procedure is implemented in WannierTools.

Topological materials feature characteristic boundary modes that reflect the bulk topology (Hasan and Kane, 2010; Vanderbilt, 2018). In the case of Weyl semimetals, those modes take the form of "Fermi arcs" connecting the projections of bulk Weyl nodes of opposite chirality onto the surface BZ (Armitage et al., 2018; Vanderbilt, 2018). PythTB and WannierTools allow to terminate a bulk TB model along specified directions, creating ribbons or slabs whose boundary modes can then be inspected by plotting the energy bands. WannierTools also has the option to obtain a surface spectral function from the Green's function calculated for a semi-infinite system.

As already mentioned, another very useful tool for diagnosing topological behaviors is a hybrid representation of the electronic structure in terms of orbitals that are localized in one spatial direction only, remaining extended in the others (Sgiarovello et al., 2001). To define these hybrid Wannier functions (HWFs) for lattices of arbitrary symmetry, it is convenient to work in reduced coordinates. Consider a 2D crystal, and let $\mathbf{k} = k_1 \mathbf{b}_1 + k_2 \mathbf{b}_2$ and $\hat{\mathbf{r}} = \hat{x}_1 \mathbf{a}_1 + \hat{x}_2 \mathbf{a}_2$. Choosing \mathbf{b}_2 as the localization

direction, the HWFs are defined as

$$|h_{k_1 ln}\rangle = \frac{1}{N_2} \sum_{k_2} e^{-i2\pi k_2 l} |\psi_{n\mathbf{k}}\rangle ,$$
 (66)

where N_2 is the number of distinct values of k_2 in the BZ, and l labels cells along \mathbf{a}_2 . The topological indices can be determined from the hybrid Wannier centers

$$x_{2,k_1ln} = \langle h_{k_1ln} | \hat{x}_2 | h_{k_1ln} \rangle;$$
 (67)

for bulk materials, the analysis is carried out on highsymmetry BZ planes. This hybrid-Wannier (or "Wilsonloop") scheme is implemented in Z2Pack, and a detailed description of the methodology can be found in Gresch et al. (2017). In Z2Pack, the hybrid Wannier centers (67) are obtained from a parallel-transport construction, starting from the overlap matrices (8) (Taherinejad et al., 2014). The same procedure is implemented in PythTB and WannierTools for Wannier/TB Hamiltonians; the needed overlaps are then taken between TB eigenstates, as in Eq. (64) above (Z2Pack can also operate in this mode). We remark that Z2Pack (Gresch et al., 2017) allows to work both with Wannier/TB Hamiltonians, and directly with first-principles engines such as Quantum ESPRESSO and VASP.

In closing, it is worth bearing in mind the different design philosophies of the three packages surveyed in this section. As already mentioned in Sec. III.C, PythTB (PythTB, 2023a) was designed with TB "toy models" in mind, and to be used as a pedagogical tool; it allows to compute several geometric and topological quantities (Berry phases and curvatures, Chern numbers, hybrid Wannier centers), and to generate ribbons and slabs to expose their boundary modes. Although PythTB can also import large Wannier models (which can be truncated internally), the code is not optimized for speed; however, a high-performance Numba (Lam et al., 2015) implementation of PythTB better suited for that purpose is available (Numba-PythTB, 2023). WannierTools (Wu et al., 2018), on the other hand, is primarily designed to work with large Wannier models, and is parallelized using MPI. Its distinctive features include searching for band degeneracies, and plotting surface spectral functions. Finally, Z2Pack is focused on the HWF scheme; it is not primarily a "post-Wannier" code, since it can circumvent the need to use a Wannier engine by directly reading the ab initio overlap matrices, which can help streamline high-throughput calculations (Grassano et al., 2023; Marrazzo et al., 2019).

While topological invariants are generally introduced for crystalline periodic systems in PBCs, there are a number of scenarios that require either the use of open boundary conditions (OBCs) or the adoption of large supercells with Γ -only sampling; in both cases, standard approaches are of no avail. Relevant examples include the study of Anderson (Groth et al., 2009; Jiang et al.,

2009; Li et al., 2009) and amorphous topological insulators (Corbae et al., 2023), heterogeneous systems such as trivial/topological junctions (Bianco and Resta, 2011), molecular dynamics simulations, and any other use case that does not fit a small primitive cell with BZ sampling. Among many other approaches (see Corbae et al. (2023) for a dedicated overview), single-point sampling (Ceresoli and Resta, 2007; Favata and Marrazzo, 2023) and local markers (Bianco and Resta, 2011) have been introduced to study topology for non-crystalline systems.

Thanks to the use of WFs as a basis set, these techniques can be implemented seamlessly in the same framework both for model TB (like the Haldane (Haldane, 1988) or the Kane-Mele models (Kane and Mele, 2005a,b)) and ab initio TB, where the latter is obtained by constructing WFs on top of any electronic structure calculations including DFT, GW or DMFT (as discussed in Sec. III.C). This strategy has been adopted by the StraWBerryPy code (Baù and Marrazzo, 2023; Favata and Marrazzo, 2023; StraWBerryPy, 2023), where model or ab initio TB Hamiltonians are read and manipulated either through PythTB or TBmodels, allowing to calculate a few single-point and local topological invariants such as the Chern number and the \mathbb{Z}_2 invariant, as well as other quantum-geometrical quantities of the electronic structure that are relevant for topological materials.

G. Electron-phonon interactions

1. Methodology

In the past decade, we have witnessed a communitywide effort to develop advanced computational approaches and simulation tools for atomistic modeling of function-defining properties of materials. A primary focus of this ongoing research has been the accurate description of electron-phonon (e-ph) interactions from first-principles (Giustino, 2017), as they determine many materials properties of technological interest such as electrical and thermal transport (Brunin et al., 2020a,b; Chaves et al., 2020; Cheng et al., 2020; Jhalani et al., 2020; Li, 2015; Macheda et al., 2022; Macheda and Bonini, 2018; Maliyov et al., 2021; Park et al., 2020; Poncé et al., 2020; Poncé et al., 2021, 2018, 2023; Protik and Broido, 2020; Protik and Kozinsky, 2020; Zhou et al., 2021b), phonon-assisted light absorption (Bushick and Kioupakis, 2023; Noffsinger et al., 2012), phononmediated superconductivity (Errea et al., 2020; Heil et al., 2017; Lafuente-Bartolome et al., 2020; Lilia et al., 2022; Margine and Giustino, 2013), and polaron formation (Falletta and Pasquarello, 2022; Lafuente-Bartolome et al., 2022; Lee et al., 2021; Sio and Giustino, 2023; Sio et al., 2019; Zhou and Bernardi, 2019). A comprehensive review of the theory of e-ph interactions in solids from the point of view of ab initio calculations is given by

Giustino (Giustino, 2017). An important contribution to the e-ph problem has been recently made by Stefanucci and colleagues (Stefanucci et al., 2023), who have developed an ab initio many-body quantum theory of electrons and phonons in and out-of-equilibrium.

There is a well established formalism for computing the e-ph matrix elements from first-principles using DFPT (Baroni et al., 2001, 1987; Gonze, 1997; Savrasov, 1992). However, all aforementioned properties are notoriously difficult to evaluate with desired accuracy using DFPT calculations directly due to the prohibitive computational cost. To achieve numerical convergence, the e-ph matrix elements need to be computed on ultra-dense electron (k) and phonon (q) BZ grids with $10^6 - 10^7$ points. Specialized numerical techniques, such as linear (Brunin et al., 2020b; Li, 2015) or Wannier (Calandra et al., 2010; Giustino et al., 2007a,b) interpolation and Fermi-surface harmonics (Allen, 1976; Lafuente-Bartolome et al., 2020), have been developed to address this problem. In particular, the interpolation of the e-ph matrix elements using MLWFs (Marzari et al., 2012) introduced by Giustino, Cohen, and Louie (Giustino et al., 2007a) has proven very successful for enabling highly accurate and efficient calculations of e-ph interactions, and the approach has been implemented in a number of codes (Cepellotti et al., 2022; Lee et al., 2023; Marini et al., 2023; Noffsinger et al., 2010; Poncé et al., 2016; Zhou et al., 2021a).

We note that an alternative to the computation of the e-ph interaction with DFPT is offered by the finite displacement scheme in real space (Chaput et al., 2019; Engel et al., 2020, 2022). While this approach requires large supercells to reach convergence, it has the advantage of being universally applicable to any functional, including hybrid or metagradient functionals, as well as more complicated exchange-correlation potentials, where higher-order derivatives of the functional are not readily available.

Below, we focus on the DFPT approach and outline the interpolation procedure to compute the e-ph matrix elements on ultra-dense meshes using WFs. One first determines the e-ph matrix elements in the Bloch representation using the electronic and vibrational properties, computed with DFT and DFPT on coarse **k**- and **q**-point grids, respectively. The e-ph matrix element is defined as:

$$g_{mn\nu}(\mathbf{k}, \mathbf{q}) = \langle \psi_{m\mathbf{k}+\mathbf{q}} | \Delta_{\mathbf{q}\nu} V^{KS} | \psi_{n\mathbf{k}} \rangle,$$
 (68)

where $\psi_{n\mathbf{k}}$ and $\psi_{m\mathbf{k}+\mathbf{q}}$ are the KS wavefunctions of the initial and final Bloch states (with \mathbf{k} being the electron wavevector, and n being the band index), and $\Delta_{\mathbf{q}\nu}V^{\mathrm{KS}}$ is the derivative of the self-consistent potential associated with a phonon with momentum \mathbf{q} and branch index ν . The latter quantity can be obtained as:

$$\Delta_{\mathbf{q}\nu}V^{\mathrm{KS}} = \sum_{\kappa\alpha p} e^{i\mathbf{q}\cdot\mathbf{R}_p} \frac{\partial V^{\mathrm{KS}}}{\partial \tau_{\kappa\alpha p}} u_{\kappa\alpha,\mathbf{q}\nu}, \tag{69}$$

with

$$u_{\kappa\alpha,\mathbf{q}\nu} = \sqrt{\frac{\hbar}{2M_{\kappa}\omega_{\mathbf{q}\nu}}} e_{\kappa\alpha,\mathbf{q}\nu}.$$
 (70)

Here \mathbf{R}_p is the lattice vector identifying the unit cell p, $\tau_{\kappa\alpha p}$ is the position of atom κ in unit cell p in the Cartesian direction α , M_{κ} is the mass of atom κ , $\omega_{\mathbf{q}\nu}$ is the phonon frequency, and $e_{\kappa\alpha,\mathbf{q}\nu}$ is the eigendisplacement vector corresponding to atom κ in the Cartesian direction α for a collective phonon mode $\mathbf{q}\nu$.

Next, one finds the e-ph matrix elements in the Wannier representation:

$$g_{ij\kappa\alpha}(\mathbf{R}_e, \mathbf{R}_p) = \left\langle \mathbf{0}_e i \left| \frac{\partial V^{KS}}{\partial \tau_{\kappa\alpha p}} \right| \mathbf{R}_e j \right\rangle,$$
 (71)

where \mathbf{R}_e and \mathbf{R}_p are the Bravais lattice vectors associated to the electron and phonon WS supercells, and $|\mathbf{R}_e j\rangle$ are the MLWFs with index j and centered in the cell at \mathbf{R}_e . This is done by transforming the e-ph matrix elements from the coarse BZ (\mathbf{k}, \mathbf{q}) grids into the corresponding real-space supercells $(\mathbf{R}_e, \mathbf{R}_p)$ as:

$$g_{ij\kappa\alpha}(\mathbf{R}_e, \mathbf{R}_p) = \frac{1}{N_e N_p} \sum_{\mathbf{k}, \mathbf{q}} e^{-i(\mathbf{k} \cdot \mathbf{R}_e + \mathbf{q} \cdot \mathbf{R}_p)}$$

$$\times \sum_{mn\nu} V_{\mathbf{k}+\mathbf{q}, im}^{\dagger} g_{mn\nu}(\mathbf{k}, \mathbf{q}) V_{\mathbf{k}, nj} u_{\kappa\alpha, \mathbf{q}\nu}^{-1}. \tag{72}$$

In Eq. (72), N_e and N_p are the number of unit cells in the periodic BvK supercells corresponding to the number of \mathbf{k} and \mathbf{q} points on the coarse electron and phonon grids, respectively, and $V_{\mathbf{k}}$ is the Wannierization matrix introduced in Eq. (5). That matrix is provided by the Wannier engine, while $u_{\kappa\alpha,\mathbf{q}\nu}$ is obtained by diagonalizing the dynamical matrix at wavevector \mathbf{q} .

Finally, performing the inverse Fourier transform of Eq. (72), the e-ph matrix elements on very fine $(\mathbf{k}', \mathbf{q}')$ BZ grids are given by:

$$g_{mn\nu}(\mathbf{k}', \mathbf{q}') = \sum_{ep} e^{i(\mathbf{k}' \cdot \mathbf{R}_e + \mathbf{q}' \cdot \mathbf{R}_p)}$$

$$\times \sum_{ij\kappa\alpha} \mathcal{U}_{\mathbf{k}' + \mathbf{q}', mi} g_{ij\kappa\alpha}(\mathbf{R}_e, \mathbf{R}_p) \mathcal{U}_{\mathbf{k}', jn}^{\dagger} u_{\kappa\alpha, \mathbf{q}'\nu}. \tag{73}$$

In this step, it is assumed that the e-ph matrix elements outside of the WS supercells defined by the initial coarse grids can be neglected. Prior to computing Eq. (73), the transformation matrices $\mathcal{U}_{\mathbf{k}',nj}$ given by Eq. (14) and the phonon eigenvectors $u_{\kappa\alpha,\mathbf{q}'\nu}$ for the new set of points $(\mathbf{k}',\mathbf{q}')$ must be found as described in Giustino et al. (2007a).

The accuracy of the Wannier–Fourier interpolation approach depends on the spatial localization of the $g_{ij\kappa\alpha}(\mathbf{R}_e,\mathbf{R}_p)$ matrix elements. Eq. (71) can be seen as a hopping integral between two localized WFs, one at $\mathbf{0}_e$ and one at \mathbf{R}_e , due to a perturbation caused by

the displacement of the atom at $\tau_{\kappa p}$. If the e-ph interactions are short-ranged in real space, the quantity $g_{ij\kappa\alpha}(\mathbf{R}_e,\mathbf{R}_p)$ decays rapidly with $|\mathbf{R}_e|$ and $|\mathbf{R}_p|$, and it is sufficient to only compute the matrix elements on a small set of $(\mathbf{R}_e, \mathbf{R}_p)$ lattice vectors to fully capture the coupling between electrons and phonons. As discussed in Giustino (2017) and Giustino et al. (2007a), the spatial decay is bound by the limiting cases $g_{ij\kappa\alpha}(\mathbf{R}_e,\mathbf{0}_p)$ and $g_{ij\kappa\alpha}(\mathbf{0}_e,\mathbf{R}_p)$. In the first case, the matrix element decays in the variable \mathbf{R}_e at least as fast as the MLWFs. In the second case, the matrix element decays with the variable \mathbf{R}_p at the same rate as the screened Coulomb potential generated by the atomic displacements. Thus, the localization of $g_{ij\kappa\alpha}(\mathbf{R}_e,\mathbf{R}_p)$ depends strongly on the dielectric properties of the system. In metals and non-polar semiconductors, the screening properties are dictated by Friedel oscillations (Fetter and Walecka, 2003) $|\mathbf{R}_p|^{-4}$ and quadrupole behavior (Pick et al., 1970) $|\mathbf{R}_p|^{-3}$, respectively. In polar materials (i.e., ionic and polar covalent crystals), the dominant contribution to the potential is the dipole Fröhlich term (Vogl, 1976), which is long-ranged and decays as $|\mathbf{R}_p|^{-2}$. As a consequence, some of the matrix elements in reciprocal space diverge as $|\mathbf{q}|^{-1}$ in the long-wavelength limit $(\mathbf{q} \rightarrow 0)$, and cannot be directly interpolated from a coarse to a fine grid using the Wannier-based interpolation approach. Recent methodologies have been developed for including long-range dipole (Deng et al., 2021; Sjakste et al., 2015; Sohier et al., 2016; Verdi and Giustino, 2015) and quadrupole (Brunin et al., 2020a,b; Jhalani et al., 2020; Park et al., 2020; Zhang and Liu, 2022) corrections in the interpolation of the e-ph matrix elements.

2. Codes

EPW (EPW, 2023; Lee et al., 2023; Noffsinger et al., 2010; Poncé et al., 2016), the first open-source code for the study of e-ph interaction using MLWFs, was publicly released in 2010 and has been distributed within the Quantum ESPRESSO suite (Giannozzi et al., 2017; Quantum ESPRESSO, 2023) since 2016. eral Wannier-based open-source codes exist today to compute physical properties related to e-ph interactions such as Perturbo (PERTURBO, 2023; Zhou et al., 2021a), Phoebe (Cepellotti et al., 2022; Phoebe, 2023), elphbolt (EPIq, 2023a; Protik et al., 2022), and EPIq (EPIq, 2023b; Marini et al., 2023). At present, EPW, Perturbo, Phoebe, and EPIq are all interfaced with Quantum ESPRESSO (Giannozzi et al., 2017) to generate the relevant first-principles input data, and use Wannier90 (Pizzi et al., 2020) in standalone or library mode to compute the required quantities in the Wannier representation. elphbolt, on the other hand, relies on EPW to generate the required Wannier space information. All codes follow an overall similar workflow to compute

e-ph matrix elements on fine grids, as outlined below and summarized in Fig. 7.

- 1. The initial step is to perform DFT calculations with Quantum ESPRESSO on a uniform coarse electronic k-point grid to obtain the band energies and Bloch wavefunctions, and DFPT calculations with Quantum ESPRESSO on an irreducible coarse q-point grid to obtain the dynamical matrices and the derivatives of the self-consistent potential with respect to the phonon perturbations. Phoebe and EPIq require that the e-ph matrix elements on the coarse electron and phonon grids are also computed with Quantum ESPRESSO since these quantities are later passed to the two codes. EPW and PERTURBO, on the other hand, compute the e-ph matrix elements on the coarse k- and q-point grids internally by reading the files generated from the DFT and DFPT calculations.
- 2. Next, one must perform a precise Wannierization of the system using Wannier90 in standalone mode with PERTURBO, Phoebe, and EPIq, or in library mode with EPW. This step produces the MLWFs and the Wannierization matrices $V_{\mathbf{k}}$ that transform the DFT Bloch wavefunctions into MLWFs.
- 3. The next step is to compute the e-ph matrix elements on the coarse **k** and **q**-point grids in the Bloch representation and transform them, along with the electronic Hamiltonian and the dynamical matrix, from the Bloch to the Wannier representation. As noticed at point 2, Phoebe and EPIq uses the e-ph matrix elements on the coarse electron and phonon grids computed directly with Quantum ESPRESSO.
- 4. The final step is to perform an inverse Fourier transform of the electronic Hamiltonian, dynamical matrix, and e-ph matrix elements from the Wannier to the Bloch representation. At this stage, the electronic eigenvalues, phonon frequencies, and e-ph matrix elements can be efficiently computed on ultra-dense \mathbf{k}' and \mathbf{q}' -point grids and further used to carry out calculations of various materials properties.

To extend the Wannier-based interpolation scheme to systems with long-range e-ph contributions, the strategy is to split the e-ph matrix elements into a short- and long-range part. Then, the short-range e-ph matrix elements are interpolated to ultra-dense \mathbf{k}' - and \mathbf{q}' -point grids using MLWFs, while the long-range e-ph matrix elements are computed using derived first-principles expressions for the dipole and quadrupole e-ph interactions. Finally, the short- and long-range components are summed up to recover the total e-ph matrix elements.

A wide range of properties can be currently computed with EPW, Perturbo, Phoebe, elphbolt, and EPIq. A full list of the capabilities for the released version of each code can be found on the respective website. In particular, EPW computes phonon-limited transport properties in the framework of the BTE, magnetotransport, phonon-mediated superconducting properties based on the Migdal–Eliashberg formalism, phonon-assisted op-

tical processes, and polarons (EPW, 2023; Lee et al., 2023). EPW also comes with the ZG toolkit for calculations of temperature-dependent e-ph properties for harmonic and anharmonic phonons via the special displacement method (Zacharias and Giustino, 2016, 2020; Zacharias et al., 2023a,b). Perturbo calculates phonon-limited transport properties using BTE, ultrafast carrier dynamics, magnetotransport, and high-field transport (PER-TURBO, 2023; Zhou et al., 2021a). Perturbo is interfaced with TDEP (TDEP, 2023) to compute anharmonic phonons. Phoebe provides various tools to predict electron and phonon transport properties at different levels of theory and accuracy, such as the BTE or models based on the Wigner distribution (Cepellotti et al., 2022; Phoebe, 2023). elphbolt solves the coupled electron and phonon BTEs, and the effect of the mutual eph drag on the electrical and thermal transport coefficients (EPIq, 2023a; Protik et al., 2022). EPIq computes phonon-mediated superconducting properties based on the Migdal-Eliashberg formalism, double resonant Raman intensities, and excited carriers lifetimes (EPIq, 2023b; Marini et al., 2023).

H. Beyond DFT with localized orbitals

While in most cases DFT is the method of choice for electronic ground state calculations, and even the ground state properties of certain materials, may require a "beyond-DFT" treatment for accurate first-principles predictions. Two examples are finite-temperature and spectroscopic properties, as observed in direct and inverse photoemission experiments, which cannot be addressed adequately within conventional DFT. Similarly, the complex physics arising from strong local Coulomb interaction in partially filled orbitals is beyond the scope of a single-particle picture, which can manifest itself in an inaccurate description of the material. In such cases, more advanced methods are needed. One class of approaches is based on diagrammatic many-body perturbation theory; examples include the GW approximation or DMFT (see Sec. III.H.1). Since such methods are often computationally costly and complex, it may be necessary to extract accurate low-energy effective Hamiltonians that are treated using these methods in a postprocessing step. An efficient alternative is to retain the functional character of DFT and apply physically motivated corrections, as in hybrid or Koopmans-compliant functionals (see Sec. III.H.2). In this case the theory is no longer based on a pure functional of the density, but the orbitals themselves or their orbital densities become the key variables. Common to both approaches is the importance of improving the description of local, orbitaldependent physics. This is where WFs come in, providing a useful basis for such applications and supporting the physical understanding with chemical intuition.

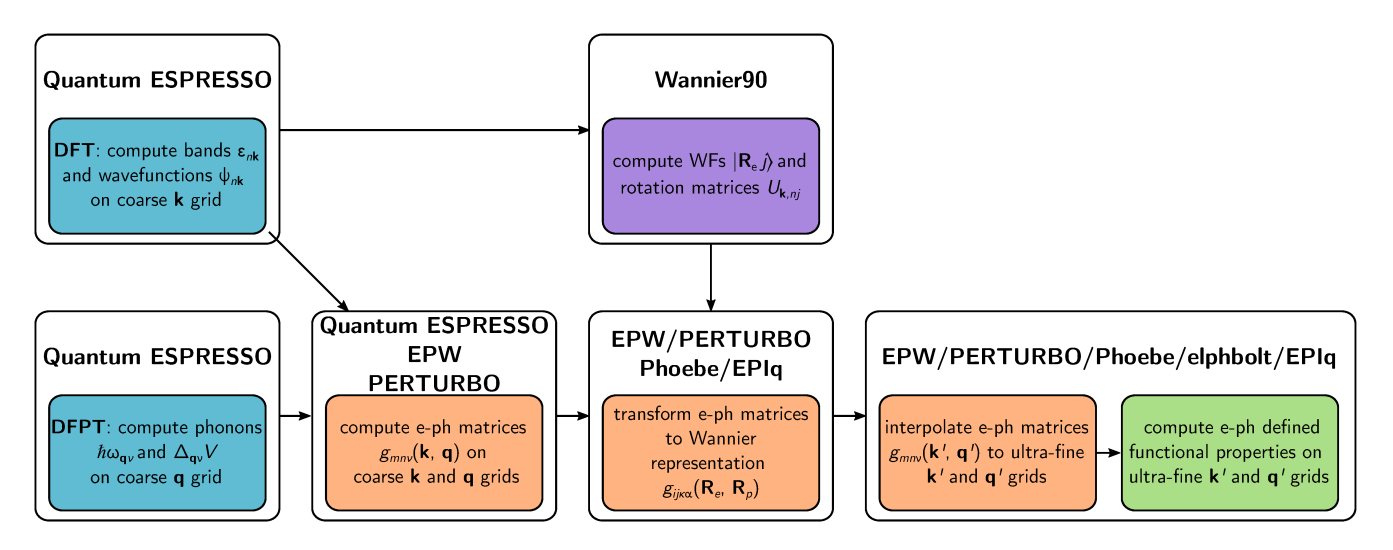


FIG. 7 Workflow to compute e-ph interactions on ultra-fine grids using WFs. The user performs DFT and DFPT calculations on coarse **k** and **q**-point grids with **Quantum ESPRESSO**. Next, the user computes the e-ph matrix elements on the coarse grids and transforms them in localized Wannier basis using the rotation matrices obtained with **Wannier90**. Note that **Phoebe** and **EPIq** read the e-ph matrix elements on the coarse grids computed with **Quantum ESPRESSO**, while **EPW** and **PERTURBO** compute them internally. Finally, **EPW/PERTURBO/Phoebe/EPIq** interpolate the band structure, phonon dispersion, and e-ph matrix elements on ultra-fine **k**'- and **q**'-point grids, and perform calculations of various materials properties.

1. Dynamical mean-field theory and embedding

Strongly correlated electron systems host a wide variety of physical phenomena, ranging from Mott physics to high-temperature superconductivity to exotic ordered phases (Tokura et al., 2017). Fundamental to these phenomena is the competition of itinerant versus localized character of electrons, which requires computational methods beyond the single-particle picture. While the representation of electronic states in reciprocal space can be beneficial, the theory of strong local correlations is most naturally formulated in a real-space basis. A key aspect of many beyond-DFT schemes is therefore the combination of itinerant Bloch states with localized molecular orbitals, which can be elegantly formalized with WFs (Lechermann et al., 2006).

Beyond-DFT schemes are typically computationally demanding and require a compromise in terms of the number of orbitals that can be treated. Starting from an ab initio description of a large number of bands, it is common practice to select a subset of correlated orbitals, such as those describing electronic states in the vicinity of the Fermi level, using projector functions. The result is a so-called downfolded model, which contains only the relevant degrees of freedom (Kotliar et al., 2006). It divides the total system into a subspace of localized orbitals, for which a higher-level method is used, and the remaining KS states, for which the single-particle description within DFT accurately reflects the physics. The embedding ansatz is further justified by the observation that correlated physics phenomena typically occur on energy scales of meV to a few eV (Chen et al., 2022). For the

remainder of this subsection we focus on DMFT as the higher-level method to solve the downfolded many-body problem, but the concepts can be similarly applied to its extensions (see below) and conceptual other approaches (see, e.g., Eskridge *et al.* (2019); Muechler *et al.* (2022); Sheng *et al.* (2022); and Zgid and Gull (2017)).

While the multiband Hubbard model studied with DMFT is naturally related to TB models, a rigorous formalism based on energy functionals allows the combined approach with ab initio methods, as in DFT+DMFT (Kotliar et al., 2006). The development of DFT+DMFT methods and software for strongly correlated materials has seen a tremendous surge in the last few decades (Held, 2007; Paul and Birol, 2019; Pavarini et al., 2011). Routine calculations allow to compute single-particle spectra (Anisimov et al., 2005; Nekrasov et al., 2006; Pavarini et al., 2004), optical conductivity (Haule et al., 2005; Wissgott et al., 2012), transport (Oudovenko et al., 2006; Zingl et al., 2019) and thermoelectric properties (Arita et al., 2008; Tomczak et al., 2012; Wissgott et al., 2010), electronic Raman (Blesio et al., 2023), and two-particle correlation functions (susceptibilities) (Boehnke et al., 2011; Kuneš, 2011; Park et al., 2011). Recent advances include interactions with core holes as in x-ray absorption and photoemission spectroscopy, and resonant inelastic x-ray scattering (Hariki et al., 2017, 2018; Haverkort et al., 2012; Lüder et al., 2017). Furthermore, routines for lattice optimization (Haule and Pascut, 2016; Leonov et al., 2014; Plekhanov et al., 2021) and for computing phonon spectra (Kocer et al., 2020) have been formalized. This list of references is by no means exhaustive, but is intended to serve as a starting point for the respective topics.

In beyond-DFT methods, it is convenient to describe the total system of interacting electrons in a periodic solid in terms of the momentum- and frequencydependent retarded single-particle Green's function

$$\hat{G}(\mathbf{k},\omega) = \left[(\omega + \mu) \mathbb{1} - \hat{H}(\mathbf{k}) - \hat{\Sigma}(\mathbf{k},\omega) + i\eta \right]^{-1}, \quad (74)$$

where μ is the chemical potential and $H(\mathbf{k})$ represents the non-interacting Hamiltonian. The frequency- and momentum-dependent electron self-energy is given by $\Sigma(\mathbf{k},\omega)$, and η is an infinitesimal positive parameter to ensure physical correctness. For clarity, we have omitted the double-counting correction here, and we refer to Karolak et al. (2010) for an overview. Starting from a DFT-derived downfolded Hamiltonian, the challenge is to compute the corresponding self-energy correction that accounts for dynamical interaction effects. ious approaches can be formalized, but for the purpose of this review we outline the workflow of single-site DMFT (Georges et al., 1996). In DMFT, the self-energy becomes a site-local quantity for a given atomic site \mathcal{R} within the unit cell when expressed in a localized orbital basis. This approximation is conceptually similar to DFT+U (Anisimov et al., 1997), but in DMFT the full frequency dependence of the interaction is taken into account. Following this approach, in the DMFT selfconsistency cycle, the local lattice self-energy $\Sigma^{\mathcal{R}}(\omega)$ is approximated by that of an auxiliary quantum impurity problem. The most computationally challenging step of the DMFT loop is typically to find the solution to the impurity problem, which allows to infer the impurity selfenergy via the Dyson equation. The self-energy is embedded into the Hilbert space of the effective Hamiltonian as

$$\Sigma_{mn}(\mathbf{k},\omega) = \sum_{\mathcal{R},ij} P_{mi}^{\mathcal{R}*}(\mathbf{k}) \Sigma_{ij}^{\mathcal{R}}(\omega) P_{jn}^{\mathcal{R}}(\mathbf{k}).$$
 (75)

Approximating the lattice self-energy in Eq. (74) by the upfolded impurity self-energy becomes exact for infinite connectivity of the lattice (Georges and Kotliar, 1992; Metzner and Vollhardt, 1989). The projector functions $P_{jn}^{\mathcal{R}}(\mathbf{k})$ in (75) encode the basis transformation from band to orbital basis, i.e., from $|\psi_{n\mathbf{k}}\rangle$, with band index n and wavevector \mathbf{k} , to $|\psi_{\mathcal{R}_{j}\mathbf{k}}^{W}\rangle$, with orbital index j at site \mathcal{R} (i.e., j is an intrasite index here):

$$P_{jn}^{\mathcal{R}}(\mathbf{k}) = \langle \psi_{\mathcal{R}_j \mathbf{k}}^{\mathbf{W}} | \psi_{n\mathbf{k}} \rangle . \tag{76}$$

The local Green's function is then computed as $G_{ij}^{\mathrm{loc},\mathcal{R}}(\omega) = \frac{1}{N} \sum_{\mathbf{k},mn} P_{im}^{\mathcal{R}}(\mathbf{k}) G_{mn}(\mathbf{k},\omega) P_{nj}^{\mathcal{R}*}(\mathbf{k})$, where N is the total number of k-points of the grid. To determine a suitable localized basis set, some DFT+DMFT codes use projections on atomic orbitals, others rely on Wannier90 directly for a simple and user-friendly interface. While the two approaches are conceptually similar

(for a more detailed overview see Chen et al. (2022)), the choice of projectors may affect the results and therefore needs to be carefully analyzed (Karp et al., 2021). Note that Eq. (76) assumes that the DFT+DMFT calculation is performed in the band basis in a charge self-consistent mode (i.e., $P(\mathbf{k})$ corresponds to $V_{\mathbf{k}}$ in Eq. (5b)). However, for one-shot calculations, the equations simplify (Beck et al., 2022). Wannier interpolation can be used in the DMFT self-consistent loop for an isolated set of bands or at the TB level, which is crucial for accurately resolving low-energy physics (Kaye et al., 2023).

Multiple schemes go beyond standard DMFT, but the discussion above carries over directly to these extensions. Examples include cluster-DMFT approaches (either in real or reciprocal space) or diagrammatic extensions of the self-energy such as the DΓA (Galler et al., 2017, 2019) and the TRILEX method (Ayral and Parcollet, 2015, 2016), as well as non-equilibrium DMFT (Aoki et al., 2014). To improve some of the shortcomings of the DFT+DMFT method, a better starting point than DFT may be GW, which combined with DMFT allows to include non-local effects beyond DFT as well as to formalize the double-counting correction term (Biermann, 2014).

a. DFT+DMFT codes From the previous section, it becomes clear that a fully integrated DFT+DMFT software suite requires three main components: 1) a DFT implementation (ab initio engine) and a routine to construct the localized basis set (e.g., a Wannier engine), 2) a Green's function formalism to implement the DMFT equations, and 3) an impurity solver. At present, there are several open-source implementations that meet these requirements to varying degrees. On the side of more monolithic, publicly available beyond-DFT codes, there are implementations in, for example, CASTEP (Plekhanov et al., 2018), Abinit (Romero et al., 2020), RSPt (Di Marco et al., 2009; Grechnev et al., 2007; Thunström et al., 2009), Amulet (AMULET, 2023), and eDMFT (Haule et al., 2010), which include an implementation of DFT and a downfolding routine, as well as choices of internal and externally linked impurity solvers. ComDMFT (Choi et al., 2019), on the other hand, interfaces directly with Wannier90 for the downfolding procedure. All codes support charge self-consistency.

An alternative philosophy is a more modular library approach, focusing on providing the framework for performing DMFT calculations based on input from a DFT calculation. For this purpose, most codes directly rely on Wannier90 to benefit from a generic, robust, and flexible interface independent of the flavor of DFT. Examples include w2dynamics (Wallerberger et al., 2019) and DCORE (Shinaoka et al., 2021), as well as EDIpack (Amaricci et al., 2022), DMFTwDFT (Singh et al., 2021), and

TRIQS (Aichhorn et al., 2016; Merkel et al., 2022; Parcollet et al., 2015), with only the latter two packages supporting charge self-consistency at present (Beck et al., 2022; James et al., 2021; Schüler et al., 2018; Singh et al., 2021). All packages contain a number of internal and external impurity solvers. A list of all currently available impurity solvers is beyond the scope of this article, but can be found on the respective websites.

b. Interaction-parameters codes As in DFT+U, the local interaction parameters that enter the Hubbard model in DFT+DMFT must be chosen appropriately. Starting from a local basis set, the Coulomb integrals can be evaluated, ideally taking into account screening processes and the symmetries of the system to simplify the parametrization of the interaction Hamiltonian (Chen et al., 2022). The most widely used approach is the constrained Random Phase Approximation (cRPA) (Aryasetiawan et al., 2004). Currently, the method is implemented in ABINIT (Romero et al., 2020), SPEX (Friedrich et al., 2010), VASP (Kaltak, 2015), and RESPACK (Nakamura et al., 2021), with the latter three offering the possibility to use WFs constructed by Wannier90. Alternatively, the interaction parameters are treated as free parameters that must be adjusted to match experimental observables.

c. Post-processing Once the solution to the DFT+DMFT scheme is found (charge) self-consistently (see Fig. 8), converged DMFT quantities such as the selfenergy, the local Green's function, or the hybridization function allow to compute several physical observables in post-processing applications. Depending on the frequency domain in which the impurity solver operates, it may be necessary to use analytic continuation to obtain the self-energy in the real frequency domain (Gubernatis et al., 1991; Wang et al., 2009). Such programs are often included in the respective software packages. Since the post-processing step is performed only once after convergence, and therefore does not significantly contribute to the overall computational cost, Wannier interpolation (see Sec. III.C) is particularly beneficial A standard observable is the lattice at this stage. or impurity spectral function, which is directly related to photoemission and absorption spectra. Most software packages provide tools for users to compute such quantities routinely. Transport tensors based on Kubo's linear response theory (Kubo, 1957), such as optical and thermal conductivities, as well as Hall and Seebeck coefficients, can be computed using various tools, including TRIQS/DFTTools (Aichhorn et al., 2016) and the woptic package (Assmann et al., 2016). Another option is LinReTraCe (Pickem et al., 2023), which relies on a semi-analytical approach valid when

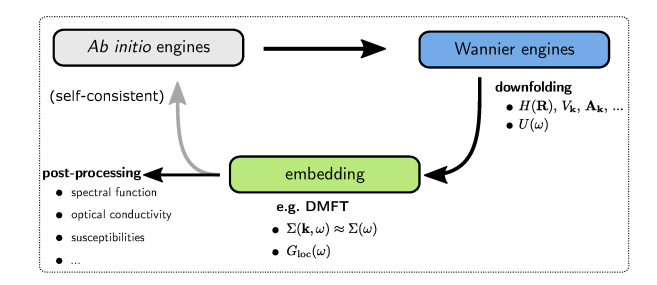


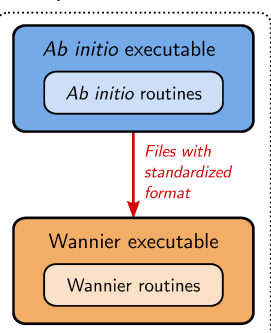
FIG. 8 Typical workflow of the embedding formalism. First, the user performs an *ab initio* calculation from which a downfolded model is derived in the basis of localized orbitals. The downfolded model is solved using an appropriate manybody method such as DMFT (depicted). Physical observables can be computed in a post-processing step. For full self-consistency the cycle is iterated until convergence.

a linear expansion of the self-energy is adequate. Tools to evaluate core level spectroscopies within different levels of approximations are available, for example, in Quanty (Haverkort, 2016) and EDRIXS (Wang *et al.*, 2019b).

2. Koopmans functionals

Koopmans-compliant (KC) functionals (Borghi et al., 2014; Colonna et al., 2022, 2018, 2019; Dabo et al., 2010; De Gennaro et al., 2022; Elliott et al., 2019; Nguyen et al., 2018) are orbital-dependent functionals capable of delivering accurate spectral properties for molecular and extended systems at low computational cost. Remarkably, the KC approach maintains a simple functional formulation while being more accurate than G_0W_0 and comparable to quasi-particle self-consistent GW with vertex correction (QSGW) (Colonna et al., 2022, 2019; Nguyen et al., 2018), at a cost which is broadly comparable to standard DFT. The simplicity and accuracy of the KC framework rests on three fundamental concepts: linearization, screening, and localization. First, a generalized linearization condition is imposed on each charged excitation: the energy of any orbital must be independent of the occupation of the orbital itself. This implies that the KC total energy functional is piecewise linear with respect to fractional occupations, and essentially implements a generalized definition of self-interaction-free orbital. Second, electronic screening and orbital relaxation (due to the electron addition/removal process) are taken into account by orbital-dependent screening coefficients, which can be calculated by finite differences (Nguyen et al., 2018) or linear-response approaches (Colonna et al., 2022, 2018). Finally, the Koopmans compliance condition is imposed on those variational orbitals—i.e., those minimizing the KC energy functional—which are localized. For periodic systems, these variational orbitals resemble MLWFs (Colonna et al., 2022, 2018, 2019;

Independent executables



Library mode

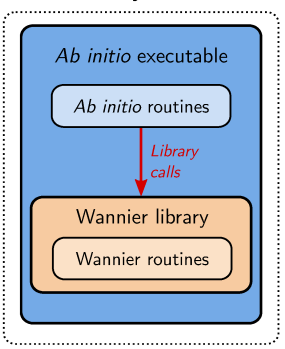


FIG. 9 Different approaches for interaction of the *ab initio* codes with the library routines. Left: the *ab initio* codes and the Wannier engine are compiled independently in two different executables. Data exchange happens via files with standardized formats (see also discussion in Secs. III.B and III.1.2). Right: the Wannier engine provides a library mode. The *ab initio* code is linked at compile time to the Wannier library, and a single executable is created. The *ab initio* routines call directly the routines from the Wannier engine via library calls.

Nguyen et al., 2018).

Using WFs as a proxy for variational orbitals has allowed the development of a Wannier-interpolation and unfolding scheme to calculate the band structure from a supercell Koopmans-functional calculation (De Gennaro et al., 2022). In addition, WFs have fostered the development of a convenient Koopmans formulation that operates fully under PBCs, and is based on explicit BZ sampling and DFPT (Colonna et al., 2022). This Koopmans-Wannier implementation, which goes under the name of KCW, is available in the Quantum ESPRESSO distribution; it delivers improved scaling with system size, and makes band-structure calculations with Koopmans functionals straightforward. KC functionals resonate with other efforts aimed at calculating excitation energies where WFs and localized orbitals are often a key ingredient (Anisimov and Kozhevnikov, 2005; Anisimov et al., 2007; Kraisler and Kronik, 2013; Li et al., 2015, 2017; Ma and Wang, 2016; Skone et al., 2014; Wing et al.. 2021).

I. Interoperability between codes in the ecosystem

1. Library mode for the Wannier engines

When combining two (or more) codes, various approaches are possible. While the most common approach has been to compile the Wannier engine into a different executable than the *ab initio* code, with data being transferred via files with standardized formats, an alternative approach is to expose the Wannier routines via a library interface, as schematically depicted in Fig. 9. In this

second approach, a single executable is created, and the main *ab initio* code is responsible for calling the appropriate routines from the Wannier-engine library.

Making sure that the library interface is both easily usable and covers all possible use cases, however, is a non-trivial task. In the specific case of Wannier90, for instance, its first release contained a simple interface to allow it to be called as a library from another Fortran program, with the necessary data being passed by the calling program rather than by file. Over time, however, it became apparent that this original library interface did not provide the full functionality needed by an ecosystem of codes, presenting three main issues. First, the interface was not fully compatible with parallel calling codes, because there was no means to distribute the data and make use of Wannier90's internal parallelism. Second, the use of global module variables meant that Wannier90 was not thread-safe, i.e., a calling program could not call more than one instance of Wannier90. The third issue concerns error handling. On detecting an error, Wannier90 would abort, causing the calling program to crash. The desired behavior would be instead to return an error code, allowing the calling program to decide how to handle it (for instance, exiting gracefully or retrying with different parameters). Work to address all three of these issues has been carried out by a team at the Scientific Computing Department of STFC at Daresbury Laboratory, UK, in collaboration with three of the present authors (AAM, JRY and GP). A development version is available in the Wannier90 GitHub repository and will be merged into a future Wannier90 release.

2. File I/O generation and parsing

In the first approach mentioned earlier, intermediate files (as listed in Tab. I) are used to decouple the first-principles calculations from the Wannierization step. As already discussed earlier, the formats defined by Wannier90 became the de facto standards for the codes in the Wannier-functions software ecosystem. For instance, many TB codes can read the so-called _tb.dat or _hr.dat files (as already mentioned, these contain onsite energies, hopping terms, ...) to further process the Wannier Hamiltonian. In the past few years many software packages have thus started to implement their own parsers for these I/O files, often focusing only on a specific subset of the file formats relevant for their own use case. However, this leads to a duplication of efforts, also considering that maintaining robust and featurecomplete parsers is a non-trivial task. As many of these codes use Python as the programming language of choice, such as TBmodels (TBmodels, 2023), PythTB (PythTB, 2023a), WannierBerri (Tsirkin, 2021), and AiiDA (Huber et al., 2020; Pizzi et al., 2016; Uhrin et al., 2021), a community effort has been initiated by Jamal I. Mustafa

and others, to implement a centralized reference set of parsers for the Wannier90 input/output files in Python, hosted at https://github.com/wannier-developers/wannier90io-python/. The goal of this project is not only to provide a parser library for developers, but also to provide a convenient package directly for users, allowing them to easily load and manipulate the Wannier90 input/output files for their own use case.

In addition, part of the Wannier90 code base already outputs Python scripts for post-processing; one example is the berry module, which outputs scripts using the matplotlib (Hunter, 2007) library to plot the Berry curvature. However, these scripts are hard-coded into the Wannier90 codebase as a series of write Fortran statements that output Python code, which makes them very difficult to update and maintain. The aforementioned Python library will also facilitate future efforts on moving these post-processing functions into a dedicated Python package, in the hope of smoothening the development experience, as well as allowing users to easily postprocess and visualize the calculation results.

The concept of a common parsing library is not limited to the Python language, and can also be applied to other emerging languages. For example, the Julia package WannierIO.jl (Qiao et al., 2023c) provides functions to read/write Wannier90 file formats, and is used by the Wannier.jl (Qiao et al., 2023d) and DFTK.jl (Herbst et al., 2023) packages as their I/O backend.

J. Automation, workflows and high-throughput

The diversity of the software ecosystem demonstrates the effectiveness of WFs. However, all methods face the need of a robust Wannierization, which used to be a not very straightforward process, since it involves a series of DFT calculations and construction of WFs, and more importantly it also depends sensitively on various input parameters (number of WFs, initial projections for ML-WFs, energy windows, k-point sampling, etc.). Their selection often required experience and chemical intuition, and was often a major challenge not only for beginners, but even for experienced researchers. Fully automated Wannierizations would make the procedure straightforward, and, as a consequence, allow any researcher to easily use all capabilities of the whole ecosystem, while also enabling high-throughput studies for accelerated materials discovery. To this end, it became urgent and necessary to perform algorithmic developments on the Wannierization itself, and to implement robust workflows combining multiple software packages in the ecosystem. On the algorithmic side, Wannierization should provide well-localized WFs without user input (for initial projections or energy windows, for instance); on the workflow side, one would like to orchestrate all different steps from the initial DFT calculations to the Wannier-engine executions to the post-processing steps, while dynamically parsing the outputs and generating new inputs. Moreover, the workflow engine should provide a set of well-tested convergence parameters, and it should be able to handle common errors, and to automatically restart failed calculations.

Recent development of novel algorithms have largely solved the Wannierization challenge, starting from the "selected columns of the density matrix" SCDM (Damle and Lin, 2018; Damle et al., 2015, 2017) algorithms, which generate initial projections by decomposing the density matrix, to the "projectability disentanglement" PDWF (Qiao et al., 2023b), that uses projectability thresholds on atomic orbitals, rather than energy windows, to select which states to drop, keep frozen, or throw in the disentanglement algorithm. Together with the "manifold remixing" MRWF (Qiao et al., 2023a) using parallel transport (Gontier et al., 2019) these approaches remove what had been up to now a critical stumbling block.

On the workflow-engine side, several software packages are able to automate the electronic-structure calculations, such as pymatgen (Ong et al., 2013) and FireWorks (Jain et al., 2015), AFLOW π (Supka et al., 2017), mkite (Schwalbe-Koda, 2023), ASE (Larsen et al., 2017) and ASR (Gjerding et al., 2021), and AiiDA (Huber et al., 2020; Pizzi et al., 2016; Uhrin et al., 2021); some of them, such as ASE and AiiDA, also provide functionalities or workflows to compute WFs. Equipped with automated Wannierization algorithms and robust workflow engines, it has become now possible to create workflows for automated Wannierizations. For instance, Gresch et al. (2018) implemented AiiDA workflows and gathered Wannier TB models for a group of III-V semiconductor materials; Vitale et al. (2020) used SCDM algorithm together with AiiDA workflows, carefully tested convergence parameters, and benchmarked Wannier interpolation accuracy on a set of 200 structures for entangled bands and a set of 81 structures for isolated bands; Garrity and Choudhary (2021) created a database of Wannier Hamiltonians for 1771 materials; Fontana et al. (2021) implemented workflows in ASE and Wannierized 30 inorganic monolayer materials using an automated protocol; and finally Qiao et al. (2023b) used PDWF to automate the Wannierization, obtaining over 1.3 million MLWF for over 20,000 3D inorganics from the Materials Cloud (Talirz et al., 2020) MC3D database, then using manifold remixing (Qiao et al., 2023a) to separately Wannierize back these into the valence and conduction bands of 77 insulators. These high-throughput studies can not only expedite materials discoveries, but also help identify challenging cases for the Wannierization algorithm, and promote further development of robust and automated Wannierization approaches.

IV. Conclusions and perspectives

The WFs software ecosystem represents a positive model for interoperability and decentralized code development in electronic-structure simulations, very much in the spirit of CECAM's Electronic Structure Library (Oliveira et al., 2020). This was made possible both by the nature of the scientific problem and physical quantities involved, and by the design choices originally made in Wannier77 and Wannier90, planned early on as Wannierization engines decoupled from the ab initio codes used to compute the electronic structure. The availability of a well-documented, maintained, and modular open-source Wannier engine has pushed scientists to extend Wannier90's functionalities or, when deemed more practical or efficient, to develop novel packages targeting specific materials properties. The growing availability of post-processing features has ignited a positive loop which further attracted developers from different electronic structure domains to work and use WFs, strengthening the interest in WF-related methods and resulting in the current ecosystem of interoperable software. The ecosystem has been reinforced by the organization of coding weeks and developer workshops, that have proven to be crucial to keep the community engaged and synced, to avoid duplication of efforts, and to collaborate on code maintenance.

While we could not cover here all the existing applications and codes leveraging WFs, we have outlined some of the most popular applications and summarized how they can be implemented in software packages and workflows to calculate advanced materials properties.

Looking forward, we expect that the ongoing efforts in the redesigned Wannier90's library mode will be instrumental in smoothly integrating automated Wannierization procedures within ab initio and post-processing codes, with the benefit of reduced file I/O and code maintenance. As Wannierization becomes increasingly automated, we expect scientists to focus on calculations of complex properties, either through high-level programming of simulation workflows, or through the development and extension of post-processing packages. As a result, even more materials properties will become computationally accessible thanks to WFs, and available to the community through the release of dedicated functionalities, either in existing or in new packages of the ecosystem.

Finally, it is worth commenting on two crucial features of an ecosystem, being it biological or software: biodiversity and resilience. A certain level of biodiversity within a software ecosystem, i.e., the existence of multiple software packages with partially overlapping functionalities, can increase its robustness. First, it enables cross-verification of different implementations, increasing the reliability of the results and facilitating a rapid identification of bugs. Second, it can ensure that the

ecosystem capabilities are not lost if a package goes unmaintained or disappears. This aspect is connected to resilience, i.e., the capability of the ecosystem to deliver functionalities—such as the calculation of materials properties—under the loss of some of its components, an especially relevant issue in a scientific community where developers might not be able to guarantee long-term support for their code. We highlight that a software ecosystem might display the same dynamics that can be seen in biological settings, including competition and extinction. While a certain level of competition can result in code improvements regarding feature coverage, efficiency, and robustness, we caution that extreme competition might undermine biodiversity. It is thus important to sustain the work of individual developers who contribute to the progress and maintenance of an active, heterogeneous, and efficient ecosystem, encouraging measures to ensure proper scientific recognition. More broadly, the challenge will be to support the software development work, which is crucial for the long-term maintenance and integration of heterogeneous software packages.

We believe that a diverse, resilient, and open WF software ecosystem is a major asset for the electronic structure community in its quest to understand, discover, and design materials.

V. Acknowledgements

The authors acknowledge especially the generous and crucial support (in alphabetical order) of CCP9, CECAM, E-CAM, ICTP, IYBSSD, MaX, NCCR MARVEL, Psi-k, SISSA, STFC and University of Trieste in the organization of summer schools and developer workshops related to the Wannier-functions software ecosystem. Pivotal to the move to the present community model were the 2016 San Sebastián workshop, which was funded by E-CAM, NCCR MARVEL, and by the CECAM JC-Maxwell node, and the 2022 ICTP Trieste Wannier Developers Meeting and Wannier Summer School, which was funded by CECAM, ICTP, IYBSSD, MaX, NCCR MARVEL, Psi-k, SISSA, and by the University of Trieste, where the present work was conceived and organized.

A.M. acknowledges support from the ICSC – Centro Nazionale di Ricerca in High Performance Computing, Big Data and Quantum Computing, funded by European Union - NextGenerationEU – PNRR, Missione 4 Componente 2 Investimento 1.4. S.B. acknowledges the Flatiron Institute, a division of the Simons Foundation. E.R.M. acknowledges support from the National Science Foundation under Grant No. DMR-2035518 and Grant No. OAC-2103991. N.M. acknowledges early support by the US National Science Foundation under Grant No. ASC-96-25885. N.M., G.P. and J.Q. acknowledge support from the NCCR MARVEL (a National Centre of Competence in Research, funded by the Swiss National Science

Foundation, grant No. 205602). A.A.M. acknowledges the European Science Foundation INTELBIOMAT programme, and the Thomas Young Centre (grant TYC-101) for support. The work of I.S. and S.S.T. was supported by Grant No. PID2021-129035NB-I00 funded by MCIN/AEI/10.13039/501100011033, and by the IKUR Strategy under the collaboration agreement between the Ikerbasque Foundation and the Material Physics Center on behalf of the Department of Education of the Basque Government. G.P. acknowledges support from the Swiss National Science Foundation (SNSF) Project Funding (grant 200021E-206190 "FISH4DIET"), and from the Open Research Data Program of the ETH Board (project "PREMISE": Open and Reproducible Materials Science Research).

References

- Agapito, Luis A, Andrea Ferretti, Arrigo Calzolari, Stefano Curtarolo, and Marco Buongiorno Nardelli (2013), "Effective and accurate representation of extended Bloch states on finite Hilbert spaces," Phys. Rev. B 88, 165127.
- Aguilera, Irene, Christoph Friedrich, Gustav Bihlmayer, and Stefan Blügel (2013), "GW study of topological insulators Bi₂Se₃, Bi₂Te₃, and Sb₂Te₃: Beyond the perturbative one-shot approach," Phys. Rev. B 88, 045206.
- Aichhorn, Markus, Leonid Pourovskii, Priyanka Seth, Veronica Vildosola, Manuel Zingl, Oleg Peil, Xiaoyu Deng, Jernej Mravlje, Gernot J. Kraberger, Cyril Martins, Michel Ferrero, and Olivier Parcollet (2016), "TRIQS/DFTTools: A TRIQS application for ab initio calculations of correlated materials," Comput. Phys. Commun. 204, 200–208.
- Allen, Philip B (1976), "Fermi-surface harmonics: A general method for nonspherical problems. Application to Boltzmann and Eliashberg equations," Phys. Rev. B 13, 1416– 1427.
- Amaricci, A, L. Crippa, A. Scazzola, F. Petocchi, G. Mazza, L. de Medici, and M. Capone (2022), "EDIpack: A parallel exact diagonalization package for quantum impurity problems," Comput. Phys. Commun. 273, 108261.
- AMULET, (2023), "The AMULET code," http://amulet-code.org, accessed on 2023-12-17.
- Anderson, E, Z. Bai, C. Bischof, S. Blackford, J. Demmel, J. Dongarra, J. Du Croz, A. Greenbaum, S. Hammarling, A. McKenney, and D. Sorensen (1999), LAPACK Users' Guide, 3rd ed. (Society for Industrial and Applied Mathematics, Philadelphia, PA).
- Anderson, PW (1972), "More is different," Science **177**, 393–396.
- Anisimov, VI, F. Aryasetiawan, and A. I. Lichtenstein (1997), "First-principles calculations of the electronic structure and spectra of strongly correlated systems: the LDA+U method," J. Phys. Condens. Matter 9 (4), 767–808.
- Anisimov, V I, D. E. Kondakov, A. V. Kozhevnikov, I. A. Nekrasov, Z. V. Pchelkina, J. W. Allen, S.-K. Mo, H.-D. Kim, P. Metcalf, S. Suga, A. Sekiyama, G. Keller, I. Leonov, X. Ren, and D. Vollhardt (2005), "Full orbital calculation scheme for materials with strongly correlated electrons," Phys. Rev. B 71, 125119.
- Anisimov, VI, and A. V. Kozhevnikov (2005), "Transition

- state method and Wannier functions," Phys. Rev. B 72, 075125.
- Anisimov, V I, A V Kozhevnikov, M A Korotin, A V Lukoyanov, and D A Khafizullin (2007), "Orbital density functional as a means to restore the discontinuities in the totalenergy derivative and the exchange-correlation potential," J. Phys.: Condens. Matter 19 (10), 106206.
- Aoki, Hideo, Naoto Tsuji, Martin Eckstein, Marcus Kollar, Takashi Oka, and Philipp Werner (2014), "Nonequilibrium dynamical mean-field theory and its applications," Rev. Mod. Phys. 86, 779–837.
- Arita, R, K. Kuroki, K. Held, A. V. Lukoyanov, S. Skornyakov, and V. I. Anisimov (2008), "Origin of large thermopower in LiRh₂O₄: Calculation of the seebeck coefficient by the combination of local density approximation and dynamical mean-field theory," Phys. Rev. B 78, 115121.
- Armitage, N P, E. J. Mele, and Ashvin Vishwanath (2018), "Weyl and Dirac semimetals in three-dimensional solids," Rev. Mod. Phys. **90**, 015001.
- Aryasetiawan, F, M. Imada, A. Georges, G. Kotliar, S. Biermann, and A. I. Lichtenstein (2004), "Frequency-dependent local interactions and low-energy effective models from electronic structure calculations," Phys. Rev. B 70, 195104.
- Assmann, E, P. Wissgott, J. Kuneš, A. Toschi, P. Blaha, and K. Held (2016), "woptic: Optical conductivity with Wannier functions and adaptive k-mesh refinement," Comput. Phys. Commun. 202, 1–11.
- Aversa, Claudio, and J. E. Sipe (1995), "Nonlinear optical susceptibilities of semiconductors: Results with a length-gauge analysis," Phys. Rev. B **52**, 14636.
- Ayral, Thomas, and Olivier Parcollet (2015), "Mott physics and spin fluctuations: A unified framework," Phys. Rev. B 92, 115109.
- Ayral, Thomas, and Olivier Parcollet (2016), "Mott physics and spin fluctuations: A functional viewpoint," Phys. Rev. B 93, 235124.
- Ibañez Azpiroz, Julen, Stepan S. Tsirkin, and Ivo Souza (2018), "Ab initio calculation of the shift photocurrent by Wannier interpolation," Phys. Rev. B 97, 245143.
- Baroni, S, S. de Gironcoli, A. Dal Corso, and P. Giannozzi (2001), "Phonons and related properties of extended systems from density-functional perturbation theory," Rev. Mod. Phys. 73, 515.
- Baroni, Stefano, Paolo Giannozzi, and Andrea Testa (1987), "Green's-function approach to linear response in solids," Phys. Rev. Lett. 58, 1861–1864.
- Baù, Nicolas, and Antimo Marrazzo (2023), "Local Chern Marker for Periodic Systems," arXiv:2310.15783 [condmat.mes-hall].
- Beck, Sophie, Alexander Hampel, Olivier Parcollet, Claude Ederer, and Antoine Georges (2022), "Charge self-consistent electronic structure calculations with dynamical mean-field theory using Quantum ESPRESSO, Wannier 90 and TRIQS," J. Phys.: Condens. Matter 34 (23), 235601.
- Becke, A D (1988), "Density-functional exchange-energy approximation with correct asymptotic behavior," Phys. Rev. A 38, 3098–3100.
- Becke, Axel D (2014), "Perspective: Fifty years of density-functional theory in chemical physics," J. Chem. Phys. **140** (18), 18A301.
- Bernevig, B Andrei, and Shou-Cheng Zhang (2006), "Quantum Spin Hall Effect," Phys. Rev. Lett. **96**, 106802.
- Bernevig, BA, and T.L. Hughes (2013), *Topological Insulators and Topological Superconductors* (Princeton University

- Press).
- Bezanson, Jeff, Alan Edelman, Stefan Karpinski, and Viral B. Shah (2017), "Julia: A Fresh Approach to Numerical Computing," SIAM Review **59** (1), 65–98.
- Bianco, Raffaello, and Raffaele Resta (2011), "Mapping topological order in coordinate space," Phys. Rev. B 84, 241106.
- Bianco, Raffaello, and Raffaele Resta (2013), "Orbital Magnetization as a Local Property," Phys. Rev. Lett. 110, 087202.
- Biermann, Silke (2014), "Dynamical screening effects in correlated electron materials—a progress report on combined many-body perturbation and dynamical mean field theory: "GW + DMFT"," J. Phys.: Condens. Matter **26** (17), 173202.
- Birner, Stefan, Tobias Zibold, Till Andlauer, Tillmann Kubis, Matthias Sabathil, Alex Trellakis, and Peter Vogl (2007), "nextnano: General Purpose 3-D Simulations," IEEE Transactions on Electron Devices **54** (9), 2137–2142.
- Blackford, L Susan, Antoine Petitet, Roldan Pozo, Karin Remington, R Clint Whaley, James Demmel, Jack Dongarra, Iain Duff, Sven Hammarling, Greg Henry, et al. (2002), "An updated set of basic linear algebra subprograms (BLAS)," ACM Transactions on Mathematical Software 28 (2), 135–151.
- Blaha, Peter, Karlheinz Schwarz, Fabien Tran, Robert Laskowski, Georg K. H. Madsen, and Laurence D. Marks (2020), "WIEN2k: An APW+lo program for calculating the properties of solids," J. Chem. Phys. **152** (7), 074101.
- Blesio, Germán, Sophie Beck, Antoine Georges, and Jernej Mravlje (2023), "Signatures of Hund Metal and Fermi Liquid Behavior in Sr₂RuO₄ Revealed by Electronic Raman Scattering," arXiv **2304.13563**, 10.48550/arXiv.2304.13563.
- Bloch, F (1929), "Über die Quantenmechanik der Elektronen in Kristallgittern," Zeitschrift für Physik **52**, 555.
- Blount, E I (1962), "Formalisms of band theory," in *Solid State Phys.*, Vol. 13 (Elsevier) p. 305.
- Boehnke, Lewin, Hartmut Hafermann, Michel Ferrero, Frank Lechermann, and Olivier Parcollet (2011), "Orthogonal polynomial representation of imaginary-time Green's functions," Phys. Rev. B 84, 075145.
- Borghi, Giovanni, Andrea Ferretti, Ngoc Linh Nguyen, Ismaila Dabo, and Nicola Marzari (2014), "Koopmans-compliant functionals and their performance against reference molecular data," Phys. Rev. B **90**, 075135.
- Bosoni, Emanuele, Louis Beal, Marnik Bercx, Peter Blaha, Stefan Blügel, Jens Bröder, Martin Callsen, Stefaan Cottenier, Augustin Degomme, Vladimir Dikan, Kristjan Eimre, Espen Flage-Larsen, Marco Fornari, Alberto Garcia, Luigi Genovese, Matteo Giantomassi, Sebastiaan P. Huber, Henning Janssen, Georg Kastlunger, Matthias Krack, Georg Kresse, Thomas D. Kühne, Kurt Lejaeghere, Georg K. H. Madsen, Martijn Marsman, Nicola Marzari, Gregor Michalicek, Hossein Mirhosseini, Tiziano M. A. Müller, Guido Petretto, Chris J. Pickard, Samuel Poncé, Gian-Marco Rignanese, Oleg Rubel, Thomas Ruh, Michael Sluydts, Danny E. P. Vanpoucke, Sudarshan Vijay, Michael Wolloch, Daniel Wortmann, Aliaksandr V. Yakutovich, Jusong Yu, Austin Zadoks, Bonan Zhu, and Giovanni Pizzi (2023), "How to verify the precision of density-functionaltheory implementations via reproducible and universal workflows," Nat. Rev. Phys. 10.1038/s42254-023-00655-3.
- Boys, S F (1966), "Localized Orbitals and Localized Adjustment Functions," in *Quantum Theory of Atoms, Molecules*,

- and the Solid State, edited by P.-O. Löwdin (Academic Press. New York).
- Bradlyn, B, L. Elcoro, J. Cano, M. G. Vergniory, Z. Wang, C. Felser, M. I. Aroyo, and B. A. Bernevig (2017), "Topological quantum chemistry," Nature 547, 298.
- Brandbyge, Mads, José-Luis Mozos, Pablo Ordejón, Jeremy Taylor, and Kurt Stokbro (2002), "Density-functional method for nonequilibrium electron transport," Phys. Rev. B 65, 165401.
- Brouder, Christian, Gianluca Panati, Matteo Calandra, Christophe Mourougane, and Nicola Marzari (2007), "Exponential Localization of Wannier Functions in Insulators," Phys. Rev. Lett. 98, 046402.
- Brunin, Guillaume, Henrique Pereira Coutada Miranda, Matteo Giantomassi, Miquel Royo, Massimiliano Stengel, Matthieu J. Verstraete, Xavier Gonze, Gian-Marco Rignanese, and Geoffroy Hautier (2020a), "Electron-Phonon beyond Fröhlich: Dynamical Quadrupoles in Polar and Covalent Solids," Phys. Rev. Lett. 125, 136601.
- Brunin, Guillaume, Henrique Pereira Coutada Miranda, Matteo Giantomassi, Miquel Royo, Massimiliano Stengel, Matthieu J. Verstraete, Xavier Gonze, Gian-Marco Rignanese, and Geoffroy Hautier (2020b), "Phonon-limited electron mobility in Si, GaAs, and GaP with exact treatment of dynamical quadrupoles," Phys. Rev. B 102, 094308.
- Bruzzone, Samantha, Giuseppe Iannaccone, Nicola Marzari, and Gianluca Fiori (2014), "An Open-Source Multiscale Framework for the Simulation of Nanoscale Devices," IEEE Transactions on Electron Devices **61** (1), 48–53.
- Buongiorno Nardelli, Marco, Frank T. Cerasoli, Marcio Costa, Stefano Curtarolo, Riccardo De Gennaro, Marco Fornari, Laalitha Liyanage, Andrew R. Supka, and Haihang Wang (2018), "PAOFLOW: A utility to construct and operate on ab initio Hamiltonians from the projections of electronic wavefunctions on atomic orbital bases, including characterization of topological materials," Comput. Mater. Sci. 143, 462–472.
- Bushick, Kyle, and Emmanouil Kioupakis (2023), "Phonon-Assisted Auger-Meitner Recombination in Silicon from First Principles," Phys. Rev. Lett. 131, 076902.
- Calandra, Matteo, Gianni Profeta, and Francesco Mauri (2010), "Adiabatic and nonadiabatic phonon dispersion in a Wannier function approach," Phys. Rev. B 82, 165111.
- Callaway, Joseph, and A. James Hughes (1967), "Localized Defects in Semiconductors," Phys. Rev. 156, 860–876.
- Calzolari, Arrigo, Nicola Marzari, Ivo Souza, and Marco Buongiorno Nardelli (2004), "Ab initio transport properties of nanostructures from maximally localized Wannier functions," Phys. Rev. B 69, 035108.
- Cancès, Éric, Antoine Levitt, Gianluca Panati, and Gabriel Stoltz (2017), "Robust determination of maximally localized Wannier functions," Phys. Rev. B 95, 075114.
- Cano, Jennifer, Barry Bradlyn, Zhijun Wang, L. Elcoro, M. G. Vergniory, C. Felser, M. I. Aroyo, and B. Andrei Bernevig (2018), "Building blocks of topological quantum chemistry: Elementary band representations," Phys. Rev. B 97, 035139.
- Carnimeo, Ivan, Stefano Baroni, and Paolo Giannozzi (2019), "Fast hybrid density-functional computations using planewave basis sets," Electron. Struct. 1 (1), 015009.
- CECAM-ESL, (2023), "The CECAM Electronic Structure Library (ESL)," https://esl.cecam.org, accessed on 2023-12-14.

- Cepellotti, Andrea, Jennifer Coulter, Anders Johansson, Natalya S Fedorova, and Boris Kozinsky (2022), "Phoebe: a high-performance framework for solving phonon and electron Boltzmann transport equations," J. Phys. Mater. 5 (3), 035003.
- Ceresoli, Davide, and Raffaele Resta (2007), "Orbital magnetization and Chern number in a supercell framework: Single **k**-point formula," Phys. Rev. B **76**, 012405.
- Chaput, L, Atsushi Togo, and Isao Tanaka (2019), "Finite-displacement computation of the electron-phonon interaction within the projector augmented-wave method," Phys. Rev. B 100, 174304.
- Chaves, Anderson S, Alex Antonelli, Daniel T. Larson, and Efthimios Kaxiras (2020), "Boosting the efficiency of ab initio electron-phonon coupling calculations through dual interpolation," Phys. Rev. B 102, 125116.
- Chen, Hanghui, Alexander Hampel, Jonathan Karp, Frank Lechermann, and Andrew J. Millis (2022), "Dynamical Mean Field Studies of Infinite Layer Nickelates: Physics Results and Methodological Implications," Front. Phys. 10, 10.3389/fphy.2022.835942.
- Cheng, Long, Chenmu Zhang, and Yuanyue Liu (2020), "Why Two-Dimensional Semiconductors Generally Have Low Electron Mobility," Phys. Rev. Lett. 125, 177701.
- Choi, Sangkook, Patrick Semon, Byungkyun Kang, Andrey Kutepov, and Gabriel Kotliar (2019), "ComDMFT: A massively parallel computer package for the electronic structure of correlated-electron systems," Comput. Phys. Commun. 244, 277–294.
- Cistaro, Giovanni, Mikhail Malakhov, Juan José Esteve-Paredes, Alejandro José Uría-Álvarez, Rui E. F. Silva, Fernando Martín, Juan José Palacios, and Antonio Picón (2023), "Theoretical Approach for Electron Dynamics and Ultrafast Spectroscopy (EDUS)," J. Chem. Theory Comput. 19 (1), 333.
- Clark, S J, M. D. Segall, C. J. Pickard, P. J. Hasnip, M. J. Probert, K. Refson, and M. C. Payne (2005), "First principles methods using CASTEP," Zeitschrift für Kristallographie 220, 567.
- Clausius, R (1879), Die Mechanische Behandlung der Electrica
- Clement, Marjory C, Xiao Wang, and Edward F. Valeev (2021), "Robust Pipek-Mezey Orbital Localization in Periodic Solids," J. Chem. Theory Comput. 17 (12), 7406-7415.
- Colonna, Nicola, Riccardo De Gennaro, Edward Linscott, and Nicola Marzari (2022), "Koopmans Spectral Functionals in Periodic Boundary Conditions," J. Chem. Theory Comput. 18 (9), 5435–5448.
- Colonna, Nicola, Ngoc Linh Nguyen, Andrea Ferretti, and Nicola Marzari (2018), "Screening in Orbital-Density-Dependent Functionals," J. Chem. Theory Comput. 14 (5), 2549–2557.
- Colonna, Nicola, Ngoc Linh Nguyen, Andrea Ferretti, and Nicola Marzari (2019), "Koopmans-Compliant Functionals and Potentials and Their Application to the GW100 Test Set," J. Chem. Theory Comput. 15 (3), 1905–1914.
- Corbae, Paul, Julia D. Hannukainen, Quentin Marsal, Daniel Muñoz-Segovia, and Adolfo G. Grushin (2023), "Amorphous topological matter: Theory and experiment," Europhys. Lett. 142 (1), 16001.
- Dabo, Ismaila, Andrea Ferretti, Nicolas Poilvert, Yanli Li, Nicola Marzari, and Matteo Cococcioni (2010), "Koopmans' condition for density-functional theory," Phys. Rev. B 82, 115121.

- Damle, A, and L. Lin (2018), "Disentanglement via Entanglement: A Unified Method for Wannier Localization," Multiscale Model. Simul. 16 (3), 1392–1410.
- Damle, Anil, Antoine Levitt, and Lin Lin (2019), "Variational Formulation for Wannier Functions with Entangled Band Structure," Multiscale Model. Simul. 17 (1), 167–191.
- Damle, Anil, Lin Lin, and Lexing Ying (2015), "Compressed Representation of Kohn–Sham Orbitals via Selected Columns of the Density Matrix," J. Chem. Theory Comput. 11 (4), 1463–1469.
- Damle, Anil, Lin Lin, and Lexing Ying (2017), "SCDM-k: Localized orbitals for solids via selected columns of the density matrix," J. Comput. Phys. **334**, 1 15.
- Dancoff, S M (1950), "Non-Adiabatic Meson Theory of Nuclear Forces," Phys. Rev. **78** (4), 382–385.
- De Gennaro, Riccardo, Nicola Colonna, Edward Linscott, and Nicola Marzari (2022), "Bloch's theorem in orbital-densitydependent functionals: Band structures from Koopmans spectral functionals," Phys. Rev. B 106, 035106.
- Deng, Tianqi, Gang Wu, Wen Shi, Zicong Marvin Wong, Jian-Sheng Wang, and Shuo-Wang Yang (2021), "Ab initio dipolar electron-phonon interactions in two-dimensional materials," Phys. Rev. B 103, 075410.
- Des Cloizeaux, Jacques (1964a), "Analytical Properties of *n*-Dimensional Energy Bands and Wannier Functions," Phys. Rev. **135**, A698–A707.
- Des Cloizeaux, Jacques (1964b), "Energy Bands and Projection Operators in a Crystal: Analytic and Asymptotic Properties," Phys. Rev. 135, A685–A697.
- Di Marco, I, J. Minár, S. Chadov, M. I. Katsnelson, H. Ebert, and A. I. Lichtenstein (2009), "Correlation effects in the total energy, the bulk modulus, and the lattice constant of a transition metal: Combined local-density approximation and dynamical mean-field theory applied to Ni and Mn," Phys. Rev. B 79, 115111.
- Dias, Alexandre C, Julian F.R.V. Silveira, and Fanyao Qu (2023), "WanTiBEXOS: A Wannier based Tight Binding code for electronic band structure, excitonic and optoelectronic properties of solids," Comput. Phys. Commun. 285, 108636.
- Dirac, P A M (1929), "Quantum mechanics of many-electron systems," Proceedings of the Royal Society of London. Series A, Containing Papers of a Mathematical and Physical Character 123 (792), 714–733.
- DiStasio, Robert A, Jr, Biswajit Santra, Zhaofeng Li, Xifan Wu, and Roberto Car (2014), "The individual and collective effects of exact exchange and dispersion interactions on the ab initio structure of liquid water," J. Chem. Phys. 141 (8), 084502.
- Duffin, R J (1953), Duke Mathem. J. 20, 233.
- E, Weinan, Carlos J. García-Cervera, and Jianfeng Lu (2007), "A sub-linear scaling algorithm for computing the electronic structure of materials," Commun. Math. Sci. 5 (4), 999–1026.
- Edmiston, Clyde, and Klaus Ruedenberg (1963), "Localized Atomic and Molecular Orbitals," Rev. Mod. Phys. **35**, 457–464.
- Elk, (2023), "The Elk Code," http://elk.sourceforge.net/.
- Elliott, Joshua D, Nicola Colonna, Margherita Marsili, Nicola Marzari, and Paolo Umari (2019), "Koopmans Meets Bethe–Salpeter: Excitonic Optical Spectra without GW," J. Chem. Theory Comput. 15 (6), 3710–3720.
- Engel, Manuel, Martijn Marsman, Cesare Franchini, and

- Georg Kresse (2020), "Electron-phonon interactions using the projector augmented-wave method and Wannier functions," Phys. Rev. B **101**, 184302.
- Engel, Manuel, Henrique Miranda, Laurent Chaput, Atsushi Togo, Carla Verdi, Martijn Marsman, and Georg Kresse (2022), "Zero-point renormalization of the band gap of semiconductors and insulators using the projector augmented wave method," Phys. Rev. B 106, 094316.
- Enkovaara, J, C. Rostgaard, J. J. Mortensen, J. Chen, M. Dułak, L. Ferrighi, J. Gavnholt, C. Glinsvad, V. Haikola, H. A. Hansen, H. H. Kristoffersen, M. Kuisma, A. H. Larsen, L. Lehtovaara, M. Ljungberg, O. Lopez-Acevedo, P. G. Moses, J. Ojanen, T. Olsen, V. Petzold, N. A. Romero, J. Stausholm-Møller, M. Strange, G. A. Tritsaris, M. Vanin, M. Walter, B. Hammer, H. Häkkinen, G. K. H. Madsen, R. M. Nieminen, J. K. Nørskov, M. Puska, T. T. Rantala, J. Schiøtz, K. S. Thygesen, and K. W. Jacobsen (2010), "Electronic structure calculations with GPAW: a real-space implementation of the projector augmented-wave method," J. Phys.: Condens. Matter 22 (25), 253202.
- EPIq, (2023a), "The elphbolt code," https://github.com/nakib/elphbolt.
- EPIq, (2023b), "The EPIq code," https://the-epiq-team.gitlab.io/epiq-site/.
- EPW, (2023), "The EPW code," https://epw-code.org/.
- Errea, Ion, Francesco Belli, Lorenzo Monacelli, Antonio Sanna, Takashi Koretsune, Terumasa Tadano, Raffaello Bianco, Matteo Calandra, Ryotaro Arita, Francesco Mauri, and Jos´A. Flores-Livas (2020), "Quantum crystal structure in the 250-kelvin superconducting lanthanum hydride," Nature 578, 66.
- Eskridge, Brandon, Henry Krakauer, and Shiwei Zhang (2019), "Local Embedding and Effective Downfolding in the Auxiliary-Field Quantum Monte Carlo Method," Journal of Chemical Theory and Computation 15 (7), 3949–3959.
- Falletta, Stefano, and Alfredo Pasquarello (2022), "Polarons free from many-body self-interaction in density functional theory," Phys. Rev. B 106, 125119.
- Fang, Chen, Matthew J. Gilbert, Xi Dai, and B. Andrei Bernevig (2012), "Multi-Weyl Topological Semimetals Stabilized by Point Group Symmetry," Phys. Rev. Lett. 108, 266802.
- Fang, Chen, Hongming Weng, Xi Dai, and Zhong Fang (2016), "Topological nodal line semimetals," Chin. Phys. B 25 (11), 117106.
- Fang, Zhong, Naoto Nagaosa, Kei S. Takahashi, Atsushi Asamitsu, Roland Mathieu, Takeshi Ogasawara, Hiroyuki Yamada, Masashi Kawasaki, Yoshinori Tokura, and Kiyoyuki Terakura (2003), "The Anomalous Hall Effect and Magnetic Monopoles in Momentum Space," Science 302 (5642), 92.
- Favata, Roberta, and Antimo Marrazzo (2023), "Single-point spin Chern number in a supercell framework," Electron. Struct. 5 (1), 014005.
- Ferretti, A, A Calzolari, B Bonferroni, and R Di Felice (2007), "Maximally localized Wannier functions constructed from projector-augmented waves or ultrasoft pseudopotentials," J. Phys.: Condens. Matter 19 (3), 036215.
- Ferretti, Andrea, Giuseppe Mallia, Layla Martin-Samos, Giovanni Bussi, Alice Ruini, Barbara Montanari, and Nicholas M. Harrison (2012), "Ab initio complex band structure of conjugated polymers: Effects of hydrid den-

- sity functional theory and GW schemes," Phys. Rev. B $\bf 85$, 235105.
- Fetter, A L, and J. D. Walecka (2003), Quantum theory of many-particle systems (Dover Publications, New York).
- Fidkowski, L, T. S. Jackson, and I. Klich (2011), "Model Characterization of Gapless Edge Modes of Topological Insulators Using Intermediate Brillouin-Zone Functions," Phys. Rev. Lett. 107, 036601.
- Fiori, Gianluca, and Giuseppe Iannaccone (2007), "Simulation of Graphene Nanoribbon Field-Effect Transistors," IEEE Electron Device Letters 28 (8), 760–762.
- Fonseca, J E, T. Kubis, M. Povolotskyi, B. Novakovic, A. Ajoy, G. Hegde, H. Ilatikhameneh, Z. Jiang, P. Sengupta, Y. Tan, and G. Klimeck (2013), "Efficient and realistic device modeling from atomic detail to the nanoscale," J. Comput. Electron. 12 (4), 592–600.
- Fontana, Pietro F, Ask H. Larsen, Thomas Olsen, and Kristian S. Thygesen (2021), "Spread-balanced Wannier functions: Robust and automatable orbital localization," Phys. Rev. B 104, 125140.
- Foreman, Bradley A (2002), "Consequences of local gauge symmetry in empirical tight-binding theory," Phys. Rev. B 66, 165212.
- Freimuth, F, Y. Mokrousov, D. Wortmann, S. Heinze, and S. Blügel (2008), "Maximally localized Wannier functions within the FLAPW formalism," Phys. Rev. B 78, 035120.
- Friedrich, Christoph, Stefan Blügel, and Arno Schindlmayr (2010), "Efficient implementation of the *GW* approximation within the all-electron FLAPW method," Phys. Rev. B **81**, 125102.
- Frigo, Matteo, and Steven G. Johnson (2005), "The Design and Implementation of FFTW3," Proceedings of the IEEE 93 (2), 216–231.
- Fu, Liang (2011), "Topological Crystalline Insulators," Phys. Rev. Lett. 106, 106802.
- Fu, Liang, C. L. Kane, and E. J. Mele (2007), "Topological Insulators in Three Dimensions," Phys. Rev. Lett. 98, 106803.
- Galler, Anna, Patrik Thunström, Patrik Gunacker, Jan M. Tomczak, and Karsten Held (2017), "Ab initio dynamical vertex approximation," Phys. Rev. B 95, 115107.
- Galler, Anna, Patrik Thunström, Josef Kaufmann, Matthias Pickem, Jan M. Tomczak, and Karsten Held (2019), "The AbinitioDγA Project v1.0: Non-local correlations beyond and susceptibilities within dynamical mean-field theory," Comput. Phys. Commun. 245, 106847.
- Gao, Yang (2019), "Semiclassical dynamics and nonlinear charge current," Front. Phys. 14, 33404.
- Gao, Yang, Shengyuan A. Yang, and Qian Niu (2017), "Intrinsic relative magnetoconductivity of nonmagnetic metals," Phys. Rev. B 95, 165135.
- García-Cervera, C J, Jianfeng Lu, Yulin Xuan, and Weinan E (2009), "Linear-scaling subspace-iteration algorithm with optimally localized nonorthogonal wave functions for Kohn-Sham density functional theory," Phys. Rev. B 79, 115110.
- Garrity, Kevin F, and Kamal Choudhary (2021), "Database of Wannier tight-binding Hamiltonians using high-throughput density functional theory," Sci. Data 8 (1), 106.
- Georges, Antoine, and Gabriel Kotliar (1992), "Hubbard model in infinite dimensions," Phys. Rev. B 45, 6479–6483.
- Georges, Antoine, Gabriel Kotliar, Werner Krauth, and Marcelo J. Rozenberg (1996), "Dynamical mean-field theory of strongly correlated fermion systems and the limit of infinite dimensions," Rev. Mod. Phys. 68, 13–125.

- Ghim, Minsu (2022), "Accurate calculation of Wannier centers and position matrix elements II: Higher-order finite difference," Wannier 2022 Developers Meeting, http://video.ictp.it/WEB/2022/2022_05_23-smr3757/2022_05_23-11_20-smr3757.mp4.
- Giannozzi, P, O Andreussi, T Brumme, O Bunau, M Buongiorno Nardelli, M Calandra, R Car, C Cavazzoni, D Ceresoli, M Cococcioni, N Colonna, I Carnimeo, A Dal Corso, S de Gironcoli, P Delugas, R A DiStasio, A Ferretti, A Floris, G Fratesi, G Fugallo, R Gebauer, U Gerstmann, F Giustino, T Gorni, J Jia, M Kawamura, H-Y Ko, A Kokalj, E Küçükbenli, M Lazzeri, M Marsili, N Marzari, F Mauri, N L Nguyen, H-V Nguyen, A Otero de-la Roza, L Paulatto, S Poncé, D Rocca, R Sabatini, B Santra, M Schlipf, A P Seitsonen, A Smogunov, I Timrov, T Thonhauser, P Umari, N Vast, X Wu, and S Baroni (2017), "Advanced capabilities for materials modelling with Quantum ESPRESSO," J. Phys.: Condens. Matter 29 (46), 465901.
- Giannozzi, Paolo, Stefano Baroni, Nicola Bonini, Matteo Calandra, Roberto Car, Carlo Cavazzoni, Davide Ceresoli, Guido L Chiarotti, Matteo Cococcioni, Ismaila Dabo, Andrea Dal Corso, Stefano de Gironcoli, Stefano Fabris, Guido Fratesi, Ralph Gebauer, Uwe Gerstmann, Christos Gougoussis, Anton Kokalj, Michele Lazzeri, Layla Martin-Samos, Nicola Marzari, Francesco Mauri, Riccardo Mazzarello, Stefano Paolini, Alfredo Pasquarello, Lorenzo Paulatto, Carlo Sbraccia, Sandro Scandolo, Gabriele Sclauzero, Ari P Seitsonen, Alexander Smogunov, Paolo Umari, and Renata M Wentzcovitch (2009), "QUANTUM ESPRESSO: a modular and open-source software project for quantum simulations of materials," J. Phys.: Condens. Matter 21 (39), 395502.
- Gibertini, Marco, Giovanni Pizzi, and Nicola Marzari (2014), "Engineering polar discontinuities in honeycomb lattices," Nat. Commun. 5 (1), 5157.
- Giustino, F (2014), Materials Modelling using Density Functional Theory (Oxford University Press).
- Giustino, Feliciano (2017), "Electron-phonon interactions from first principles," Rev. Mod. Phys. 89, 015003.
- Giustino, Feliciano, Marvin L. Cohen, and Steven G. Louie (2007a), "Electron-phonon interaction using Wannier functions," Phys. Rev. B **76**, 165108.
- Giustino, Feliciano, Marvin L. Cohen, and Steven G. Louie (2010), "GW method with the self-consistent Sternheimer equation," Phys. Rev. B 81 (11), 115105.
- Giustino, Feliciano, and Alfredo Pasquarello (2006), "Mixed Wannier-Bloch Functions for Electrons and Phonons in Periodic Systems," Phys. Rev. Lett. 96, 216403.
- Giustino, Feliciano, Jonathan R. Yates, Ivo Souza, Marvin L. Cohen, and Steven G. Louie (2007b), "Electron-Phonon Interaction via Electronic and Lattice Wannier Functions: Superconductivity in Boron-Doped Diamond Reexamined," Phys. Rev. Lett. 98, 047005.
- Gjerding, Morten, Thorbjørn Skovhus, Asbjørn Rasmussen, Fabian Bertoldo, Ask Hjorth Larsen, Jens Jørgen Mortensen, and Kristian Sommer Thygesen (2021), "Atomic Simulation Recipes: A Python framework and library for automated workflows," Comput. Mater. Sci. 199, 110731.
- Golze, Dorothea, Marc Dvorak, and Patrick Rinke (2019), "The GW Compendium: A Practical Guide to Theoretical Photoemission Spectroscopy," Front. Chem. 7, 10.3389/fchem.2019.00377.
- Gontier, D, A. Levitt, and S. Siraj-dine (2019), "Numerical

- construction of Wannier functions through homotopy," J. Math. Phys. **60** (3), 031901.
- Gonze, Xavier (1997), "First-principles responses of solids to atomic displacements and homogeneous electric fields: Implementation of a conjugate-gradient algorithm," Phys. Rev. B 55, 10337–10354.
- Gonze, Xavier, Bernard Amadon, Gabriel Antonius, Frédéric Arnardi, Lucas Baguet, Jean-Michel Beuken, Jordan Bieder, François Bottin, Johann Bouchet, Eric Bousquet, Nils Brouwer, Fabien Bruneval, Guillaume Brunin, Théo Cavignac, Jean-Baptiste Charraud, Wei Chen, Michel Côté, Stefaan Cottenier, Jules Denier, Grégory Geneste, Philippe Ghosez, Matteo Giantomassi, Yannick Gillet, Olivier Gingras, Donald R. Hamann, Geoffroy Hautier, Xu He, Nicole Helbig, Natalie Holzwarth, Yongchao Jia, François Jollet, William Lafargue-Dit-Hauret, Kurt Lejaeghere, Miguel A.L. Marques, Alexandre Martin, Cyril Martins, Henrique P.C. Miranda, Francesco Naccarato, Kristin Persson, Guido Petretto, Valentin Planes, Yann Pouillon, Sergei Prokhorenko, Fabio Ricci, Gian-Marco Rignanese, Aldo H. Romero, Michael Marcus Schmitt, Marc Torrent, Michiel J. van Setten, Benoit Van Troeye, Matthieu J. Verstraete, Gilles Zérah, and Josef W. Zwanziger (2020), "The Abinit project: Impact, environment and recent developments," Comput. Phys. Commun. **248**, 107042.
- Gosálbez-Martínez, Daniel, Ivo Souza, and David Vanderbilt (2015), "Chiral degeneracies and Fermi-surface Chern numbers in bcc Fe," Phys. Rev. B **92**, 085138.
- Graf, M, and P. Vogl (1995), "Electromagnetic fields and dielectric response in empirical tight-binding theory," Phys. Rev. B **51**, 4940–4949.
- Grassano, Davide, Davide Campi, Antimo Marrazzo, and Nicola Marzari (2023), "Complementary screening for quantum spin Hall insulators in two-dimensional exfoliable materials," Phys. Rev. Mater. 7, 094202.
- Grechnev, Alexei, I. Di Marco, M. I. Katsnelson, A. I. Lichtenstein, John Wills, and Olle Eriksson (2007), "Theory of bulk and surface quasiparticle spectra for Fe, Co, and Ni," Phys. Rev. B 76, 035107.
- Gresch, Dominik, Gabriel Autès, Oleg V. Yazyev, Matthias Troyer, David Vanderbilt, B. Andrei Bernevig, and Alexey A. Soluyanov (2017), "Z2Pack: Numerical implementation of hybrid wannier centers for identifying topological materials," Phys. Rev. B 95, 075146.
- Gresch, Dominik, QuanSheng Wu, Georg W. Winkler, Rico Häuselmann, Matthias Troyer, and Alexey A. Soluyanov (2018), "Automated construction of symmetrized Wannier-like tight-binding models from ab initio calculations," Phys. Rev. Mater. 2, 103805.
- Groth, C. W., M. Wimmer, A. R. Akhmerov, J. Tworzydło, and C. W. J. Beenakker (2009), "Theory of the Topological Anderson Insulator," Phys. Rev. Lett. 103, 196805.
- Groth, Christoph W, Michael Wimmer, Anton R Akhmerov, and Xavier Waintal (2014), "Kwant: a software package for quantum transport," New J. Phys. 16 (6), 063065.
- Gubernatis, J E, Mark Jarrell, R. N. Silver, and D. S. Sivia (1991), "Quantum Monte Carlo simulations and maximum entropy: Dynamics from imaginary-time data," Phys. Rev. B 44, 6011–6029.
- Gunawardana, Thivan M, Ari M. Turner, and Ryan Barnett (2023), "Optimally Localized Wannier Functions for 2D Chern Insulators," arXiv 2309.07242, 10.48550/arXiv.2309.07242.

- Gygi, F (2008), "Architecture of Qbox: A scalable first-principles molecular dynamics code," IBM Journal of Research and Development **52** (1.2), 137–144.
- Gygi, François, Jean-Luc Fattebert, and Eric Schwegler (2003), "Computation of Maximally Localized Wannier Functions using a simultaneous diagonalization algorithm," Comput. Phys. Commun. 155 (1), 1–6.
- Haldane, F D M (1988), "Model for a Quantum Hall Effect without Landau Levels: Condensed-Matter Realization of the "Parity Anomaly"," Phys. Rev. Lett. 61, 2015–2018.
- Hamann, D R, and David Vanderbilt (2009), "Maximally localized Wannier functions for GW quasiparticles," Phys. Rev. B 79, 045109.
- Hariki, Atsushi, Takayuki Uozumi, and Jan Kuneš (2017), "LDA+DMFT approach to core-level spectroscopy: Application to 3d transition metal compounds," Phys. Rev. B **96**, 045111.
- Hariki, Atsushi, Mathias Winder, and Jan Kuneš (2018), "Continuum Charge Excitations in High-Valence Transition-Metal Oxides Revealed by Resonant Inelastic X-Ray Scattering," Phys. Rev. Lett. 121, 126403.
- Hasan, M Z, and C. L. Kane (2010), "Colloquium: Topological insulators," Rev. Mod. Phys. 82, 3045–3067.
- Haule, Kristjan, Viktor Oudovenko, Sergej Y. Savrasov, and Gabriel Kotliar (2005), "The $\alpha \to \gamma$ Transition in Ce: A Theoretical View from Optical Spectroscopy," Phys. Rev. Lett. **94**, 036401.
- Haule, Kristjan, and Gheorghe L. Pascut (2016), "Forces for structural optimizations in correlated materials within a DFT+embedded DMFT functional approach," Phys. Rev. B 94, 195146.
- Haule, Kristjan, Chuck-Hou Yee, and Kyoo Kim (2010), "Dynamical mean-field theory within the full-potential methods: Electronic structure of ceirin₅, cecoin₅, and cerhin₅," Phys. Rev. B **81**, 195107.
- Haverkort, M W, M. Zwierzycki, and O. K. Andersen (2012), "Multiplet ligand-field theory using Wannier orbitals," Phys. Rev. B 85, 165113.
- Haverkort, Maurits W (2016), "Quanty for core level spectroscopy excitons, resonances and band excitations in time and frequency domain," Journal of Physics: Conference Series 712 (1), 012001.
- Heil, Christoph, Samuel Poncé, Henry Lambert, Martin Schlipf, Elena R. Margine, and Feliciano Giustino (2017),
 "Origin of Superconductivity and Latent Charge Density Wave in NbS₂," Phys. Rev. Lett. 119, 087003.
- Held, K (2007), "Electronic structure calculations using dynamical mean field theory," Advances in Physics 56 (6), 829–926.
- Herbst, Michael F, Antoine Levitt, and Eric Cancès (2023), "DFTK: The Density-functional toolkit," https://dftk.org.
- Heyd, Jochen, Gustavo E. Scuseria, and Matthias Ernzerhof (2003), "Hybrid functionals based on a screened Coulomb potential," J. Chem. Phys. 118 (18), 8207–8215.
- Hirata, So, and Martin Head-Gordon (1999), "Time-dependent density functional theory within the Tamm-Dancoff approximation," Chem. Phys. Lett. **314** (3), 291–299.
- Huber, Sebastiaan P, Emanuele Bosoni, Marnik Bercx, Jens Bröder, Augustin Degomme, Vladimir Dikan, Kristjan Eimre, Espen Flage-Larsen, Alberto Garcia, Luigi Genovese, Dominik Gresch, Conrad Johnston, Guido Petretto, Samuel Poncé, Gian-Marco Rignanese, Christo-

- pher J. Sewell, Berend Smit, Vasily Tseplyaev, Martin Uhrin, Daniel Wortmann, Aliaksandr V. Yakutovich, Austin Zadoks, Pezhman Zarabadi-Poor, Bonan Zhu, Nicola Marzari, and Giovanni Pizzi (2021), "Common workflows for computing material properties using different quantum engines," npj Comput. Mater. 7 (1), 136.
- Huber, Sebastiaan P, Spyros Zoupanos, Martin Uhrin, Leopold Talirz, Leonid Kahle, Rico Häuselmann, Dominik Gresch, Tiziano Müller, Aliaksandr V. Yakutovich, Casper W. Andersen, Francisco F. Ramirez, Carl S. Adorf, Fernando Gargiulo, Snehal Kumbhar, Elsa Passaro, Conrad Johnston, Andrius Merkys, Andrea Cep ellotti, Nicolas Mounet, Nicola Marzari, Boris Kozinsky, and Giovanni Pizzi (2020), "AiiDA 1.0, a scalable computational infrastructure for automated reproducible workflows and data provenance," Sci. Data 7 (1), 300.
- Hunter, J D (2007), "Matplotlib: A 2D graphics environment," Comput. Sci. Eng. 9 (3), 90–95.
- Ibañez-Azpiroz, Julen, Fernando de Juan, and Ivo Souza (2022), "Assessing the role of interatomic position matrix elements in tight-binding calculations of optical properties," SciPost Phys. 12, 070.
- Jain, Anubhav, Shyue Ping Ong, Wei Chen, Bharat Medasani, Xiaohui Qu, Michael Kocher, Miriam Brafman, Guido Petretto, Gian-Marco Rignanese, Geoffroy Hautier, Daniel Gunter, and Kristin A. Persson (2015), "Fire-Works: a dynamic workflow system designed for highthroughput applications," Concurrency Computat.: Pract. Exper. 27 (17), 5037–5059.
- James, A D N, E. I. Harris-Lee, A. Hampel, M. Aichhorn, and S. B. Dugdale (2021), "Wave functions, electronic localization, and bonding properties for correlated materials beyond the Kohn-Sham formalism," Phys. Rev. B 103, 035106.
- Jhalani, Vatsal A, Jin-Jian Zhou, Jinsoo Park, Cyrus E. Dreyer, and Marco Bernardi (2020), "Piezoelectric Electron-Phonon interaction from *ab initio* Dynamical Quadrupoles: Impact on Charge Transport in Wurtzite GaN," Phys. Rev. Lett. **125**, 136602.
- Jiang, Hua, Lei Wang, Qing-feng Sun, and X. C. Xie (2009), "Numerical study of the topological Anderson insulator in HgTe/CdTe quantum wells," Phys. Rev. B 80, 165316.
- Jin, Gan, Daye Zheng, and Lixin He (2021), "Calculation of Berry curvature using non-orthogonal atomic orbitals," J. Phys.: Condens. Matter 33 (32), 325503.
- Jónsson, Elvar Ö, Susi Lehtola, Martti Puska, and Hannes Jónsson (2017), "Theory and Applications of Generalized Pipek-Mezey Wannier Functions," J. Chem. Theory Comput. 13 (2), 460–474.
- Kaltak, Merzuk (2015), Merging GW with DMFT, Ph.D. thesis (University of Vienna).
- Kane, C L, and E. J. Mele (2005a), "Z₂ Topological Order and the Quantum Spin Hall Effect," Phys. Rev. Lett. 95, 146802.
- Kane, C L, and E. J. Mele (2005b), "Quantum Spin Hall Effect in Graphene," Phys. Rev. Lett. 95, 226801.
- Kapil, Venkat, Mariana Rossi, Ondrej Marsalek, Riccardo Petraglia, Yair Litman, Thomas Spura, Bingqing Cheng, Alice Cuzzocrea, Robert H. Meißner, David M. Wilkins, Benjamin A. Helfrecht, Przemysław Juda, Sébastien P. Bienvenue, Wei Fang, Jan Kessler, Igor Poltavsky, Steven Vandenbrande, Jelle Wieme, Clemence Corminboeuf, Thomas D. Kühne, David E. Manolopoulos, Thomas E.

- Markland, Jeremy O. Richardson, Alexandre Tkatchenko, Gareth A. Tribello, Veronique Van Speybroeck, and Michele Ceriotti (2019), "i-PI 2.0: A universal force engine for advanced molecular simulations," Comput. Phys. Commun. 236, 214–223.
- Karolak, M, G. Ulm, T. Wehling, V. Mazurenko,
 A. Poteryaev, and A. Lichtenstein (2010), "Double counting in LDA+DMFT—The example of NiO," Journal of Electron Spectroscopy and Related Phenomena 181 (1), 11–15, proceedings of International Workshop on Strong Correlations and Angle-Resolved Photoemission Spectroscopy 2009.
- Karp, Jonathan, Alexander Hampel, and Andrew J. Millis (2021), "Dependence of DFT + DMFT results on the construction of the correlated orbitals," Phys. Rev. B 103, 195101.
- Kaye, Jason, Sophie Beck, Alex Barnett, Lorenzo Van Muñoz, and Olivier Parcollet (2023), "Automatic, high-order, and adaptive algorithms for Brillouin zone integration," SciPost Phys. 15, 062.
- Khalaf, Eslam, Hoi Chun Po, Ashvin Vishwanath, and Haruki Watanabe (2018), "Symmetry Indicators and Anomalous Surface States of Topological Crystalline Insulators," Phys. Rev. X 8, 031070.
- King-Smith, R D, and David Vanderbilt (1993), "Theory of polarization of crystalline solids," Phys. Rev. B 47, 1651– 1654.
- Kivelson, S (1982), "Wannier functions in one-dimensional disordered systems: Application to fractionally charged solitons," Phys. Rev. B 26, 4269-4277.
- Koçer, Can P, Kristjan Haule, G. Lucian Pascut, and Bartomeu Monserrat (2020), "Efficient lattice dynamics calculations for correlated materials with DFT+DMFT," Phys. Rev. B 102, 245104.
- Koelling, DD, and J.H Wood (1986), "On the interpolation of eigenvalues and a resultant integration scheme," J. Comput. Phys. **67** (2), 253–262.
- Kohn, W (1996), "Density Functional and Density Matrix Method Scaling Linearly with the Number of Atoms," Phys. Rev. Lett. 76, 3168–3171.
- Koretsune, Takashi (2023), "Construction of maximally-localized Wannier functions using crystal symmetry," Comput. Phys. Commun. 285, 108645.
- Kotliar, G, S. Y. Savrasov, K. Haule, V. S. Oudovenko, O. Parcollet, and C. A. Marianetti (2006), "Electronic structure calculations with dynamical mean-field theory," Rev. Mod. Phys. 78, 865–951.
- Kraisler, Eli, and Leeor Kronik (2013), "Piecewise Linearity of Approximate Density Functionals Revisited: Implications for Frontier Orbital Energies," Phys. Rev. Lett. 110, 126403.
- Kresse, G, and D. Joubert (1999), "From ultrasoft pseudopotentials to the projector augmented-wave method," Phys. Rev. B **59** (3), 1758–1775.
- Kruthoff, Jorrit, Jan de Boer, Jasper van Wezel, Charles L. Kane, and Robert-Jan Slager (2017), "Topological Classification of Crystalline Insulators through Band Structure Combinatorics," Phys. Rev. X 7, 041069.
- Kubo, Ryogo (1957), "Statistical-Mechanical Theory of Irreversible Processes. I. General Theory and Simple Applications to Magnetic and Conduction Problems," J. Phys. Soc. Jpn. 12 (6), 570–586.
- Kümmel, Stephan, and Leeor Kronik (2008), "Orbital-dependent density functionals: Theory and applications,"

- Rev. Mod. Phys. 80, 3-60.
- Kune, Jan, Ryotaro Arita, Philipp Wissgott, Alessandro Toschi, Hiroaki Ikeda, and Karsten Held (2010), "Wien2wannier: From linearized augmented plane waves to maximally localized Wannier functions," Comput. Phys. Commun. 181 (11), 1888–1895.
- Kuneš, Jan (2011), "Efficient treatment of two-particle vertices in dynamical mean-field theory," Phys. Rev. B 83, 085102.
- Kühne, Thomas D, Marcella Iannuzzi, Mauro Del Ben, Vladimir V. Rybkin, Patrick Seewald, Frederick Stein, Teodoro Laino, Rustam Z. Khaliullin, Ole Schütt, Florian Schiffmann, Dorothea Golze, Jan Wilhelm, Sergey Chulkov, Mohammad Hossein Bani-Hashemian, Valéry Weber, Urban Borštnik, Mathieu Taillefumier, Alice Shoshana Jakobovits, Alfio Lazzaro, Hans Pabst, Tiziano Müller, Robert Schade, Manuel Guidon, Samuel Andermatt, Nico Holmberg, Gregory K. Schenter, Anna Hehn, Augustin Bussy, Fabian Belleflamme, Gloria Tabacchi, Andreas Glöß, Michael Lass, Iain Bethune, Christopher J. Mundy, Christian Plessl, Matt Watkins, Joost VandeVondele, Matthias Krack, and Jürg Hutter (2020), "CP2K: An electronic structure and molecular dynamics software package - Quickstep: Efficient and accurate electronic structure calculations," J. Chem. Phys. 152 (19), 194103.
- Lafuente-Bartolome, Jon, Idoia G. Gurtubay, and Asier Eiguren (2020), "Symmetric Helmholtz Fermi-surface harmonics for an optimal representation of anisotropic quantities on the Fermi surface: Application to the electron-phonon problem," Phys. Rev. B 102, 165113.
- Lafuente-Bartolome, Jon, Chao Lian, Weng Hong Sio, Idoia G. Gurtubay, Asier Eiguren, and Feliciano Giustino (2022), "Unified Approach to Polarons and Phonon-Induced Band Structure Renormalization," Phys. Rev. Lett. 129, 076402.
- Lam, Siu Kwan, Antoine Pitrou, and Stanley Seibert (2015), "Numba: A LLVM-Based Python JIT Compiler," in Proceedings of the Second Workshop on the LLVM Compiler Infrastructure in HPC, LLVM '15 (Association for Computing Machinery, New York, NY, USA).
- Landauer, Rolf (1970), "Electrical resistance of disordered one-dimensional lattices," The Philosophical Magazine: A Journal of Theoretical Experimental and Applied Physics 21 (172), 863–867.
- Larsen, Ask Hjorth, Jens Jørgen Mortensen, Jakob Blomqvist, Ivano E Castelli, Rune Christensen, Marcin Dułak, Jesper Friis, Michael N Groves, Bjørk Hammer, Cory Hargus, Eric D Hermes, Paul C Jennings, Peter Bjerre Jensen, James Kermode, John R Kitchin, Esben Leonhard Kolsbjerg, Joseph Kubal, Kristen Kaasbjerg, Steen Lysgaard, Jón Bergmann Maronsson, Tristan Maxson, Thomas Olsen, Lars Pastewka, Andrew Peterson, Carsten Rostgaard, Jakob Schiøtz, Ole Schütt, Mikkel Strange, Kristian S Thygesen, Tejs Vegge, Lasse Vilhelmsen, Michael Walter, Zhenhua Zeng, and Karsten W Jacobsen (2017), "The atomic simulation environment—a Python library for working with atoms," J. Phys.: Condens. Matter 29 (27), 273002.
- Lechermann, F, A. Georges, A. Poteryaev, S. Biermann, M. Posternak, A. Yamasaki, and O. K. Andersen (2006), "Dynamical mean-field theory using Wannier functions: A flexible route to electronic structure calculations of strongly correlated materials," Phys. Rev. B 74, 125120.

- Lee, Chengteh, Weitao Yang, and Robert G. Parr (1988), "Development of the Colle-Salvetti correlation-energy formula into a functional of the electron density," Phys. Rev. B 37, 785–789.
- Lee, Chi-Cheng, Yung-Ting Lee, Masahiro Fukuda, and Taisuke Ozaki (2018), "Tight-binding calculations of optical matrix elements for conductivity using nonorthogonal atomic orbitals: Anomalous Hall conductivity in bcc Fe," Phys. Rev. B 98, 115115.
- Lee, D H, and J. D. Joannopoulos (1981a), "Simple scheme for surface-band calculations. I," Phys. Rev. B 23, 4988–4996.
- Lee, D H, and J. D. Joannopoulos (1981b), "Simple scheme for surface-band calculations. II. The Green's function," Phys. Rev. B 23, 4997–5004.
- Lee, Hyungjun, Samuel Poncé, Kyle Bushick, Samad Hajinazar, Jon Lafuente-Bartolome, Joshua Leveillee, Chao Lian, Jae-Mo Lihm, Francesco Macheda, Hitoshi Mori, Hari Paudyal, Weng Hong Sio, Sabyasachi Tiwar, Marios Zacharias, Xiao Zhang, Nicola Bonini, Emmanouil Kioupakis, Elena R. Margine, and Feliciano Giustino (2023), "Electron-phonon physics from first principles using the EPW code," npj Comput. Mater. 9 (1), 156.
- Lee, Nien-En, Hsiao-Yi Chen, Jin-Jian Zhou, and Marco Bernardi (2021), "Facile ab initio approach for self-localized polarons from canonical transformations," Phys. Rev. Materials 5, 063805.
- Lee, Young-Su, Marco Buongiorno Nardelli, and Nicola Marzari (2005), "Band Structure and Quantum Conductance of Nanostructures from Maximally Localized Wannier Functions: The Case of Functionalized Carbon Nanotubes," Phys. Rev. Lett. 95, 076804.
- Leonov, I, V. I. Anisimov, and D. Vollhardt (2014), "First-Principles Calculation of Atomic Forces and Structural Distortions in Strongly Correlated Materials," Phys. Rev. Lett. 112, 146401.
- Li, Chen, Xiao Zheng, Aron J. Cohen, Paula Mori-Sánchez, and Weitao Yang (2015), "Local Scaling Correction for Reducing Delocalization Error in Density Functional Approximations," Phys. Rev. Lett. 114, 053001.
- Li, Chen, Xiao Zheng, Neil Qiang Su, and Weitao Yang (2017), "Localized orbital scaling correction for systematic elimination of delocalization error in density functional approximations," Natl. Sci. Rev. 5 (2), 203–215.
- Li, Jian, Rui-Lin Chu, J. K. Jain, and Shun-Qing Shen (2009), "Topological Anderson Insulator," Phys. Rev. Lett. 102, 136806.
- Li, Wu (2015), "Electrical transport limited by electronphonon coupling from boltzmann transport equation: An ab initio study of Si, Al, and MoS₂," Phys. Rev. B **92**, 075405.
- Lihm, Jae-Mo (2022), "Accurate calculation of Wannier centers and position matrix elements I: Translationally-invariant formula," Wannier 2022 Developers Meeting, http://video.ictp.it/WEB/2022/2022_05_23-smr3757/2022_05_23-11_00-smr3757.mp4.
- Lihm, Jae-Mo, and Cheol-Hwan Park (2019), "Reliable methods for seamless stitching of tight-binding models based on maximally localized Wannier functions," Phys. Rev. B 99, 125117.
- Lihm, Jae-Mo, and Cheol-Hwan Park (2021), "Wannier Function Perturbation Theory: Localized Representation and Interpolation of Wave Function Perturbation," Phys. Rev. X $\bf 11$, 041053.
- Lilia, Boeri, Richard Hennig, Peter Hirschfeld, Gianni Pro-

- feta, Antonio Sanna, Eva Zurek, Warren E Pickett, Maximilian Amsler, Ranga Dias, Mikhail I Eremets, Christoph Heil, Russell J Hemley, Hanyu Liu, Yanming Ma, Carlo Pierleoni, Aleksey N Kolmogorov, Nikita Rybin, Dmitry Novoselov, Vladimir Anisimov, Artem R Oganov, Chris J Pickard, Tiange Bi, Ryotaro Arita, Ion Errea, Camilla Pellegrini, Ryan Requist, E K U Gross, Elena Roxana Margine, Stephen R Xie, Yundi Quan, Ajinkya Hire, Laura Fanfarillo, G R Stewart, J J Hamlin, Valentin Stanev, Renato S Gonnelli, Erik Piatti, Davide Romanin, Dario Daghero, and Roser Valenti (2022), "The 2021 roomtemperature superconductivity roadmap," J. Phys.: Condens. Matter 34 (18), 183002.
- Liu, Xiaoxiong, Stepan S. Tsirkin, and Ivo Souza (2023), "Covariant derivatives of Berry-type quantities: Application to nonlinear transport," arXiv 2303.10129, 10.48550/arXiv.2303.10129.
- Lopez, M G, David Vanderbilt, T. Thonhauser, and Ivo Souza (2012), "Wannier-based calculation of the orbital magnetization in crystals," Phys. Rev. B 85, 014435.
- Lüder, Johann, Johan Schött, Barbara Brena, Maurits W. Haverkort, Patrik Thunström, Olle Eriksson, Biplab Sanyal, Igor Di Marco, and Yaroslav O. Kvashnin (2017), "Theory of l-edge spectroscopy of strongly correlated systems," Phys. Rev. B 96, 245131.
- Ma, Jie, and Lin-Wang Wang (2016), "Using Wannier functions to improve solid band gap predictions in density functional theory," Sci. Rep. 6 (1), 24924.
- Macheda, Francesco, Paolo Barone, and Francesco Mauri (2022), "Electron-Phonon Interaction and Longitudinal-Transverse Phonon Splitting in Doped Semiconductors," Phys. Rev. Lett. 129, 185902.
- Macheda, Francesco, and Nicola Bonini (2018), "Magneto-transport phenomena in *p*-doped diamond from first principles," Phys. Rev. B **98**, 201201.
- Madsen, Georg KH, Jesús Carrete, and Matthieu J. Verstraete (2018), "BoltzTraP2, a program for interpolating band structures and calculating semi-classical transport coefficients," Comput. Phys. Commun. 231, 140–145.
- Madsen, Georg KH, and David J. Singh (2006), "BoltzTraP. A code for calculating band-structure dependent quantities," Comput. Phys. Commun. 175, 67–71.
- Mahler, Aaron, Jacob Williams, Neil Qiang Su, and Weitao Yang (2022), "Localized orbital scaling correction for periodic systems," Phys. Rev. B 106, 035147.
- Maliyov, Ivan, Jinsoo Park, and Marco Bernardi (2021), "Ab initio electron dynamics in high electric fields: Accurate prediction of velocity-field curves," Phys. Rev. B **104**, L100303.
- Margine, E R, and F. Giustino (2013), "Anisotropic Migdal-Eliashberg theory using Wannier functions," Phys. Rev. B 87, 024505.
- Marini, Giovanni, Guglielmo Marchese, Gianni Profeta, Jelena Sjakste, Francesco Macheda, Nathalie Vast, Francesco Mauri, and Matteo Calandra (2023), "EPIq: an open-source software for the calculation of electron-phonon interaction related properties," Comput. Phys. Commun., 108950.
- Markel, J (1971), "FFT pruning," IEEE Transactions on Audio and Electroacoustics 19 (4), 305–311.
- Marrazzo, Antimo, Marco Gibertini, Davide Campi, Nicolas Mounet, and Nicola Marzari (2019), "Relative Abundance of \mathbb{Z}_2 Topological Order in Exfoliable Two-Dimensional Insulators," Nano Lett. **19** (12), 8431–8440.

- Marrazzo, Antimo, and Raffaele Resta (2016), "Irrelevance of the Boundary on the Magnetization of Metals," Phys. Rev. Lett. 116, 137201.
- Marrazzo, Antimo, and Raffaele Resta (2019), "Local Theory of the Insulating State," Phys. Rev. Lett. 122, 166602.
- Marsili, Margherita, Edoardo Mosconi, Filippo De Angelis, and Paolo Umari (2017), "Large-scale GW-BSE calculations with N^3 scaling: Excitonic effects in dye-sensitized solar cells," Phys. Rev. B **95** (7), 075415.
- Martin, Richard M (2004), Electronic Structure: Basic Theory and Practical Methods (Cambridge University Press).
- Martin, Richard M (2020), *Electronic Structure: Basic The*ory and Practical Methods, 2nd ed. (Cambridge University Press).
- Marzari, Nicola, Andrea Ferretti, and Chris Wolverton (2021), "Electronic-structure methods for materials design," Nature Materials **20** (6), 736–749.
- Marzari, Nicola, Arash A. Mostofi, Jonathan R. Yates, Ivo Souza, and David Vanderbilt (2012), "Maximally localized Wannier functions: Theory and applications," Rev. Mod. Phys. 84, 1419–1475.
- Marzari, Nicola, and David Vanderbilt (1997), "Maximally localized generalized Wannier functions for composite energy bands," Phys. Rev. B **56**, 12847–12865.
- Marzari, Nicola, David Vanderbilt, and M. C. Payne (1997), "Ensemble Density-Functional Theory for Ab Initio Molecular Dynamics of Metals and Finite-Temperature Insulators," Phys. Rev. Lett. 79, 1337–1340.
- Mauri, Francesco, Giulia Galli, and Roberto Car (1993), "Orbital formulation for electronic-structure calculations with linear system-size scaling," Phys. Rev. B 47, 9973–9976.
- Merkel, Maximilian E, Alberto Carta, Sophie Beck, and Alexander Hampel (2022), "solid_dmft: gray-boxing DFT+ DMFT materials simulations with TRIQS," J. Open Source Software 7 (77), 4623.
- Metzner, Walter, and Dieter Vollhardt (1989), "Correlated Lattice Fermions in $d = \infty$ Dimensions," Phys. Rev. Lett. **62**, 324–327.
- Michel, L, and J. Zak (1999), "Connectivity of energy bands in crystals," Phys. Rev. B **59**, 5998–6001.
- Mossotti, O F (1850), Memorie di Matematica e di Fisica della Società Italiana delle Scienze Residente in Modena 24.
- Mostofi, Arash A, Jonathan R. Yates, Young-Su Lee, Ivo Souza, David Vanderbilt, and Nicola Marzari (2008), "Wannier90: A tool for obtaining maximally-localised wannier functions," Comput. Phys. Commun. 178 (9), 685—699.
- Mostofi, Arash A, Jonathan R. Yates, Giovanni Pizzi, Young-Su Lee, Ivo Souza, David Vanderbilt, and Nicola Marzari (2014), "An updated version of wannier90: A tool for obtaining maximally-localised Wannier functions," Comput. Phys. Commun. 185 (8), 2309–2310.
- Mountjoy, Jeff, Michelle Todd, and Nicholas J. Mosey (2017), "Exact exchange with non-orthogonal generalized Wannier functions," J. Chem. Phys. **146** (10), 104108.
- Muechler, Lukas, Danis I. Badrtdinov, Alexander Hampel, Jennifer Cano, Malte Rösner, and Cyrus E. Dreyer (2022), "Quantum embedding methods for correlated excited states of point defects: Case studies and challenges," Phys. Rev. B **105**, 235104.
- Mulliken, R S (2004), "Electronic Population Analysis on LCAO-MO Molecular Wave Functions. I," J. Chem. Phys. 23 (10), 1833–1840.
- Mustafa, Jamal I, Sinisa Coh, Marvin L. Cohen, and

- Steven G. Louie (2015), "Automated construction of maximally localized Wannier functions: Optimized projection functions method," Phys. Rev. B **92**, 165134.
- Nakamura, Kazuma, Yoshihide Yoshimoto, Yusuke Nomura, Terumasa Tadano, Mitsuaki Kawamura, Taichi Kosugi, Kazuyoshi Yoshimi, Takahiro Misawa, and Yuichi Motoyama (2021), "RESPACK: An ab initio tool for derivation of effective low-energy model of material," Comput. Phys. Commun. 261, 107781.
- Nardelli, Marco Buongiorno (1999), "Electronic transport in extended systems: Application to carbon nanotubes," Phys. Rev. B 60, 7828–7833.
- Nekrasov, I A, K. Held, G. Keller, D. E. Kondakov, Th. Pruschke, M. Kollar, O. K. Andersen, V. I. Anisimov, and D. Vollhardt (2006), "Momentum-resolved spectral functions of SrVO₃ calculated by LDA+DMFT," Phys. Rev. B 73, 155112.
- Nenciu, G (1991), "Dynamics of band electrons in electric and magnetic fields: rigorous justification of the effective Hamiltonians," Rev. Mod. Phys. 63, 91–127.
- Neupert, T, and F. Schindler (2018), "Lecture Notes on Topological Crystalline Insulators," in *Topological Matter Lectures from the Topological Matter School 2017*, edited by D. Bercioux, J. Cayssol, M. G. Vergniory, and M. Reyes Calvo, Chap. 2 (Springer, Cham) p. 31.
- Nguyen, Ngoc Linh, Nicola Colonna, Andrea Ferretti, and Nicola Marzari (2018), "Koopmans-Compliant Spectral Functionals for Extended Systems," Phys. Rev. X 8, 021051.
- Nikolaev, S A, and I. V. Solovyev (2014), "Orbital magnetization of insulating perovskite transition-metal oxides with a net ferromagnetic moment in the ground state," Phys. Rev. B 89, 064428.
- Noffsinger, Jesse, Feliciano Giustino, Brad D. Malone, Cheol-Hwan Park, Steven G. Louie, and Marvin L. Cohen (2010), "EPW: A program for calculating the electron-phonon coupling using maximally localized wannier functions," Comput. Phys. Commun. **181** (12), 2140–2148.
- Noffsinger, Jesse, Emmanouil Kioupakis, Chris G. Van de Walle, Steven G. Louie, and Marvin L. Cohen (2012), "Phonon-Assisted Optical Absorption in Silicon from First Principles," Phys. Rev. Lett. 108, 167402.
- Numba-PythTB, (2023), The high-performance Numba implementation of PYTHTB is available at https://github.com/mikelgda/yeet-pythtb.
- Nunes, R W, and David Vanderbilt (1994), "Generalization of the density-matrix method to a nonorthogonal basis," Phys. Rev. B 50, 17611–17614.
- Oliveira, Micael J T, Nick Papior, Yann Pouillon, Volker Blum, Emilio Artacho, Damien Caliste, Fabiano Corsetti, Stefano de Gironcoli, Alin M. Elena, Alberto García, Víctor M. García-Suárez, Luigi Genovese, William P. Huhn, Georg Huhs, Sebastian Kokott, Emine Küçükbenli, Ask H. Larsen, Alfio Lazzaro, Irina V. Lebedeva, Yingzhou Li, David López-Durán, Pablo López-Tarifa, Martin Lüders, Miguel A. L. Marques, Jan Minar, Stephan Mohr, Arash A. Mostofi, Alan O'Cais, Mike C. Payne, Thomas Ruh, Daniel G. A. Smith, José M. Soler, David A. Strubbe, Nicolas Tancogne-Dejean, Dominic Tildesley, Marc Torrent, and Victor Wen-zhe Yu (2020), "The CECAM electronic structure library and the modular software development paradigm," J. Chem. Phys. 153 (2), 024117.
- Ong, Shyue Ping, William Davidson Richards, Anubhav Jain, Geoffroy Hautier, Michael Kocher, Shreyas Cholia, Dan

- Gunter, Vincent L. Chevrier, Kristin A. Persson, and Gerbrand Ceder (2013), "Python Materials Genomics (pymatgen): A robust, open-source python library for materials analysis," Comput. Mater. Sci. 68, 314–319.
- Onida, Giovanni, Lucia Reining, and Angel Rubio (2002), "Electronic excitations: density-functional versus manybody green's-function approaches," Rev. Mod. Phys. 74, 601–659.
- Ordejón, Pablo, David A. Drabold, Matthew P. Grumbach, and Richard M. Martin (1993), "Unconstrained minimization approach for electronic computations that scales linearly with system size," Phys. Rev. B 48, 14646–14649.
- Oudovenko, V S, G. Pálsson, K. Haule, G. Kotliar, and S. Y. Savrasov (2006), "Electronic structure calculations of strongly correlated electron systems by the dynamical mean-field method," Phys. Rev. B 73, 035120.
- Ozaki, T, and H. Kino (2005), "Efficient projector expansion for the ab initio LCAO method," Phys. Rev. B 72, 045121.
- Ozaki, Taisuke, Kengo Nishio, and Hiori Kino (2010), "Efficient implementation of the nonequilibrium Green function method for electronic transport calculations," Phys. Rev. B 81, 035116.
- Panati, Gianluca (2007), "Triviality of Bloch and Bloch-Dirac Bundles," Annales Henri Poincaré 8 (5), 995–1011.
- Panati, Gianluca, and Adriano Pisante (2013), "Bloch Bundles, Marzari-Vanderbilt Functional and Maximally Localized Wannier Functions," Commun. Math. Phys. **322** (3), 835–875.
- Parcollet, Olivier, Michel Ferrero, Thomas Ayral, Hartmut Hafermann, Igor Krivenko, Laura Messio, and Priyanka Seth (2015), "TRIQS: A toolbox for research on interacting quantum systems," Comput. Phys. Commun. 196 (Supplement C), 398 415.
- Park, Hyowon, Kristjan Haule, and Gabriel Kotliar (2011), "Magnetic Excitation Spectra in bafe₂as₂: A Two-Particle Approach within a Combination of the Density Functional Theory and the Dynamical Mean-Field Theory Method," Phys. Rev. Lett. **107**, 137007.
- Park, Jinsoo, Jin-Jian Zhou, Vatsal A. Jhalani, Cyrus E. Dreyer, and Marco Bernardi (2020), "Long-range quadrupole electron-phonon interaction from first principles," Phys. Rev. B 102, 125203.
- Paul, Arpita, and Turan Birol (2019), "Applications of DFT + DMFT in Materials Science," Annual Review of Materials Research 49 (1), 31–52.
- Pavarini, E, S. Biermann, A. Poteryaev, A. I. Lichtenstein, A. Georges, and O. K. Andersen (2004), "Mott Transition and Suppression of Orbital Fluctuations in Orthorhombic $3d^1$ Perovskites," Phys. Rev. Lett. **92**, 176403.
- Pavarini, Eva, Erik Koch, Alexander Lichtenstein, and Dieter Vollhardt, Eds. (2011), *The LDA+DMFT approach to strongly correlated materials*, Schriften des Forschungszentrums Jülich. Reihe modeling and simulation, Vol. 1 (Forschungszenrum Jülich GmbH Zentralbibliothek, Verlag, Jülich) record converted from VDB: 12.11.2012.
- Pedersen, Thomas Garm, Kjeld Pedersen, and Thomas Brun Kriestensen (2001), "Optical matrix elements in tight-binding calculations," Phys. Rev. B 63, 201101.
- Perdew, John P, Matthias Ernzerhof, and Kieron Burke (1996), "Rationale for mixing exact exchange with density functional approximations," J. Chem. Phys. **105** (22), 9982–9985.
- PERTURBO, (2023), "The PERTURBO code," https://perturbo-code.github.io/.

- Phoebe, (2023), "Phoebe, A high-performance framework for solving Phonon and Electron Boltzmann transport Equations," https://mir-group.github.io/phoebe/.
- Pick, Robert M, Morrel H. Cohen, and Richard M. Martin (1970), "Microscopic Theory of Force Constants in the Adiabatic Approximation," Phys. Rev. B 1, 910–920.
- Pickem, Matthias, Emanuele Maggio, and Jan M. Tomczak (2023), "LinReTraCe: The linear response transport centre," SciPost Phys. Codebases, 16.
- Pickett, Warren E (1989), "Pseudopotential methods in condensed matter applications," Computer Physics Reports 9 (3), 115–197.
- Pickett, Warren E, Henry Krakauer, and Philip B. Allen (1988), "Smooth Fourier interpolation of periodic functions," Phys. Rev. B 38, 2721–2726.
- Pipek, János, and Paul G. Mezey (1989), "A fast intrinsic localization procedure applicable for ab initio and semiempirical linear combination of atomic orbital wave functions," J. Chem. Phys. 90 (9), 4916–4926.
- Pizzi, Giovanni, Andrea Cepellotti, Riccardo Sabatini, Nicola Marzari, and Boris Kozinsky (2016), "AiiDA: automated interactive infrastructure and database for computational science," Comput. Mater. Sci. 111, 218–230.
- Pizzi, Giovanni, Valerio Vitale, Ryotaro Arita, Stefan Blügel, Frank Freimuth, Guillaume Géranton, Marco Gibertini, Dominik Gresch, Charles Johnson, Takashi Koretsune, Julen Ibañez-Azpiroz, Hyungjun Lee, Jae-Mo Lihm, Daniel Marchand, Antimo Marrazzo, Yuriy Mokrousov, Jamal I Mustafa, Yoshiro Nohara, Yusuke Nomura, Lorenzo Paulatto, Samuel Poncé, Thomas Ponweiser, Junfeng Qiao, Florian Thöle, Stepan S Tsirkin, Małgorzata Wierzbowska, Nicola Marzari, David Vanderbilt, Ivo Souza, Arash A Mostofi, and Jonathan R Yates (2020), "Wannier90 as a community code: new features and applications," J. Phys. Condens. Matter 32 (16), 165902.
- Pizzi, Giovanni, Dmitri Volja, Boris Kozinsky, Marco Fornari, and Nicola Marzari (2014), "BoltzWann: A code for the evaluation of thermoelectric and electronic transport properties with a maximally-localized Wannier functions basis," Comput. Phys. Commun. 185 (1), 422–429.
- Plekhanov, Evgeny, Nicola Bonini, and Cedric Weber (2021), "Calculating dynamical mean-field theory forces in ab initio ultrasoft pseudopotential formalism," Phys. Rev. B 104, 235131.
- Plekhanov, Evgeny, Phil Hasnip, Vincent Sacksteder, Matt Probert, Stewart J. Clark, Keith Refson, and Cedric Weber (2018), "Many-body renormalization of forces in f-electron materials," Phys. Rev. B 98, 075129.
- Po, Hoi Chun, Ashvin Vishwanath, and Haruki Watanabe (2017), "Symmetry-based indicators of band topology in the 230 space groups," Nat. Commun. 8 (1), 10.1038/s41467-017-00133-2.
- Poncé, S, E. R. Margine, C. Verdi, and F. Giustino (2016), "EPW: Electron-phonon coupling, transport and superconducting properties using maximally localized Wannier functions," Comput. Phys. Commun. 209, 116.
- Poncé, Samuel, Wenbin Li, Sven Reichardt, and Feliciano Giustino (2020), "First-principles calculations of charge carrier mobility and conductivity in bulk semiconductors and two-dimensional materials," Rep. Prog. Phys. 83 (3), 036501.
- Poncé, Samuel, Francesco Macheda, Elena Roxana Margine, Nicola Marzari, Nicola Bonini, and Feliciano Giustino (2021), "First-principles predictions of hall and drift mo-

- bilities in semiconductors," Phys. Rev. Research 3, 043022. Poncé, Samuel, Elena R. Margine, and Feliciano Giustino
- (2018), "Towards predictive many-body calculations of phonon-limited carrier mobilities in semiconductors," Phys. Rev. B **97**, 121201.
- Poncé, Samuel, Miquel Royo, Marco Gibertini, Nicola Marzari, and Massimiliano Stengel (2023), "Accurate Prediction of Hall Mobilities in Two-Dimensional Materials through Gauge-Covariant Quadrupolar Contributions," Phys. Rev. Lett. 130, 166301.
- Posternak, Michel, Alfonso Baldereschi, Sandro Massidda, and Nicola Marzari (2002), "Maximally localized Wannier functions in antiferromagnetic MnO within the FLAPW formalism," Phys. Rev. B 65, 184422.
- Óscar Pozo Ocaña,, and Ivo Souza (2023), "Multipole theory of optical spatial dispersion in crystals," SciPost Phys. 14, 118.
- Prentice, Joseph C A, Jolyon Aarons, James C. Womack, Alice E. A. Allen, Lampros Andrinopoulos, Lucian Anton, Robert A. Bell, Arihant Bhandari, Gabriel A. Bramley, Robert J. Charlton, Rebecca J. Clements, Daniel J. Cole, Gabriel Constantinescu, Fabiano Corsetti, Simon M.-M. Dubois, Kevin K. B. Duff, José María Escartín, Andrea Greco, Quintin Hill, Louis P. Lee, Edward Linscott, David D. O'Regan, Maximillian J. S. Phipps, Laura E. Ratcliff, Álvaro Ruiz Serrano, Edward W. Tait, Gilberto Teobaldi, Valerio Vitale, Nelson Yeung, Tim J. Zuehlsdorff, Jacek Dziedzic, Peter D. Haynes, Nicholas D. M. Hine, Arash A. Mostofi, Mike C. Payne, and Chriskriton Skylaris (2020), "The ONETEP linear-scaling density functional theory program," J. Chem. Phys. 152 (17), 10.1063/5.0004445.
- Protik, Nakib H, and David A. Broido (2020), "Coupled transport of phonons and carriers in semiconductors: A case study of *n*-doped GaAs," Phys. Rev. B **101**, 075202.
- Protik, Nakib H, and Boris Kozinsky (2020), "Electronphonon drag enhancement of transport properties from a fully coupled *ab initio* Boltzmann formalism," Phys. Rev. B **102**, 245202.
- Protik, Nakib H, Chunhua Li, Miguel Pruneda, David Broido, and Pablo Ordejón (2022), "The elphbolt ab initio solver for the coupled electron-phonon Boltzmann transport equations," npj Comput. Mater. 8 (1), 28.
- Provost, J P, and G. Vallee (1980), "Riemannian structure on manifolds of quantum states," Commun. Math. Phys. **76** (3), 289 301.
- PythTB, (2023a), The PYTHTB code package is available at http://www.physics.rutgers.edu/pythtb/about.html.
- PythTB, (2023b), "Pythtb tight-binding formalism and conventions," https://www.physics.rutgers.edu/pythtb/_downloads/e39c23ce476d399b268efa520e7a9091/pythtb-formalism.pdf, accessed: 2023-06-20.
- Qian, Xiaofeng, Ju Li, Liang Qi, Cai-Zhuang Wang, Tzu-Liang Chan, Yong-Xin Yao, Kai-Ming Ho, and Sidney Yip (2008), "Quasiatomic orbitals for ab initio tight-binding analysis," Phys. Rev. B 78, 245112.
- Qiao, Junfeng, Giovanni Pizzi, and Nicola Marzari (2023a), "Automated mixing of maximally localized Wannier functions into target manifolds," npj Comput. Mater. 9 (1), 206
- Qiao, Junfeng, Giovanni Pizzi, and Nicola Marzari (2023b), "Projectability disentanglement for accurate and automated electronic-structure Hamiltonians," npj Comput. Mater. 9 (1), 208.

- Qiao, Junfeng, Giovanni Pizzi, and Nicola Marzari (2023c), "WannierIO.jl: A Julia package for reading/writing wannier90 file formats," https://github.com/qiaojunfeng/WannierIO.jl, accessed on 2023-12-11.
- Qiao, Junfeng, Giovanni Pizzi, and Nicola Marzari (2023d), "Wannier.jl: A playground for Wannier functions," https://wannierjl.org, accessed on 2023-07-05.
- Qiao, Junfeng, Jiaqi Zhou, Zhe Yuan, and Weisheng Zhao (2018), "Calculation of intrinsic spin Hall conductivity by Wannier interpolation," Phys. Rev. B 98, 214402.
- Quantum ESPRESSO, (2023), "The Quantum ESPRESSO suite of codes," https://www.quantum-espresso.org.
- Ratcliff, Laura E, William Dawson, Giuseppe Fisicaro, Damien Caliste, Stephan Mohr, Augustin Degomme, Brice Videau, Viviana Cristiglio, Martina Stella, Marco D'Alessandro, Stefan Goedecker, Takahito Nakajima, Thierry Deutsch, and Luigi Genovese (2020), "Flexibilities of wavelets as a computational basis set for large-scale electronic structure calculations," J. Chem. Phys. 152 (19), 194110.
- Resta, Raffaele (1992), "Theory of the electric polarization in crystals," Ferroelectrics **136** (1), 51–55.
- Resta, Raffaele (1994), "Macroscopic polarization in crystalline dielectrics: the geometric phase approach," Rev. Mod. Phys. **66**, 899–915.
- Rew, R, and G. Davis (1990), "NetCDF: an interface for scientific data access," IEEE Computer Graphics and Applications 10 (4), 76–82.
- Rocca, Dario, Ralph Gebauer, Yousef Saad, and Stefano Baroni (2008), "Turbo charging time-dependent densityfunctional theory with Lanczos chains," J. Chem. Phys. 128 (15), 154105.
- Rocca, Dario, Deyu Lu, and Giulia Galli (2010), "Ab initio calculations of optical absorption spectra: Solution of the Bethe–Salpeter equation within density matrix perturbation theory," J. Chem. Phys. 133 (16), 164109.
- Rocha, A R, V. M. García-Suárez, S. Bailey, C. Lambert, J. Ferrer, and S. Sanvito (2006), "Spin and molecular electronics in atomically generated orbital landscapes," Phys. Rev. B 73, 085414.
- Rohlfing, Michael, and Steven G. Louie (2000), "Electron-hole excitations and optical spectra from first principles," Phys. Rev. B **62**, 4927–4944.
- Romero, Aldo H, Douglas C. Allan, Bernard Amadon, Gabriel Antonius, Thomas Applencourt, Lucas Baguet, Jordan Bieder, François Bottin, Johann Bouchet, Eric Bousquet, Fabien Bruneval, Guillaume Brunin, Damien Caliste, Michel Côté, Jules Denier, Cyrus Dreyer, Philippe Ghosez, Matteo Giantomassi, Yannick Gillet, Olivier Gingras, Donald R. Hamann, Geoffroy Hautier, François Jollet, Gérald Jomard, Alexandre Martin, Henrique P. C. Miranda, Francesco Naccarato, Guido Petretto, Nicholas A. Pike, Valentin Planes, Sergei Prokhorenko, Tonatiuh Rangel, Fabio Ricci, Gian-Marco Rignanese, Miquel Royo, Massimiliano Stengel, Marc Torrent, Michiel J. van Setten, Benoit Van Troeye, Matthieu J. Verstraete, Julia Wiktor, Josef W. Zwanziger, and Xavier Gonze (2020), "ABINIT: Overview and focus on selected capabilities," J. Chem. Phys. **152** (12), 124102.
- Ryoo, Ji Hoon, Cheol-Hwan Park, and Ivo Souza (2019), "Computation of intrinsic spin Hall conductivities from first principles using maximally localized Wannier functions," Phys. Rev. B 99, 235113.
- Sakuma, R (2013), "Symmetry-adapted Wannier functions

- in the maximal localization procedure," Phys. Rev. B 87, 235109.
- Sancho, M P Lopez, J M Lopez Sancho, and J Rubio (1984), "Quick iterative scheme for the calculation of transfer matrices: application to Mo (100)," J. Phys. F: Met. Phys. 14 (5), 1205.
- Sangalli, D, A Ferretti, H Miranda, C Attaccalite, I Marri, E Cannuccia, P Melo, M Marsili, F Paleari, A Marrazzo, G Prandini, P Bonfà, M O Atambo, F Affinito, M Palummo, A Molina-Sánchez, C Hogan, M Grüning, D Varsano, and A Marini (2019), "Many-body perturbation theory calculations using the yambo code," J. Phys. Condens. Matter 31 (32), 325902.
- Satpathy, S, and Z. Pawlowska (1988), "Construction of Bond-Centered Wannier Functions for Silicon Valence Bands," physica status solidi (b) **145** (2), 555–565.
- Savrasov, S Yu (1992), "Linear response calculations of lattice dynamics using muffin-tin basis sets," Phys. Rev. Lett. 69, 2819–2822.
- Schüler, M, O E Peil, G J Kraberger, R Pordzik, M Marsman, G Kresse, T O Wehling, and M Aichhorn (2018), "Charge self-consistent many-body corrections using optimized projected localized orbitals," J. Phys. Condens. Matter 30 (47), 475901.
- Schulz, Werner W, Philip B. Allen, and Nandini Trivedi (1992), "Hall coefficient of cubic metals," Phys. Rev. B 45, 10886–10890.
- Schwalbe-Koda, Daniel (2023), "mkite: A distributed computing platform for high-throughput materials simulations," arXiv **2301.08841**, 10.48550/arXiv.2301.08841, arXiv:2301.08841 [physics.comp-ph].
- Sgiarovello, Claudia, Maria Peressi, and Raffaele Resta (2001), "Electron localization in the insulating state: Application to crystalline semiconductors," Phys. Rev. B **64**, 115202.
- Shelley, Matthew, Nicolas Poilvert, Arash A. Mostofi, and Nicola Marzari (2011), "Automated quantum conductance calculations using maximally-localised Wannier functions," Comput. Phys. Commun. 182 (10), 2174–2183.
- Sheng, Nan, Christian Vorwerk, Marco Govoni, and Giulia Galli (2022), "Green's Function Formulation of Quantum Defect Embedding Theory," Journal of Chemical Theory and Computation 18 (6), 3512–3522.
- Shinaoka, Hiroshi, Junya Otsuki, Mitsuaki Kawamura, Nayuta Takemori, and Kazuyoshi Yoshimi (2021), "DCore: Integrated DMFT software for correlated electrons," Sci-Post Phys. 10, 117.
- Silvestrelli, Pier Luigi (1999), "Maximally localized Wannier functions for simulations with supercells of general symmetry," Phys. Rev. B **59**, 9703–9706.
- Singh, Vijay, Uthpala Herath, Benny Wah, Xingyu Liao, Aldo H. Romero, and Hyowon Park (2021), "DMFTwDFT: An open-source code combining Dynamical Mean Field Theory with various density functional theory packages," Comput. Phys. Commun. 261, 107778.
- Sio, Weng Hong, and Feliciano Giustino (2023), "Polarons in two-dimensional atomic crystals," Nat. Phys. 19, 629.
- Sio, Weng Hong, Carla Verdi, Samuel Poncé, and Feliciano Giustino (2019), "Polarons from First Principles, without Supercells," Phys. Rev. Lett. 122, 246403.
- Sjakste, J, N. Vast, M. Calandra, and F. Mauri (2015), "Wannier interpolation of the electron-phonon matrix elements in polar semiconductors: Polar-optical coupling in GaAs," Phys. Rev. B 92, 054307.

- Skone, Jonathan H, Marco Govoni, and Giulia Galli (2014), "Self-consistent hybrid functional for condensed systems," Phys. Rev. B 89, 195112.
- Sodemann, Inti, and Liang Fu (2015), "Quantum Nonlinear Hall Effect Induced by Berry Curvature Dipole in Time-Reversal Invariant Materials," Phys. Rev. Lett. 115, 216806.
- Sohier, Thibault, Matteo Calandra, and Francesco Mauri (2016), "Two-dimensional Fröhlich interaction in transition-metal dichalcogenide monolayers: Theoretical modeling and first-principles calculations," Phys. Rev. B 94, 085415.
- Soler, José M, Emilio Artacho, Julian D Gale, Alberto García, Javier Junquera, Pablo Ordejón, and Daniel Sánchez-Portal (2002), "The SIESTA method for ab initio order-N materials simulation," J. Phys.: Condens. Matter 14 (11), 2745–2779.
- Soluyanov, Alexey A, and David Vanderbilt (2011a), "Computing topological invariants without inversion symmetry," Phys. Rev. B 83, 235401.
- Soluyanov, Alexey A, and David Vanderbilt (2011b), "Wannier representation of \mathbb{Z}_2 topological insulators," Phys. Rev. B 83, 035108.
- Song, Zhida, Tiantian Zhang, Zhong Fang, and Chen Fang (2018), "Quantitative mappings between symmetry and topology in solids," Nat. Commun. 9 (1), 10.1038/s41467-018-06010-w.
- Sorensen, HV, and C.S. Burrus (1993), "Efficient computation of the DFT with only a subset of input or output points," IEEE Transactions on Signal Processing 41 (3), 1184–1200.
- Souza, Ivo, Nicola Marzari, and David Vanderbilt (2001), "Maximally localized Wannier functions for entangled energy bands," Phys. Rev. B **65**, 035109.
- Sporkmann, B, and H. Bross (1994), "Calculation of Wannier functions for fcc transition metals by Fourier transformation of Bloch functions," Phys. Rev. B 49, 10869–10876.
- Stefanucci, Gianluca, Robert van Leeuwen, and Enrico Perfetto (2023), "In and Out-of-Equilibrium Ab Initio Theory of Electrons and Phonons," Phys. Rev. X 13, 031026.
- Stengel, Massimiliano, and Nicola A. Spaldin (2006), "Accurate polarization within a unified Wannier function formalism," Phys. Rev. B 73, 075121.
- StraWBerryPy, (2023), The STRAWBERRYPY code package is available at https://github.com/strawberrypy-developers/strawberrypy.git.
- Sun, Qiming, Timothy C. Berkelbach, Nick S. Blunt, George H. Booth, Sheng Guo, Zhendong Li, Junzi Liu, James D. McClain, Elvira R. Sayfutyarova, Sandeep Sharma, Sebastian Wouters, and Garnet Kin-Lic Chan (2018), "PySCF: the Python-based simulations of chemistry framework," WIREs Computational Molecular Science 8 (1), e1340.
- Sun, Qiming, Xing Zhang, Samragni Banerjee, Peng Bao, Marc Barbry, Nick S. Blunt, Nikolay A. Bogdanov, George H. Booth, Jia Chen, Zhi-Hao Cui, Janus J. Eriksen, Yang Gao, Sheng Guo, Jan Hermann, Matthew R. Hermes, Kevin Koh, Peter Koval, Susi Lehtola, Zhendong Li, Junzi Liu, Narbe Mardirossian, James D. McClain, Mario Motta, Bastien Mussard, Hung Q. Pham, Artem Pulkin, Wirawan Purwanto, Paul J. Robinson, Enrico Ronca, Elvira R. Sayfutyarova, Maximilian Scheurer, Henry F. Schurkus, James E. T. Smith, Chong Sun, Shi-Ning Sun, Shiv Upadhyay, Lucas K. Wagner, Xiao Wang, Alec White, James Daniel Whitfield, Mark J. Williamson, Sebastian Wouters, Jun

- Yang, Jason M. Yu, Tianyu Zhu, Timothy C. Berkelbach, Sandeep Sharma, Alexander Yu. Sokolov, and Garnet Kin-Lic Chan (2020), "Recent developments in the PySCF program package," J. Chem. Phys. **153** (2), 024109.
- Supka, Andrew R, Troy E. Lyons, Laalitha Liyanage, Pino D'Amico, Rabih Al Rahal Al Orabi, Sharad Mahatara, Priya Gopal, Cormac Toher, Davide Ceresoli, Arrigo Calzolari, Stefano Curtarolo, Marco Buongiorno Nardelli, and Marco Fornari (2017), "AFLOWπ: A minimalist approach to high-throughput ab initio calculations including the generation of tight-binding hamiltonians," Comput. Mater. Sci. 136, 76–84.
- Taherinejad, Maryam, Kevin F. Garrity, and David Vanderbilt (2014), "Wannier center sheets in topological insulators." Phys. Rev. B 89, 115102.
- Talirz, Leopold, Luca M. Ghiringhelli, and Berend Smit (2021), "Trends in Atomistic Simulation Software Usage [Article v1.0]," Living Journal of Computational Molecular Science 3 (1), 1483.
- Talirz, Leopold, Snehal Kumbhar, Elsa Passaro, Aliaksandr V. Yakutovich, Valeria Granata, Fernando Gargiulo, Marco Borelli, Martin Uhrin, S ebastiaan P. Huber, Spyros Zoupanos, Carl S. Adorf, Casper Welzel Andersen, Ole Schütt, Carlo A. Pignedoli, Daniele Passerone, Joost VandeVondele, Thomas C. Schulthess, Berend Smit, Giovanni Pizzi, and Nicola Marzari (2020), "Materials Cloud, a platform for open computational science," Sci. Data 7 (1), 299.
- Tancogne-Dejean, Nicolas, Micael J. T. Oliveira, Xavier Andrade, Heiko Appel, Carlos H. Borca, Guillaume Le Breton, Florian Buchholz, Alberto Castro, Stefano Corni, Alfredo A. Correa, Umberto De Giovannini, Alain Delgado, Florian G. Eich, Johannes Flick, Gabriel Gil, Adrián Gomez, Nicole Helbig, Hannes Hübener, René Jestädt, Joaquim Jornet-Somoza, Ask H. Larsen, Irina V. Lebedeva, Martin Lüders, Miguel A. L. Marques, Sebastian T. Ohlmann, Silvio Pipolo, Markus Rampp, Carlo A. Rozzi, David A. Strubbe, Shunsuke A. Sato, Christian Schäfer, Iris Theophilou, Alicia Welden, and Angel Rubio (2020), "Octopus, a computational framework for exploring light-driven phenomena and quantum dynamics in extended and finite systems," J. Chem. Phys. 152 (12), 10.1063/1.5142502.
- Tang, Feng, Hoi Po, Ashvin Vishwanath, and Xiangang Wan (2019), "Comprehensive search for topological materials using symmetry indicators," Nature 566, 486–489.
- TBmodels, (2023), The TBMODELS code package is available at https://tbmodels.greschd.ch/en/latest/index.html.
- TDEP, (2023), "The TDEP code," https://tdep-developers.github.io/tdep/.
- The HDF Group, (2023), "2023," https://www.hdfgroup.org/HDF5/, accessed on 2023-12-14.
- Thonhauser, T, D. Ceresoli, D. Vanderbilt, and R. Resta (2005), "Orbital Magnetization in Periodic Insulators," Phys. Rev. Lett. 95, 137205.
- Thonhauser, T, and D. Vanderbilt (2006), "Insulator/Chern-insulator transition in the Haldane model," Phys. Rev. B 74, 235111.
- Thunström, P, I. Di Marco, A. Grechnev, S. Lebègue, M. I. Katsnelson, A. Svane, and O. Eriksson (2009), "Multiplet effects in the electronic structure of intermediate-valence compounds," Phys. Rev. B 79, 165104.
- Thygesen, K S, L. B. Hansen, and K. W. Jacobsen (2005), "Partly Occupied Wannier Functions," Phys. Rev. Lett. 94,

- 026405.
- Tillack, Sebastian, Andris Gulans, and Claudia Draxl (2020), "Maximally localized wannier functions within the (L)APW + LO method," Phys. Rev. B 101, 235102.
- Tokura, Yoshinori, Masashi Kawasaki, and Naoto Nagaosa (2017), "Emergent functions of quantum materials," Nat. Phys. 13 (11), 1056–1068.
- Tomczak, Jan M, Kristjan Haule, and Gabriel Kotliar (2012), "Signatures of electronic correlations in iron silicide," Proc. Natl. Acad. Sci. U.S.A. **109** (9), 3243–3246.
- Tsirkin, Stepan S (2021), "High performance Wannier interpolation of Berry curvature and related quantities with WannierBerri code," npj Comput. Mater. 7 (1), 33.
- Tsirkin, Stepan S, Ivo Souza, and David Vanderbilt (2017), "Composite Weyl nodes stabilized by screw symmetry with and without time-reversal invariance," Phys. Rev. B **96**, 045102
- Uehara, Kentaro, and John S. Tse (2000), "Calculations of transport properties with the linearized augmented planewave method," Phys. Rev. B 61, 1639–1642.
- Uhrin, Martin, Sebastiaan P. Huber, Jusong Yu, Nicola Marzari, and Giovanni Pizzi (2021), "Workflows in AiiDA: Engineering a high-throughput, event-based engine for robust and modular computational workflows," Comput. Mater. Sci. 187, 110086.
- Umari, P, X. Qian, N. Marzari, G. Stenuit, L. Giaco-mazzi, and S. Baroni (2011), "Accelerating GW calculations with optimal polarizability basis," physica status solidi (b) 248 (3), 527–536.
- Uría-Álvarez, Alejandro José, Juan José Esteve-Paredes, Manuel Antonio García-Blázquez, and Juan José Palacios (2023), "Efficient computation of optical excitations in two-dimensional materials with the Xatu code," arXiv 2307.01572, 10.48550/arXiv.2307.01572.
- Vanderbilt, D (2018), Berry Phases in Electronic Structure Theory: Electric Polarization, Orbital Magnetization and Topological Insulators (Cambridge University Press).
- Vanderbilt, David, and R. D. King-Smith (1993), "Electric polarization as a bulk quantity and its relation to surface charge," Phys. Rev. B 48, 4442–4455.
- Varnava, Nicodemos, Ivo Souza, and David Vanderbilt (2020), "Axion coupling in the hybrid Wannier representation," Phys. Rev. B 101, 155130.
- Verdi, Carla, and Feliciano Giustino (2015), "Fröhlich Electron-Phonon vertex from First Principles," Phys. Rev. Lett. 115, 176401.
- Vergniory, M G, L. Elcoro, Zhijun Wang, Jennifer Cano, C. Felser, M. I. Aroyo, B. Andrei Bernevig, and Barry Bradlyn (2017), "Graph theory data for topological quantum chemistry," Phys. Rev. E 96 (2), 10.1103/physreve.96.023310.
- Vergniory, MG, L Elcoro, Claudia Felser, Nicolas Regnault, B Andrei Bernevig, and Zhijun Wang (2019), "A complete catalogue of high-quality topological materials," Nature 566 (7745), 480—485.
- Vitale, Valerio, Giovanni Pizzi, Antimo Marrazzo, Jonathan R. Yates, Nicola Marzari, and Arash A. Mostofi (2020), "Automated high-throughput Wannierisation," npj Comput. Mater. 6 (1), 1–18.
- Vogl, P (1976), "Microscopic theory of electron-phonon interaction in insulators or semiconductors," Phys. Rev. B 13, 694–704.
- Železný, Jakub (2023), "Linres: Wannier linear

- response," https://bitbucket.org/zeleznyj/wannier-linear-response/wiki/Home.
- Walker, Brent, A. Marco Saitta, Ralph Gebauer, and Stefano Baroni (2006), "Efficient Approach to Time-Dependent Density-Functional Perturbation Theory for Optical Spectroscopy," Phys. Rev. Lett. 96 (11), 113001.
- Wallerberger, Markus, Andreas Hausoel, Patrik Gunacker, Alexander Kowalski, Nicolaus Parragh, Florian Goth, Karsten Held, and Giorgio Sangiovanni (2019), "w2dynamics: Local one- and two-particle quantities from dynamical mean field theory," Comput. Phys. Commun. 235, 388–399.
- Wang, Chong, Xiaoyu Liu, Lei Kang, Bing-Lin Gu, Yong Xu, and Wenhui Duan (2017), "First-principles calculation of nonlinear optical responses by Wannier interpolation," Phys. Rev. B 96, 115147.
- Wang, Chong, Sibo Zhao, Xiaomi Guo, Xinguo Ren, Bing-Lin Gu, Yong Xu, and Wenhui Duan (2019a), "First-principles calculation of optical responses based on nonorthogonal localized orbitals," New J. Phys. 21 (9), 093001.
- Wang, Jing, and Shou-Cheng Zhang (2017), "Topological states of condensed matter," Nat. Mater. 16 (11), 1062–1067.
- Wang, Runzhi, Emanuel A. Lazar, Hyowon Park, Andrew J. Millis, and Chris A. Marianetti (2014), "Selectively localized wannier functions," Phys. Rev. B 90, 165125.
- Wang, Xin, Emanuel Gull, Luca de' Medici, Massimo Capone, and Andrew J. Millis (2009), "Antiferromagnetism and the gap of a Mott insulator: Results from analytic continuation of the self-energy," Phys. Rev. B 80, 045101.
- Wang, Xinjie, David Vanderbilt, Jonathan R. Yates, and Ivo Souza (2007), "Fermi-surface calculation of the anomalous Hall conductivity," Phys. Rev. B 76, 195109.
- Wang, Xinjie, Jonathan R. Yates, Ivo Souza, and David Vanderbilt (2006), "Ab initio calculation of the anomalous Hall conductivity by Wannier interpolation," Phys. Rev. B 74, 195118
- Wang, YL, G. Fabbris, M.P.M. Dean, and G. Kotliar (2019b), "EDRIXS: An open source toolkit for simulating spectra of resonant inelastic x-ray scattering," Comput. Phys. Commun. 243, 151–165.
- Wannier, Gregory H (1937), "The Structure of Electronic Excitation Levels in Insulating Crystals," Phys. Rev. **52**, 191–197.
- WannierBerri, (2023), The implementation is described in the WannierBerri documentation available at https://docs.wannier-berri.org/en/master/docs/mmn2uHu.html.
- Weng, Hongming, Taisuke Ozaki, and Kiyoyuki Terakura (2009), "Revisiting magnetic coupling in transition-metalbenzene complexes with maximally localized Wannier functions," Phys. Rev. B 79, 235118.
- Wieder, Benjamin J, Barry Bradlyn, Jennifer Cano, Zhijun Wang, Maia G. Vergniory, Luis Elcoro, Alexey A. Soluyanov, Claudia Felser, Titus Neupert, Nicolas Regnault, and B. Andrei Bernevig (2022), "Topological materials discovery from crystal symmetry," Nat. Rev. Mater. 7 (3), 196–216.
- Wing, Dahvyd, Guy Ohad, Jonah B. Haber, Marina R. Filip, Stephen E. Gant, Jeffrey B. Neaton, and Leeor Kronik (2021), "Band gaps of crystalline solids from Wannierlocalization-based optimal tuning of a screened rangeseparated hybrid functional," Proc. Natl. Acad. Sci. U.S.A. 118 (34), e2104556118.
- Wissgott, P, A. Toschi, H. Usui, K. Kuroki, and K. Held

- (2010), "Enhancement of the Na_xCoO_2 thermopower due to electronic correlations," Phys. Rev. B 82, 201106.
- Wissgott, P, J. Kuneš, A. Toschi, and K. Held (2012), "Dipole matrix element approach versus Peierls approximation for optical conductivity," Phys. Rev. B 85, 205133.
- Wortmann, Daniel, Gregor Michalicek, Nadjib Baadji, Markus Betzinger, Gustav Bihlmayer, Jens Bröder, Tobias Burnus, Jussi Enkovaara, Frank Freimuth, Christoph Friedrich, Christian-Roman Gerhorst, Sabastian Granberg Cauchi, Uliana Grytsiuk, Andrea Hanke, Jan-Philipp Hanke, Marcus Heide, Stefan Heinze, Robin Hilgers, Henning Janssen, Daniel Aaaron Klüppelberg, Roman Kovacik, Philipp Kurz, Marjana Lezaic, Georg K. H. Madsen, Yuriy Mokrousov, Alexander Neukirchen, Matthias Redies, Stefan Rost, Martin Schlipf, Arno Schindlmayr, Miriam Winkelmann, and Stefan Blügel (2023), "Fleur," Zenodo 10.5281/zenodo.7891361.
- Wu, QuanSheng, ShengNan Zhang, Hai-Feng Song, Matthias Troyer, and Alexey A. Soluyanov (2018), "WannierTools: An open-source software package for novel topological materials," Comput. Phys. Commun. 224, 405–416.
- Wu, Xifan, Annabella Selloni, and Roberto Car (2009), "Order-n implementation of exact exchange in extended insulating systems," Phys. Rev. B 79, 085102.
- Xiao, D, M.-C. Chang, and Q. Niu (2010), "Berry phase effects on electronic properties," Rev. Mod. Phys. 82, 1959.
- Xiao, Di, Junren Shi, and Qian Niu (2005), "Berry Phase Correction to Electron Density of States in Solids," Phys. Rev. Lett. 95, 137204.
- Xiao, Di, Yugui Yao, Zhong Fang, and Qian Niu (2006), "Berry-Phase Effect in Anomalous Thermoelectric Transport," Phys. Rev. Lett. 97, 026603.
- Yang, Shuo-Ying, Hao Yang, Elena Derunova, Stuart S. P. Parkin, Binghai Yan, and Mazhar N. Ali (2018), "Symmetry demanded topological nodal-line materials," Adv. Phys.: X 3 (1), 1414631.
- Yao, Yugui, Leonard Kleinman, A. H. MacDonald, Jairo Sinova, T. Jungwirth, Ding-sheng Wang, Enge Wang, and Qian Niu (2004), "First Principles Calculation of Anomalous Hall Conductivity in Ferromagnetic bcc Fe," Phys. Rev. Lett. 92, 037204.
- Yates, Jonathan R, Xinjie Wang, David Vanderbilt, and Ivo Souza (2007), "Spectral and Fermi surface properties from Wannier interpolation," Phys. Rev. B 75, 195121.
- Yin, M T, and Marvin L. Cohen (1980), "Microscopic Theory of the Phase Transformation and Lattice Dynamics of Si," Phys. Rev. Lett. 45, 1004–1007.
- Yokouchi, Tomoyuki, Yuya Ikeda, Takahiro Morimoto, and Yuki Shiomi (2023), "Giant Magnetochiral Anisotropy in Weyl Semimetal WTe₂ Induced by Diverging Berry Curvature," Phys. Rev. Lett. **130**, 136301.
- Z2pack, (2023), The Z2Pack code package is available at https://z2pack.greschd.ch/en/latest/index.html.
- Zacharias, Marios, and Feliciano Giustino (2016), "One-shot calculation of temperature-dependent optical spectra and phonon-induced band-gap renormalization," Phys. Rev. B 94, 075125.
- Zacharias, Marios, and Feliciano Giustino (2020), "Theory of the special displacement method for electronic structure calculations at finite temperature," Phys. Rev. Res. 2, 013357.
- Zacharias, Marios, George Volonakis, Feliciano Giustino, and Jacky Even (2023a), "Anharmonic lattice dynamics via the special displacement method," Phys. Rev. B 108, 035155.

- Zacharias, Marios, George Volonakis, Feliciano Giustino, and Jacky Even (2023b), "Anharmonic lattice dynamics via the special displacement method," npj Comput. Mater. 9 (1), 153.
- Zak, J (1982), "Band representations of space groups," Phys. Rev. B 26, 3010–3023.
- Zak, J (1989), "Berry's phase for energy bands in solids," Phys. Rev. Lett. 62, 2747–2750.
- Zgid, Dominika, and Emanuel Gull (2017), "Finite temperature quantum embedding theories for correlated systems," New Journal of Physics 19 (2), 023047.
- Zhang, Chenmu, and Yuanyue Liu (2022), "Phonon-limited transport of two-dimensional semiconductors: Quadrupole scattering and free carrier screening," Phys. Rev. B 106, 115423.
- Zhang, Tiantian, Yi Jiang, Zhida Song, He Huang, Yuqing He, Zhong Fang, Hongming Weng, and Chen Fang (2019), "Catalogue of topological electronic materials," Nature **566** (7745), 475–479.
- Zhou, Jin-Jian, and Marco Bernardi (2019), "Predicting charge transport in the presence of polarons: The beyond-quasiparticle regime in SrTiO₃," Phys. Rev. Research 1,

- 033138.
- Zhou, Jin-Jian, Jinsoo Park, I-Te Lu, Ivan Maliyov, Xiao Tong, and Marco Bernardi (2021a), "PERTURBO: A software package for ab initio electron-phonon interactions, charge transport and ultrafast dynamics," Comput. Phys. Commun. 264, 107970.
- Zhou, Jin-Jian, Jinsoo Park, Iurii Timrov, Andrea Floris, Matteo Cococcioni, Nicola Marzari, and Marco Bernardi (2021b), "Ab Initio Electron-Phonon Interactions in Correlated Electron Systems," Phys. Rev. Lett. 127, 126404.
- Zicovich-Wilson, Claudio M, Roberto Dovesi, and Victor R. Saunders (2001), "A general method to obtain well localized Wannier functions for composite energy bands in linear combination of atomic orbital periodic calculations," J. Chem. Phys. 115 (21), 9708–9719.
- Ziman, J (1972), Principles of the Theory of Solids, 2nd ed. (Cambridge University Press).
- Zingl, Manuel, Jernej Mravlje, Markus Aichhorn, Olivier Parcollet, and Antoine Georges (2019), "Hall coefficient signals orbital differentiation in the Hund's metal Sr₂RuO₄," npj Quantum Materials 4 (1), 35.